Split-hopper barges

Workability of a split-hopper barge in irregular seas

S.T.M Mensch

Technische Universiteit Delft

TU Delft

Split-hopper barges

Workability of a split-hopper barge in irregular seas

by

S.T.M Mensch

to obtain the degree of Master of Science

at the Delft University of Technology,

to be defended publicly on the 16th of October 2017

Student number: 4150503
Project duration: November 14, 2016 – Oktober 16, 2017

Chairman:	Prof. Dr. Ir. A. Metrikine,	TU Delft
Thesis committee:	Ir. J. S. Hoving,	TU Delft
	Dr. Ir. K. N. van Dalen,	TU Delft
	Ing. H. Duba,	Royal Boskalis Westminster

TU Delft Boskalis

Abstract

A split hopper barge is a dredging vessel that can split over its longitudinal axis to discharge its cargo. To allow for such an operation, the barge consists of two half-hulls that are connected by hinges at the top and hydraulic cylinders at the bottom. Any forces that act at the interface between the half-hulls have to be transferred by the hinges and cylinders as a result. The aim of this thesis is to develop a method to determine the workability limits of split hopper barges in irregular seas. For this workability of the barge, the design limits of the hinges and hydraulic cylinders are assumed to be governing.

A quasi-static model is formulated to determine the effects of roll, different types of cargo, opening the barge and discharging the cargo on the forces in the hinges and cylinders. The results of the quasi-static model are a set of governing load cases for the split hopper barge. From the quasi-static model, it is found that the forces of interest are the largest for a closed split hopper barge and that either a solid or a liquid cargo will yield the governing load case. To account for the dynamics in irregular sea conditions, a calculation method is proposed based on Ansys AQWA. Since AQWA is not able to account for liquid cargo motions, its effects are incorporated separately. Using WAMIT simulations, the influences of the liquid cargo to the added mass and stiffness of the barge are determined. Based on the WAMIT results the AQWA model is adjusted.

Superimposing the results from the quasi-static and dynamic models, the maximum forces in the hinges and hydraulic cylinders are obtained for the governing load cases. By comparing the obtained maximum forces to the design forces, a conclusion on the workability limits of the split hopper barge is drawn.

For the barge carrying a solid cargo only one resonance frequency is found, while, due to the liquid cargo motions, the barge with a liquid cargo has two resonance frequencies. As a result, a larger number of combinations of wave directions and periods yield considerable forces. For a 3-hour-extreme with a significant wave height of 3 meters, the governing hydraulic cylinder forces are found for a barge carrying a liquid cargo. The maximum resulting hinge forces however, are found for a barge carrying a solid cargo. Because the limits of the hinges are exceeded before the limits of the hydraulic cylinders, it is concluded that the workability limits of the split hopper barge in irregular waves are most limited, and therefore governing, for a barge carrying a solid cargo.

Preface

S.T.M Mensch
Bergambacht, October 2017

This report presents the study that I have done as a part of my thesis for the finalization of my master study in Offshore Engineering at the Delft University of Technology. The research has been conducted at the R&D department of Royal Boskalis Westminster and covers the topic of the workability of split hopper barges in irregular seas. It is a topic that has become very dear to me and has challenged me repeatedly over the past months.

I would like to thank my graduation committee Prof. Dr. Ir. A. Metrikine, Ir. J.S. Hoving and Ing. H. Duba for their guidance, effort and confidence that they putt into me and my project. In particular I feel obliged to thank Hans for his full and daily support over the duration of the project. It is really appreciated that he was willing to putt this amount of time of effort in this project next to his daily activities. Next to Hans, I would like to thank the other engineers of the R&D department as well, in special Oscar Sainz Avila and Gert-Jan Grundlehner for their ideas and support in the realization of the research goals.

Next to the supervisors and colleagues I would like to thank my fellow (graduate) students at Boskalis for the pleasant cooperation and working environment. Off course my graduation would not have been successful without the support of my family, friends and other relatives.

Thank you all!

Summary

Introduction

Split hopper barges (SHB) are dredging vessels that are used to transport and discharge dredged materials. A typical split-hopper barge is only used for transportation of dredged cargo, the dredging itself is done using other types of dredging equipment. Therefore, split hopper barges will always work together with other types of dredging vessels in a project. The SHB is build up from two half-hulls that are connected by hinges and hydraulic cylinders. Any forces that act at the interface between the half-hulls have to be transferred by the hinges and cylinders as a result. In this research the limits of the hinges and hydraulic cylinders are of concern. The aim of this thesis is to find a calculation method to determine the technical workability limits of split hopper barges in irregular seas. The assumption is made that these limits follow from the design limits of the hinges and hydraulic cylinders. In this thesis first the design/classification regulations are used to get familiar with the barge and its design. Using the obtained knowledge, a simple model is built to determine which load cases are of the most interest. For these load cases a model is built to study the dynamics. Using this model, the resulting maximum forces in the hinges and hydraulic cylinders can be found. By comparing the determined forces to the design forces that were used, a first conclusion on the limits of the barge can be made.

Design regulations for a split hopper barge

In the static design/classification regulations for the SHBs by Bureau Veritas (Bureau Veritas, 2016), a calculation method for the forces in the hinges and cylinder is presented. The reactions in the hinges and hydraulic cylinders are determined based on the equilibria of forces and moments around the hinges. Both equilibria are found using the splitting forces that act in the splitting plane of the split hopper barge, they follow from the summation of the different loads that act on one half-hull.

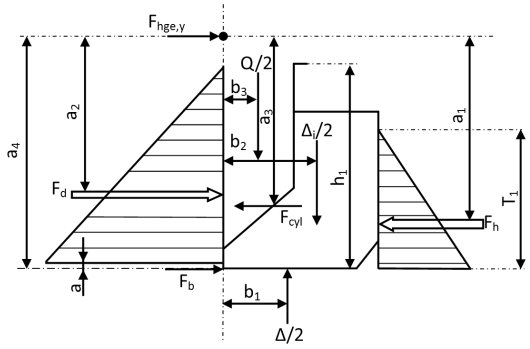

Figure 1: Static calculation method by Bureau Veritas

The opening moment around the hinges of the barge is counteracted by the cylinders. The required force in them, F_{cyl}, follows directly from the moment equilibrium around the hinges. In general the hydraulic cylinders have an overcapacity, the superfluous force in them pre-loads the barge resulting in a force in the bottom chocks. Hence, the bottom chock forces, F_b, can be obtained from the difference between the cylinder capacity and the required cylinder force. Using the cylinder and bottom chock force, a complete horizontal force equilibrium in the hinges can be made, using this it is possible to determine the reactions in the hinges.

Quasi-static model of the split hopper barge

In order to study more interesting load cases, the model from the design regulations is expanded. The result is a quasi-static model of the SHB in Matlab. In this model, again the reactions in the hinges and cylinders are determined based on the splitting forces in the splitting plane. The barge is loaded by forces resulting from hydrostatics, the cargo and its own weight. Using the quasi-static model, the effects of roll, different types of cargo, opening the barge and discharging of the cargo are determined. Using the results, the most governing load cases for the SHB are identified to model their dynamic influences.

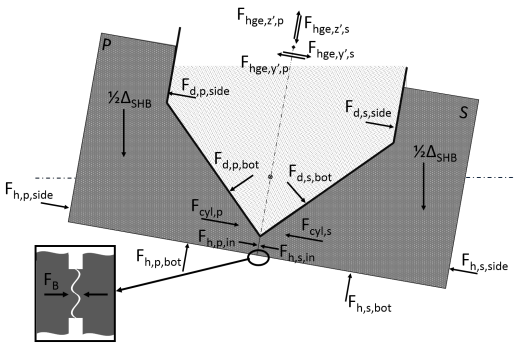

Figure 2: Quasi-static Matlab model

Using the quasi-static Matlab model, first the effect of roll is considered. The barge is modelled carrying a liquid cargo ($\rho_c = 1450 kg/m^3$) under fixed angles of roll varying between 0 and 25 degrees. The static roll is found to result in a decrease of the required cylinder forces, F_{cyl}, which is an effect of the additional closing moment due to the weight of and the hydrostatic force acting on the SHB. Through the bottom chock forces, the hydraulic cylinder force is found to have an important effect on the hinges forces. The decrease of the required cylinder forces results in an increase of the superfluous force that excites the hinges and the bottom chocks. This in combination with a decrease of the cargo forces due to outflow over the coaming, causes the horizontal hinge forces, $F_{hge,y'}$, to increase slightly for an increasing angle of roll. The vertical hinge forces, $F_{hge,z'}$, are found to increase as well. For an increasing angle of roll, the uphill half-hull of the barge starts to rest on the hinges. As a result, the weight of the lifted half-hull has to be supported by the hinges, which causes an increase of the vertical hinge reactions.

Next to the effect of roll, the effects of different types of cargo where considered. The barge was modelled carrying either a solid ($\rho_c = 2200 kg/m^3$), liquid ($\rho_c = 1450 kg/m^3$) or a sliding cargo ($\rho_c = 1600 kg/m^3$). Here, the behaviour of the cargo is determined based on the cargo density. A liquid cargo is expected to have a constant horizontal fluid surface, while a solid cargo does not move relative to the barge. The sliding cargo is expected to move in a restricted way, which is defined by a sliding law.

For all cargoes, the exciting forces that act on the hopper walls are assumed to follow from homogeneous pressure distributions. I.e. a solid cargo is modelled like a liquid cargo only it is restricted in its movements. For the cargo calculations, the barge is again considered under multiple fixed angles of roll, the differences between the resulting forces for the different types of cargo are determined. In the end, the calculations show that either a solid or a liquid cargo results in the highest reactions in the hinges and hydraulic cylinders.

To study the effect of opening the barge, it is modelled with an opening angle varying between 0 and 15 degrees. Again the opened barge is considered for multiple angles of roll, discharge of the cargo is neglected to create a conservative load case. Due to the opening of the barge, the force of the hydraulic cylinders that acts on the barge is no longer found to be equal to the maximum capacity of the cylinders. Only the force that is required to counteract the opening moment now acts on the barge. Since this means that the bottom chocks forces are zero, the horizontal hinge forces decrease. Although the opening of the barge does lead to an increasing trend in the reaction forces. The initial difference due to the loss of the superfluous force in the cylinders makes that the hinge reactions for the closed barge are larger. For the highest required cylinder forces, no difference was found between the opened and closed barge. The conclusion is drawn that the closed barge load case is governing over the opened one.

The final effect that is captured using the quasi-static model, is that of actual cargo discharge. the barge is modelled as a mass, spring, damper system from which the cargo flows out with a fixed speed. Two types of cargo outflow are considered. First a normal outflow were the cargo surface moves down through the hopper. Secondly, an inverse outflow is considered for which the cargo disappears from the bottom up. This outflow mimics the presence of cargo bridges over the opening in the barge due to cohesion and friction. For both types of outflow it is found that the resulting forces in the hinges and hydraulic cylinders decrease to almost zero after all cargo has flown out. Depending on the outflow speed, this decrease occurs rapidly. From the dynamic outflow model it is concluded that discharge of the cargo will not lead to the most governing load case.

In the end, from the quasi-static calculations of the SHB, the conclusion is drawn that the most interesting load cases to be studied further are those for a closed barge either carrying a liquid or a solid cargo.

Modelling the dynamics of a split hopper barge

To account for the dynamics of the SHB in irregular seas, a calculation method based on Ansys AQWA is proposed. Using Ansys AQWA GS, the splitting forces in the splitting plane of the SHB can be determined directly. When the splitting forces are known, the hinge and cylinders reactions follow from a calculation method similar to that used before. To run AQWA simulations, the geometry of the SHB as well as some data on its mass, mass distribution and inertia are required. This input can be determined using excel and CAD software tools.

From the splitting force RAOs that are returned by AQWA the forces that result in the hinges and hydraulic cylinders can be determined using a Matlab script. Using the resulting hinge and cylinder force RAOs in combination with a wave spectrum, the maximum dynamic forces in the hinges and cylinders are obtained. To find the overall forces, the average/static forces in the hinges and cylinders have to be added. These average force contributions are determined using the quasi-static SHB model. By comparing the obtained hinge and cylinder reaction for a certain irregular sea state to the the design limits that follow from the classification regulations, a first indication on the exceedance of the limits of the SHB is found.

Since AQWA is not capable of dealing with a free-surface liquid cargo inside the model, the effects coming from a liquid cargo have to be accounted for in the simulations separately. Based on the coupled equations of motions of the SHB and the liquid cargo, the conclusion was drawn that the liquid cargo effects are be captured well by adding additional added mass and stiffness to the system. The additional stiffness that has to be taken into account is included by reducing the stability lever arms of the barge. The additional added mass matrix, follows from a comparison of the added mass plots of a barge carrying a solid and a frozen cargo in WAMIT. The differences that are found are used to describe a relation that is used for the adjustments to the added mass matrix in AQWA.

From the WAMIT simulations with the TF501 SHB, it is found that the natural frequencies of the liquid cargo are hardly excited for the wave spectra that were considered. As a result, a constant relation between the added mass of the barge with a solid and a liquid cargo is obtained. The effects of the liquid cargo mainly affects the surge, sway, roll and yaw motions of the SHB. For heave and pitch, no significant changes are identified. Using the additional added mass determined using WAMIT in combination with the decrease of the stability lever arms of the SHB, the Ansys model is adjusted to be used for a SHB carrying a liquid cargo as well.

Results and conclusions

The calculation method is used to determine the forces in the hinges and hydraulic cylinders for one type of SHB. Using a model of the TF501 SHB it is found that beam waves yield the highest responses in the hinges and hydraulic cylinders. The limits of the hinges are found to be exceeded faster, which leads to the conclusion that the design limits of the hinges are of most interest when the limits of the SHB are considered. Due to a destabilization of the barge that results from the liquid cargo effects, a wider spectra of wave directions and periods is found to result in significant increases of the reactions in the hinges and hydraulic cylinders. For the cylinders this causes the obtained reaction forces for the barge carrying a liquid cargo to be the highest. The maximum reaction forces in the hinges however, are found for the SHB carrying a solid cargo. Due to a large difference that is found in the static hinge force contributions, the barge carrying a solid cargo yields the highest hinge force reactions. Since the limits of the hinges are exceeded first, the conclusion is drawn that the limits of the split hopper barge in irregular waves are most limited, and therefore governing, for a barge carrying a solid cargo.

Nomenclature

Abbreviations

DAF	Dynamic amplification factor	
RAO	Response amplitude operator	
CoF	Center of flotation	
CoG	Center of gravity	
p	Subscript used for variables on the port-side of the vessel	
s	Subscript used for variables of the starboard-side of the vessel	
SHB	Split hopper barge	

Constants

ρ_s	Density of seawater	1025 $\frac{kg}{m^3}$
g	Gravitational acceleration	9.81 $\frac{m}{s^2}$

Greek symbols

α_w	Wave direction	rad
δ	Angle of external friction	deg
ω	Wave frequency	rad/s
ρ_c	Density of the cargo inside the hopper	$\frac{kg}{m^3}$
σ	Normal stress	$\frac{N}{m^2}$
τ	Shear stress	$\frac{N}{m^2}$
θ_c	Angle made by the cargo relative to the barge	deg
θ_r	Angle of roll made by the barge	deg
θ_u	Upper angle in the cargo hopper	deg
$\triangle_{SHB}$	Weight of the barge	N
φ	Angle of internal friction	deg
ϑ	Wave phase angle	rad

Variables

$\overline{GG'}_x/\overline{GG'}_y$	Reduction in metacentric heights	m
B_{SHB}	Breadth of the split-hopper barge	m
c	Cohesion of soil	$\frac{N}{m^2}$
C_h	Cargo height in the hopper	m

D_{storm}	Storm duration	s
F_W	Force due to the weight of the barge	N
F_B	Force in the bottom chock	N
F_{cur}	Current force acting on the SHB	N
$F_{cyl,pre}$	Pre-tension in the hydraulic cylinder	N
$F_{cyl,req}$	Required hydraulic cylinder force	N
F_d	Force due to cargo pressure	N
F_{hge}	Resulting force in the hinge	N
F_h	Hydrostatic force	N
F_{wind}	Wind force acting on the SHB	N
$Fx/Fy/Fz$	Splitting forces in the splitting plane	N
GM_x/GM_y	Metacentric heights	m
H_s	Significant wave height	m
H_v	Height of the V-shaped part of the hopper	m
H_{bot}	Height of the bottom of the barge	m
h_{cyl}	Distance between the cylinders and the hinges	m
h_{hge}	Distance of the hinge above the baseline	m
H_{max}	Maximum loading height of the hopper	m
H_{SHB}	Height of the barge's free-board	m
I_t	Second moment of area at the water plane of the barge	m^4
$k_{xx}/k_{yy}/k_{zz}$	Radii of gyration	m
L_{hop}	Length of the cargo hopper	m
L_{SHB}	Length of the split-hopper barge	m
m_n	Spectral moment	[−]
M_{op}	Opening moment around the hinges	Nm
M_{res}	Restoring moment acting on the barge	Nm
n_B	Number of bottom chocks	-
n_{cyl}	Number of hydraulic cylinders	-
n_{hge}	Number of hinges	-
$Rx/Ry/Rz$	Splitting moments in the splitting plane	Nm
T_0	Initial mean draft of the barge in a upright position	m
T_z	Mean zero crossing period	s
TF_f	Force RAO	[−]
u_{cur}	Current speed	$knots$
u_{wind}	Wind speed	$\frac{m}{s}$

List of Figures

List of Tables

Contents

1

Introduction to the project

Figure 1.1: Cork Sand split hopper barge (Boskalis, 2014)

Split hopper barges are ships that are commonly used in dredging. They are used to transport dredged materials from a dredging site to an offshore discharge location. The barges can either be pushed, pulled or self-propelled and come in a variety of sizes and capacities. A typical split-hopper barge is only used for transportation of dredged cargo, the dredging itself is done using other types of dredging equipment. Therefore, split hopper barges will always work together with other types of dredging vessels in a project. Since the split-hopper barges are open hopper vessels, they can be versatilely used for all types of cargoes ranging from rocks to fine particles.

The basic design of the split-hopper barge has only seen minor changes over its existence, the vessel consist of two half-hulls connected by hinges and hydraulic cylinders. Using the hydraulic cylinders the two halves can be pushed open, splitting the vessel over its entire length. This allows the cargo inside the hopper to free-fall in to the sea without additional mechanical interference. In general two hinges and two hydraulic cylinders are installed on a split hopper barge one fore and one aft of the open hopper. Due to the increasing hydraulic cylinder capacity that is needed to actuate a bigger barge and due to the increase in required steel for the double hull, conventional split-hopper barge capacities in general are limited to a maximum of roughly 7000t (DWT). In an effort to increase the capacity of the barge, the conventional design has been altered in some cases.

1.1. Background

The moment the split hopper barge starts to open, only the hinges and hydraulic cylinders keep the two half-hulls together. Since the discharge of the cargo usually takes place in non-sheltered waters, the opened barge will be excited by wind and waves resulting in movement . Instinctively this causes the split hopper barge to be quite vulnerable in this situation. The technical limits of the barge for these particular situation need to be sufficient and great care is taken in judging whether or not the weather conditions allow for the split hopper barge operations.

For verification and classification of the design of the split hopper barge, static design regulations are stated. these regulations verify the design loads acting on the hinges and hydraulic cylinders for both an open and closed condition of the barge. Apart from these static guidelines, only a limited amount of information is given about the dynamics that have to be included. These dynamic contributions to the hinge and cylinders forces follow from dynamic amplification factors for which the origin is not always defined clearly.

Since the design forces cannot always be traced back properly, speculation about the true technical limits of the split hopper barges continues to exist, resulting in discussions about their workability limits . The technical workability limits result from the environmental loads acting on the barge. In practice this limit is determined based on experience, weather predictions and the given information in the stability booklet belonging to the barge. This method thus is commonly based on the judgement of one or several persons instead of on the knowledge of technical limitations of the barge.

Since a split hopper barge is usually employed in dredging projects that take place in sheltered waters, and the split hopper barge is the only vessel that has to leave these sheltered waters to discharge. The workability limit of the split hopper barge is often the limiting one for the entire project. In practice this holds that when the operations of the split hopper barge are stopped, the entire dredging process comes to a hold. This means that by making a wrong judgement about the workability of the relatively cheap split hopper barge expensive and preventable delays in the complete project can be the result.

Following from the above, to be able to describe the technical limits of the split hopper barge in greater detail, to reassure the crews about the safety of their vessel and to give the project managers a helping hand in defining the limits of their split hopper barges, this research is intended to find a method to define the limiting sea states for the split hopper barge. An ultimate goal would be to be able to describe a single limit parameter that can be measured on board the actual barge itself, giving the crew the possibility to determine the safety of their operations in real time allowing them to stretch their operational time to an absolute safe maximum.

1.2. Aim of the study

The aim of this study is to develop a method that can be used to determine the technical workability limits of a split hopper barge in irregular seas.

In the study, the maximum loads acting on the hinges and hydraulic cylinders of the split hopper barge have to be determined. These maximum loads are compared to their design limits. The interaction of the barge with the sea is included. In the intended workability study knowledge has to be obtained for at least the following conditions:

- Both open and closed conditions of the barge
- Multiple cargo conditions of the barge
- Discharge of the cargo

During this thesis the work-ability of at least one split hopper barge is determined. Yet, the goal is to develop a method that can be used for more types/sizes of split hopper barges.

1.3. Project approach

The aim of this thesis is not only to describe the reactions that act on the internal structural parts of the split hopper barge, but also to create knowledge on the influence that multiple types of cargo, configuration and orientation have on these forces. To reach the thesis goals, the following approach is used:

- First the design regulations of split hopper barges are briefly regarded to create a better understanding of the barge design and its design loads.
- The influences of multiple types of loading, configuration and orientation on the internal forces acting inside the barge are determined
- A full dynamic model is made, to obtain the limiting forces in the hinges and hydraulic cylinders of the split hopper barge.
- The proposed dynamic model will be used to determine the maximum forces in the hinges and hydraulic cylinders of one type of SHB in irregular seas.
- Finally, conclusions and recommendations can be made to finalize the research project.

1.4. Axes convention

In this report, multiple models of the split hopper barge will be made and multiple calculations on it are performed. To relate the different parts of the report with each other, the same axes convention will be used for the barge. The axes convention as it is used in this research is given in figure 1.2.

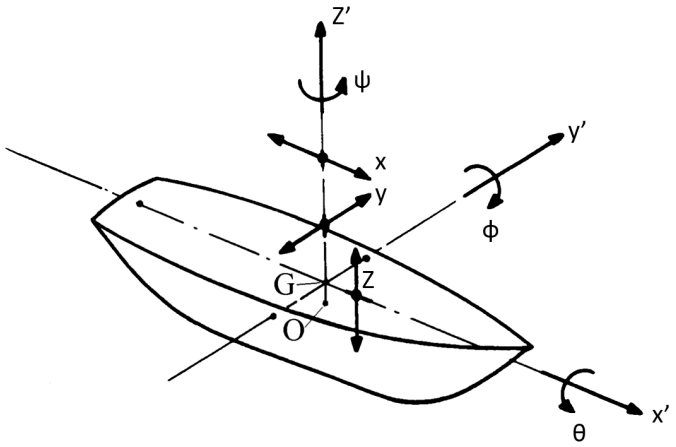

Figure 1.2: Axes convention (Journee & Massie, 2001)

Both global and local directions will be used throughout the different chapters. The global system indicates the directions in an earthbound direction, the coordinates are indicated using [X,Y,Z]. The local coordinated system is ship-bound and is indicated by [x',y',z']. The zero degree wave direction modelled to be along the positive X-axes (from stern to bow), the angle increases counter clock-wise.

2

Design regulations for a split hopper barge

Since this research is not, directly, meant to gain knowledge for a new design of split hopper barges, there is no need to define their design requirements al over again. Instead, to get familiar with the design and limits of the SHB, the already existing design regulations can be used. Do note that the study to the design regulations in this chapter is not only meant to get familiar with the topic, the obtained knowledge can be used for the modelling of the SHB in the next stages of the research as well.

This chapter describes the current design regulations for split hopper barges based on the Bureau Veritas regulations (Bureau Veritas, 2016). Note that, besides Bureau Veritas there do exist more regulating authorities. Each with its own design regulations, the basic idea in these regulations though will remain the same. The design regulations that are presented in this chapter are not intended to supply naval architects with a design for the split hopper barge, but rather are intended to verify/show that a designed and new to build vessel complies to the safety standards. The regulations describe design strengths for multiple components of the SHB. In this chapter only the regulations related to the design forces in the hinges and hydraulic cylinders are considered.

2.1. Static loads

Figure 2.1 displays the static reactions that act on one half-hull of the split hopper barge, as they are defined by the rules of Bureau Veritas (Bureau Veritas, 2016).

In the figure, F_{cyl} shows the position and orientation of the hydraulic cylinders of the barge. $F_{hge,y}$ shows the force that results in the hinge as a result from the static loads that act on the barge. Note that there exists no vertical hinge force, the barge is in perfect equilibrium. As a result, the weight of the barge and its cargo is equal to the buoyancy force that acts on the barge due to its displaced volume. From the equilibrium of forces in the vertical direction it is found that no force will result in the hinges for this direction.

Since the barge is symmetric, the forces that act on the two different half-hulls will be exactly equal for this upright position. Do note, that some of the forces for the different half-hulls do have an opposite sign.

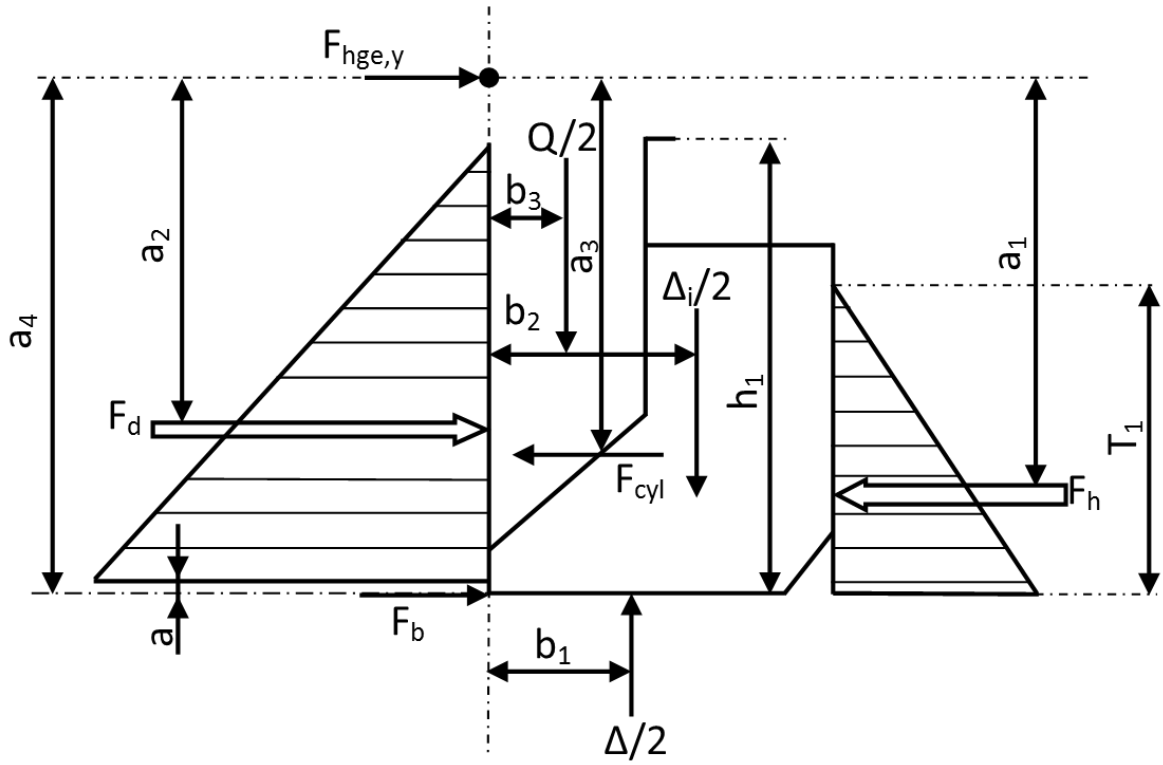

Figure 2.1: Forces acting on the half hull. (Bureau Veritas, 2016)

In the figure, F_h is the resulting force caused by the hydro-static pressure distribution on the side wall of the half-hull and follows directly from the draught of the barge. F_d is the horizontal force that results from the horizontal pressure of the cargo in the hopper. The cargo is prevented from flowing through the small gap that exists in between the two half-hulls by a bottom seal, this seal is positioned in between the bottom of the barge and the bottom of the hopper which is indicated in the figure by distance a. Q and $\triangle_i$ are the weight of the cargo and the barge respectively. Each half-hull is loaded by half the weight of the cargo and the barge. $\frac{\triangle}{2}$ is half the buoyancy force that results from the total displaced volume of the loaded barge.

The resulting opening moment, M_{op}, around the hinges are found using:

$$M_{op} = -F_h \cdot a_1 + F_d \cdot a_2 + \frac{1}{2}(\triangle \cdot b_1 - \triangle_{1l} \cdot b_2 - Q \cdot b_3) \tag{2.1}$$

Since this moment can only be counteracted by the hydraulic cylinders, the static horizontal force required in the cylinder to keep the barge closed follows directly from M_{op} and is given by:

$$F_{cyl,req} = \frac{M_{op}}{n_{cyl} a_3} \tag{2.2}$$

Here, n_{cyl} is the number of hydraulic cylinders that is installed on the barge. The cylinder force that excites the barge is not necessarily equal to this required hydraulic cylinder force. Instead, when the cylinder capacity is sufficient, the hydraulic cylinders can be used to pre-load the barge. In this case the barge is loaded with the full cylinder capacity, $F_{cyl,pre}$. Due to the presence of this pre-tension, the two half-hulls of the barge are pulled together strongly having a force in the bottom chocks as a result. This resulting bottom chock force is found by:

$$F_B = \frac{n_{cyl} \cdot a_3 \cdot F_{cyl,pre} - M_{op}}{n_B \cdot a_4} \tag{2.3}$$

Here, n_B is the number of bottom chocks that are installed. Note that when the cylinder forces are exactly equal to the force required to counteract the opening moment around the hinges, the force in the bottom chocks is equal to zero. In this case the barge is not really closed, but only held in a constant 'opened' position by the hydraulic cylinder.

Using the forces of the bottom chocks and the hydraulic cylinder, an equilibrium of the horizontal forces leads to the horizontal forces required in the hinges of the barge:

$$\begin{aligned} F_{hge,y,stat} &= 0.5[F_h - F_d + n_{cyl}\left(F_{cyl,stat} - F_B\right)] \\ &= 0.5[F_h - F_d + n_{cyl}\left(1 - \frac{a_3}{a_4}\right) F_{cyl,stat} + \frac{M_{op}}{a_4}] \end{aligned} \tag{2.4}$$

The vertical hinge forces follow from the equilibrium of forces in the vertical direction.

$$F_{hge,z,stat} = \frac{1}{2}\left(\triangle_i + Q - \triangle\right) \tag{2.5}$$

As was already mentioned in the introduction to this section, in the static upright equilibrium in which the barge is considered, this force will be equal to zero.

2.2. Dynamic loads

Currently Bureau Veritas does not supply comprehensive mathematical formulations for the calculations of the dynamic forces acting on the hinges, cylinders and chocks. The calculation of these forces is left to the designer of the barge. The calculations have to be submitted to the regulating authorities for a review. This review is done using computer software developed by Bureau Veritas itself. In a paper by Bureau Veritas (Latreille, 1982) a small description of the proposed method is given to determine the strength of the barges.

The calculation software that was developed is based on strip theory that solves the motions of the barge in a two dimensional way. Since a two-dimensional approach is used, the surge motion is not determined in the software. After the motions of the barge are solved, the hinge and hydraulic cylinder forces can be determined. This calculation of the dynamic forces in the hinges and hydraulic cylinders of the split hopper barge is done using the equilibria of forces and moments that exist around the hinges of the barge. The exciting forces that are used are expressed as the splitting forces that act in the mid-plane of the barge. For the equilibria of forces, only one half-hull of the barge is considered.

From the force and moment equilibria around the hinge four unknown forces are found, knowing, the fore and aft hinge- and cylinder forces. To determine these unknown reactions only three equations are available, one moment equilibrium around the hinges and two force equilibria in the hinges. Since in this system of equations there are too many unknowns, it cannot be solved. Therefore, Bureau Veritas assumes that the cylinder forces of the fore and aft of the barge are equal.

In line with the rules given by Bureau Veritas the dynamic forces should be calculated using a long term statistical approach taking into account the conditions defined in table 2.1.

Table 2.1: Probability for the determination of dynamic forces.

Condition	Probability
Dredging and Navigation with spoil [H_s<3m]	$p_f = 10^-5$
Navigation without spoil	$p_{f,Jack} = 10^-7$ $p_{f,Hinge} = 10^-5$

For each loading case used, the dynamic forces $F_{cyl,dyn}$,$F_{hge,y,dyn}$ and $F_{hge,z,dyn}$ should be obtained. These dynamic contributions to the load on the hinges, cylinders and chocks have to be added to their static counterparts creating a total force that has to be used for the strength calculations of the different components. The resulting forces become:

$$F_{cyl} = F_{cyl,stat} + F_{cyl,dyn} \tag{2.6}$$

$$F_{hge} = \sqrt{\left(F_{hge,y,stat} + F_{hge,y,dyn}\right)^2 + \left(F_{hge,z,stat} + F_{hge,z,dyn}\right)^2} \tag{2.7}$$

2.3. Strength calculations

2.3.1. Hinge Design

In the design regulations of Bureau Veritas two types of hinges used for the split hopper barge are considered. In figure 2.2 on the left a hinge design with a bearing is shown. The drawing on the right shows a hinge without a bearing. For both types of hinges, the exciting loads that act on them have to be compared to their design limits. For this validation of the hinge strengths, Bureau Veritas supplies a calculation method again. In table 2.3 the relations that have to be used for the validation of the hinge strengths of the split hopper barge are presented. For both types of hinges the pins, center eyes and side straps are considered separately.

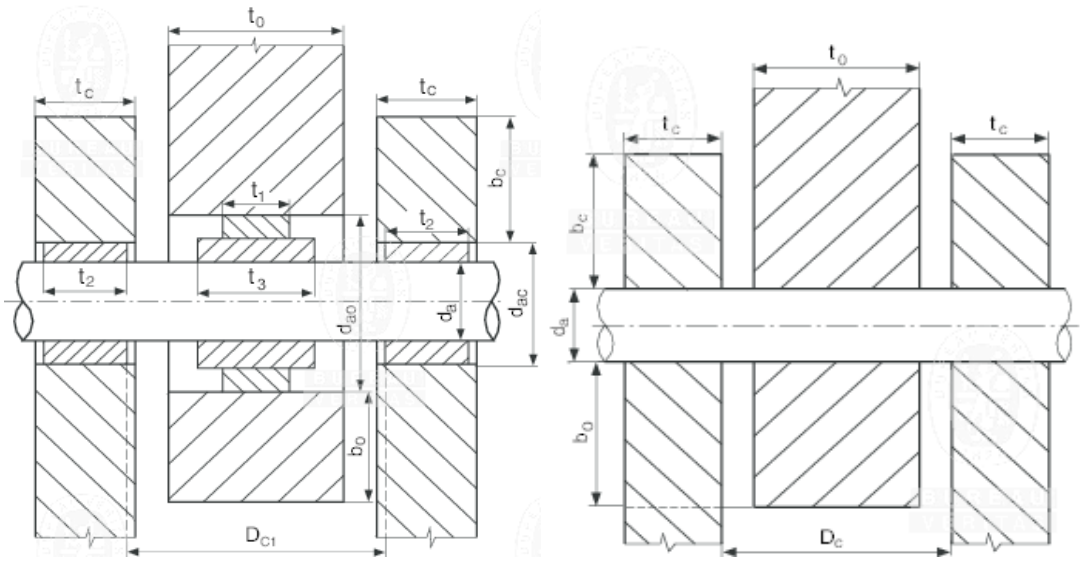

Figure 2.2: Schematic drawing of the hinges. (Bureau Veritas, 2016)

Case	Elements to be checked		
	Pins	Centre eye	Side straps
Direct bearing	$F < \frac{d_a^2 R_m}{5{,}76} 10^{-3}$ $F < \frac{2}{3} d_a t_0 R_{eH} 10^{-3}$ • if $t_0 < d_a$: $F < \frac{d_a^3}{2D_C - t_0} \frac{R_m}{5} 10^{-3}$ • if $t_0 \geq d_a$: $F < \frac{d_a^3}{2D_C - 2t_0 + d_a} \frac{R_m}{5} 10^{-3}$	$F < \frac{b_0 t_0 R_{eH}}{2{,}27} 10^{-3}$ $F < d_a t_0 R_{rad} 10^{-3}$	$F < \frac{b_C t_C R_{eH}}{1{,}14} 10^{-3}$ $F < 2 d_a t_C R_{rad} 10^{-3}$
Load transfer by bearings	$F < \frac{d_a^2 R_m}{5{,}76} 10^{-3}$ $F < \frac{2}{3} d_a t_3 R_{eH} 10^{-3}$ • if $t_3 < d_a$: $F < \frac{d_a^3}{2D_{C1} - t_3} \frac{R_m}{5} 10^{-3}$ • if $t_3 \geq d_a$: $F < \frac{d_a^3}{2D_{C1} - 2t_3 + d_a} \frac{R_m}{5} 10^{-3}$	$F < \frac{b_0 t_0 R_{eH}}{2{,}27} 10^{-3}$ $F < \frac{2}{3} d_{a0} t_1 R_{eH} 10^{-3}$	$F < \frac{b_C t_C R_{eH}}{1{,}14} 10^{-3}$ $F < \frac{4}{3} d_{aC} t_2 R_{eH} 10^{-3}$
Note 1: R_{rad} : Admissible radial pressure on the bearing, to be taken equal to 100 N/mm^2.			

Figure 2.3: Scantelings for jack hinges. (Bureau Veritas, 2016)

For all components of the hinges multiple validation relations are stated. For all these relations the limits of the hinges have to be safe of course.

2.3.2. Cylinder design

To verify the design of the hydraulic cylinders, the calculated forces from sections 2.1 and 2.2 that act on the hydraulic cylinders for the mentioned load cases have to be compared to their design limit. This limit force in the cylinders is defined by :

$$F_{cyl} = \frac{P_{system}}{A_{piston}} - \frac{P_{system}}{A_{rod}} \tag{2.8}$$

In the relation, P_{system} is the pressure inside the hydraulic cylinder that actuates the piston. A_{piston} and A_{rod} are the areas of the piston and the rod respectively. A drawing of a typical hydraulic cylinder design for the split hopper barge is shown in figure 2.4.

The cylinder forces are determined and verified for both a pull and push operation. In the situation that the hydraulic cylinder pulls on the half-hulls, it is used to close the barge. When the cylinder pushes, it causes a opening moment around the hinges. In general the force needed in the pull situation exceeds the force needed in the push situation. Due to the cargo pressures that act on the hopper wall, split hopper barges have a tendency to have a resulting opening moment around the hinges rather than a closing moment. As a result, the force needed by the hydraulic cylinder to open the barge is smaller than the force that is needed to pull the half-hulls together.

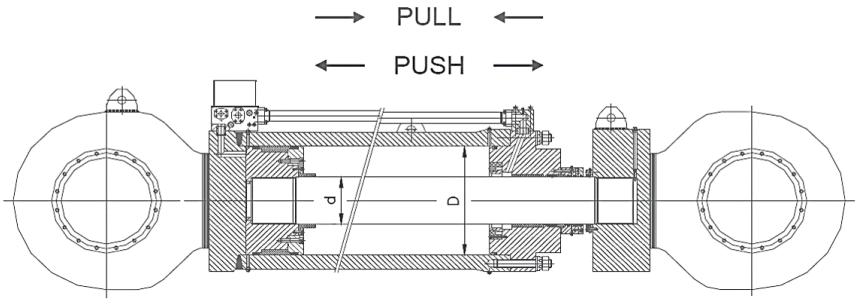

Figure 2.4: Scantelings for jack hinges. (Bureau Veritas, 2016)

3

Quasi-static calculations

A Split-hopper barge is a relatively small and simple vessel compared to other types of dredging equipment. The behaviour of the SHB in a dynamic environment however, is a complicated process in which many different motions, configurations and loads play a part. To be able to describe and understand the influence of all these separate aspects, a thorough study should be conducted. To achieve this, a straight forward implementation of the barge and all of it particulars in simulation software is not preferred. Instead it seems more appropriate to investigate the aspects and processes of interest separately first before they are combined in one dynamic model. This does not only allow for a better understanding of behaviour of the SHB on one side, it also allows for a detailed selection of processes that have to be included in a full dynamic simulation.

In this chapter the following motions, configurations and loads will be considered:

- The effect of roll.
- The effect the cargo density.
- The effect of opening the barge.
- The effect of discharge.
- The influence of environmental forces (wind & current).

To obtain the influence of these points of interest, a quasi-static model is built in Matlab. This model will be further described in the next section, after which the result obtained using it are discussed.

3.1. The quasi-static approach for the split-hopper barge

For the calculation of the static forces in the SHB, the barge was modelled in Matlab. This first section of the chapter focusses on the model that was made. The most important relations for the calculations are described and their origin will be explained. In appendix A the data from the Matlab model is compared to data from a stability booklet of an actual barge to validate the Matlab model. Differences up to 0.1% were found, which shows that the model is accurate.

3.1.1. The geometry of the barge

In the Matlab model that was made, the goal is to describe the effect of the selected scenarios on the SHB using straight forward and simple equations. To do so, the complex shape of the real barge has to be approximated using a more elementary shape. The barge hull in the model is represented by a beam of length L_{SHB}, width B_{SHB} and height H_{SHB}. The weight of the barge $\triangle_{SHB}$ then causes a initial displaced volume with a mean draft T_0 as a result.

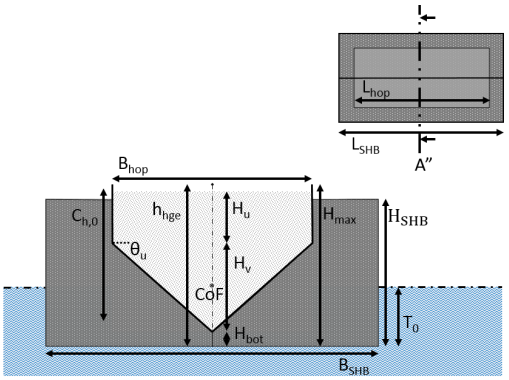

Figure 3.1: Quasi-Static model of the split-hopper barge.

The hopper itself is modelled as a fully symmetric shape. It is positioned in the exact middle of the model hull, both longitudinal as transverse. The hopper shape is built up from two parts, a triangular bottom part with a height of H_v and a inclined wall angle of θ_u. On top there is a square section with a height of H_u and a total width of B_{hop}. The total loading height of the barge H_{max} is equal to the combined height of the hopper together with the height of the barge bottom H_{bot}, this height exceeds the total height of the barge itself. The two half-hulls of the barge are supposed to close fully so that there is no gap between the two parts of the hopper in a closed configuration.

Just as with the real barge, the two half-hulls are held together by a hinge arrangement, that is placed at a height h_{hge} above the barge bottom. The hydraulic cylinders of the barge are placed at a distance h_{cyl} below the hinge. The bottom chocks are located at the bottom of the barge at a height h_{hge} below the hinges.

Figure 3.1 shows the general set-up of the model that is used for the quasi-static calculations in Matlab. The graph displays the barge model including the described particulars in both a frontal and top view.

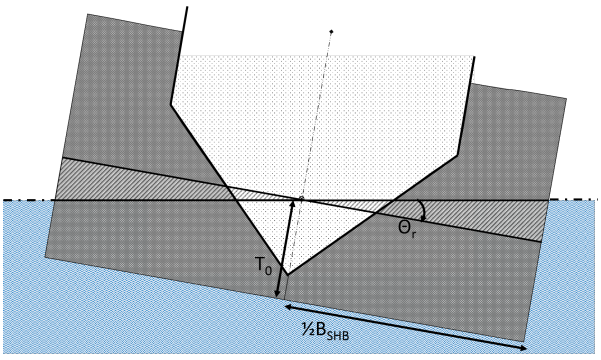

Figure 3.2: The split-hopper barge model experiencing roll.

In figure 3.1 the Center of Flotation, CoF, of the barge is shown. According to the Offshore Hydro Mechanics book by Journee (Journee & Massie, 2001), this point around which the vessel rotates is located in the exact middle of the vessels initial, upright, water plane. This holds for all vessels with a symmetric underwater geometry. Since the closed barge is a beam, it satisfies the condition of symmetry and thus the mentioned theory holds ($Y_{CoF} = \frac{1}{2}B_{SHB}$). Since the barge rotates around the point of flotation, its rotational motion causes an equal change in displacement for both half-hulls. As a result, the emerged and immersed wedges due to the rotational motion of the barge are equal. The barge under a heel angle, including the emerged and immersed wedges is shown in figure 3.2. Here, θ_r is the angle made by the barge.

3.1.2. Forces acting on the split-hopper barge

As the barge geometry is defined, the forces that load it have to be determined. The static loads that act on the SHB can be subdivided into three different types. First there are the forces that are caused by the own weight and geometry of the barge. Secondly the presence of cargo causes forces that act on the hopper walls. Lastly the outer walls of the barge are loaded by the seawater pressures.

Figure 3.3 shows a graph of all forces that act on the barge for a roll motion as well as the resulting forces in the hinges and the hydraulic cylinders which are of interest for the research.

The figure shows that due to the rolling motion of the barge the forces that act on it are no longer orientated in the global coordinate system. Instead, a local (ship fixed) coordinate system is chosen to describe the loads.

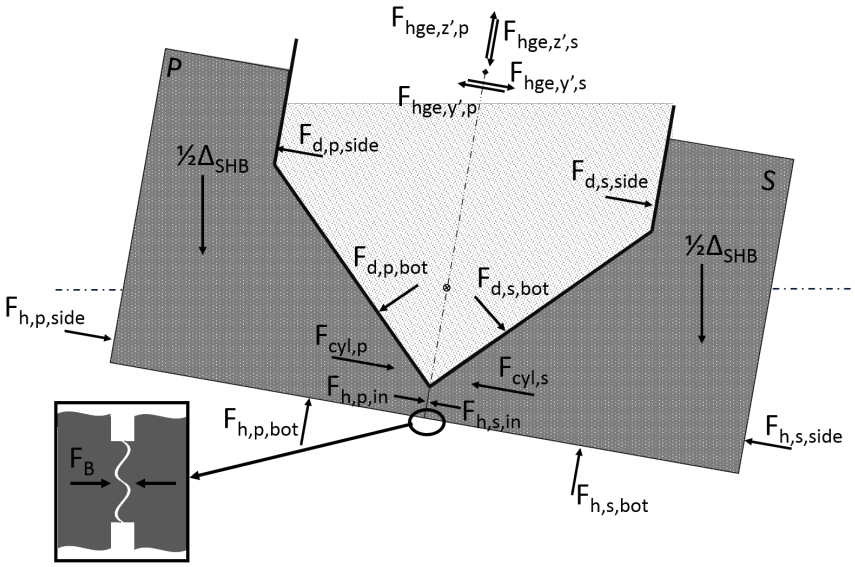

Figure 3.3: The exciting forces in the ship-bound coordinate system.

Cargo loads

For all types of cargo in the SHB it is assumed that they excite the hopper like a fluid. This means that regardless of the cargo density and the cargo behaviour, the resulting cargo forces that excite the barge follow from the pressure distributions over the hopper walls. These cargo pressures together with the forces that result from them are illustrated in figure 3.4. Note that in the figure, cargo forces parallel to the hopper walls are included as well. In general such forces follow from friction that occurs between the cargo and the hopper walls for certain cargo types. The effects of cargo friction on the SHB are discussed in more detail in appendix B.

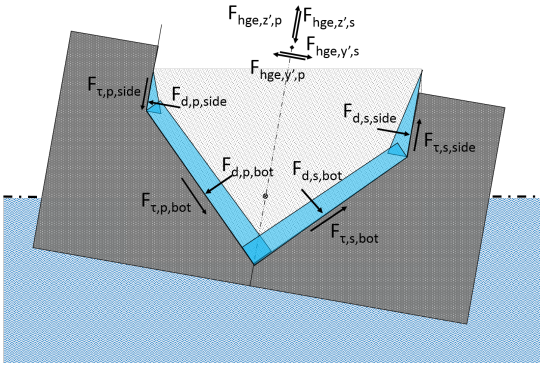

Figure 3.4: Forces, pressures and friction acting on the hopper walls.

Due to the roll of the barge, the cargo moves. The extent in which the cargo will be able to follow the motions of the barge depends on the cargo density. A fully liquid cargo is expected to follow the motions of the barge exactly. A solid cargo is defined to not move at all. In between these two extremes the cargo is of a sliding kind. The way this sliding cargo moves is assumed to depend linearly on the cargo density. The linear relations used to describe the motions of the cargo is taken from the Bureau Veritas regulations (Bureau Veritas, 2016). These relations divide the possible cargo in the hopper into three regimes depending on the cargo density, ρ_c. For each regime separate relations are given between the cargo angle and the angle of the motion of the barge:

- Liquid cargo for $\rho_c \leq 1400$ $[\frac{kg}{m^3}]$

  $\theta_c = \theta_r$

- Sliding cargo for $1400 < \rho_c < 2000$ $[\frac{kg}{m^3}]$

  $\theta_c = \frac{2000-\rho_c}{600}\theta_r$

- Solid cargo for $\rho_c \geq 2000$ $[\frac{kg}{m^3}]$

  $\theta_c = 0$

In these relations θ_c is the cargo angle with respect to the barge. θ_r is again the roll angle of the barge. Depending on the motions of the cargo, the amount of cargo that flows over the coaming and the orientation of the cargo in the hopper differs per cargo type. The result is that the cargo forces that act on the hopper change per type of cargo.

Due to the motions of the barge and the resulting motions of the cargo, the cargo pressures on the hopper walls have to be determined for inclined orientations. To do so, a relation has to be found for fluid pressures on an inclined wall.

Figure 3.5 shows a fluid pressure on an inclined wall. The resulting force acting on this wall can be found by integrating the cargo pressure over the wall area, which gives the following relation for the resulting normal force:

$$F_{res} = \int_y \int_x \cdot \rho_c \cdot g \cdot h \, dx \, dy \tag{3.1}$$

Were h is the height of the fluid column above the point of interest. Thus for a point on the wall inclined with an angle θ at a distance y of the water surface:

$$F_{res} = \rho_c \cdot g \cdot \sin\theta \int_y \int_x y \, dx \, dy \tag{3.2}$$

This eventually results in:

$$F_{res} = \rho_c \cdot g \cdot y_{cg} \cdot \sin\theta \cdot A = \rho_c \cdot g \cdot h_{cg} \cdot A \tag{3.3}$$

In which y_{cg} is the coordinate of the centroid of the wall along its length, and h_{cg} is the height of the water column above the centroid of the wall.

Thus, the resulting force on the inclined wall is the hydrostatic pressure at the centroid of the wall multiplied with the surface area. Note that the resulting force that was determined does not necessarily work at the location of the centroid. The point of engagement in which it does work has to be derived separately from the relation given above.

The obtained relation assumes that the fluid surrounding the wall always develops a perfect horizontal surface. The cargo in the hopper however, does not always behave like a perfect fluid and can therefore not always be described using a horizontal surface. In fact, according to the sliding law that was introduced in section 3.1.1, the developed cargo angle can differ from the developed angle of roll depending on the cargoes density. As a result the cargo surface will not be horizontal, which makes the found relations for the resulting wall forces less valid.

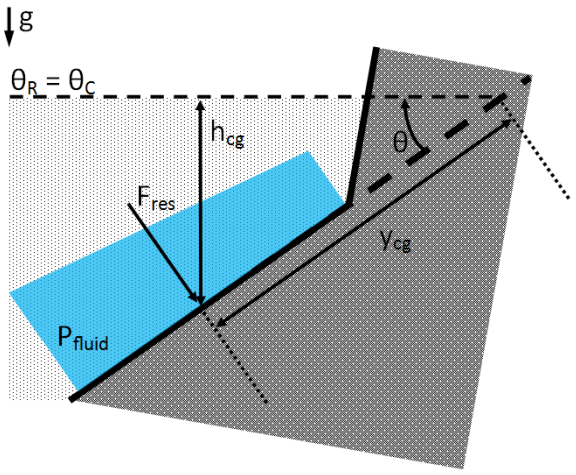

Figure 3.5: Resulting pressure force on an inclined wall.

In the situation were the cargo angle is assumed to differ from the roll angle of the barge, the cargo surface can no longer be regarded as being horizontal. For the situations where this occurs, the gravitational acceleration that works on the cargo surface can be split up into two separate parts. Figure 3.6 shows the considered situation were the cargo surface is no longer horizontal.

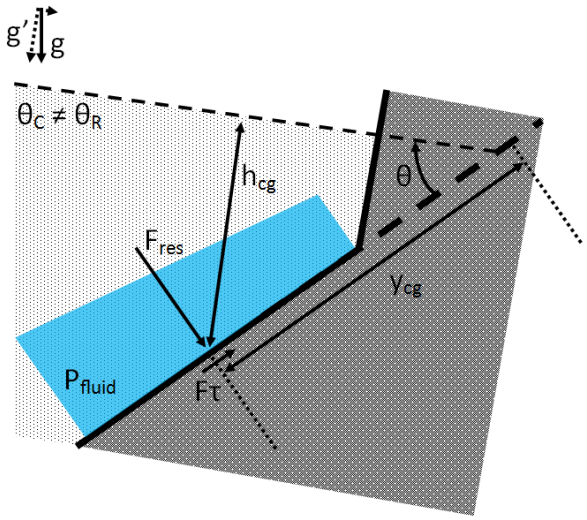

Figure 3.6: Resulting pressure force on an inclined wall for a non-horizontal fluid surface.

The figure shows that the part of the gravitational acceleration that works perpendicular to the inclined cargo surface for this situation can then be found using the relation:

$$g' = g \cdot \cos(\theta_r - \theta_c) \tag{3.4}$$

This relation can be used as a substitute of the gravitational acceleration in the previously shown relations. By doing so, the resulting cargo force on the inclined wall for a cargo with a non-horizontal surface becomes:

$$\begin{aligned} F_{res} &= \rho_c \cdot g' \cdot y_{cg} \cdot \sin\theta \cdot A \\ &= \rho_c \cdot g \cdot h_{cg} \cdot A \cdot \cos(\theta_r - \theta_c) \end{aligned} \tag{3.5}$$

However, since the gravitational acceleration was split into two parts, the effect due to the part of the gravitation that works transversal to the inclined cargo surface has to be taken into consideration as well. This component causes a force along the hopper wall surface which is given by:

$$F_\tau = F_{res} \cdot \tan(\theta_r - \theta_c) \tag{3.6}$$

Note that this force resembles a shear force that would act on the hopper wall. It is however a additional cargo force due to the angle of inclination of the cargo surface. Including this force in the cargo calculations allows the model to use the same calculation method for all types of cargo, independent of the angle of inclination of the cargo surface.

The resulting cargo forces both in the y' and z' direction are than found by summing up the cargo force contributions in both these directions.

Weight of the barge

Next, the weight of the SHB is included. This weight is a constant ,$\triangle_{SHB}$, which is evenly distributed over the two half-hulls. Hence, each half-hull is loaded with half the barge weight, $\frac{1}{2}\triangle_{SHB}$.

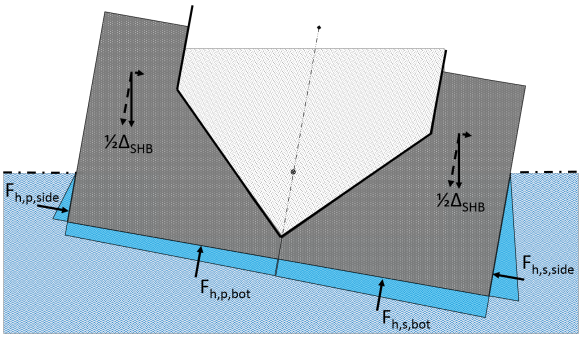

Figure 3.7: Gravitational- and hydrostatic forces.

During the rolling motion of the barge the direction of the gravitational force stays constant. Therefore, in the ship fixed coordinate system, the gravitational contribution has to be broken up into two different parts. Figure 3.7 shows the gravitational force that excites the barge, together with the components in which the barges gravitational weight can be subdivided. The force components that result from the barge weight are equal to:

$$F_{W,z'} = \frac{1}{2}\triangle_{SHB}\cos\theta_r \tag{3.7}$$

$$F_{W,y'} = \frac{1}{2}\triangle_{SHB}\sin\theta_r \tag{3.8}$$

Hydrostatic forces

The last type of load that excites the barge in the Matlab model comes from the water pressures on the outer walls of the barge. The resulting forces can be found by integrating the pressures due to the water over the submerged wall heights. Figure 3.7 shows the pressures and resulting hydro-static forces that act on the rolling barge.

Although it was assumed that no cargo flows through the gap in-between the two half-hulls, in the gap there is water the excites the barge with a hydrostatic pressure, $F_{h,in}$. For the length of the hopper, the height of this gap is limited to the height were the bottom seal of the barge is located. In this model it is assumed that the bottom seal is mounted at the bottom of the hopper. In front and aft of the hopper there is no seal. The water in between the two half-hulls is not limited and raises up to the waterline as a result. Figure 3.8 shows the two different resulting hydro static forces in between the two half-hulls.

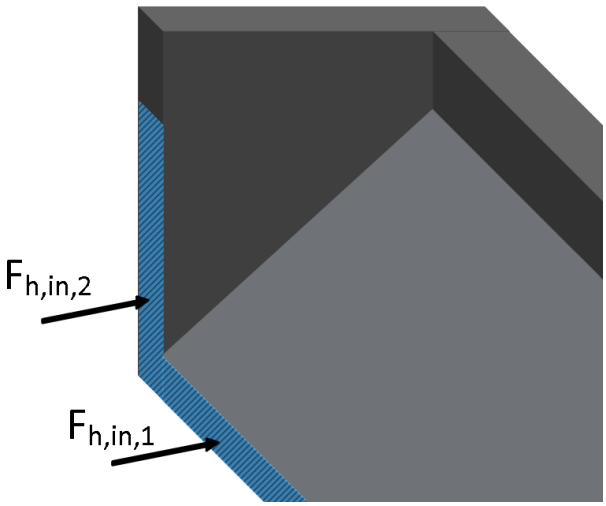

Figure 3.8: Hydrostatic forces in beween the half-hulls

To determine the contribution of the hydrostatic forces to the force equilibrium over both the half-hulls, evidently the force contributions in the y' and z' direction of the barge are found by adding up the hydrostatic forces in the two directions:

$$F_{h,y'} = \sum_{y'} F_h \tag{3.9}$$

$$F_{h,z'} = \sum_{z'} F_h \tag{3.10}$$

3.1.3. Quasi-static equilibrium

When the split hopper barge starts rolling, this rolling motion is counteracted by a restoring moment that results from the buoyancy of the barge. Due to the change in underwater geometry of the barge, the point of engagement where the resulting buoyancy force acts is no longer in the exact middle of the barge. As a direct result, a restoring moment occurs that tries to upright the barge into its equilibrium position. Therefore, barge as it is shown in figure 3.3 is not in a natural equilibrium. Instead it is kept under the fixed angle of roll by an external moment that resists the described restoring moment. In order to find the required equilibrium of forces around the hinges of the barge, this additional moment has to be included as well.

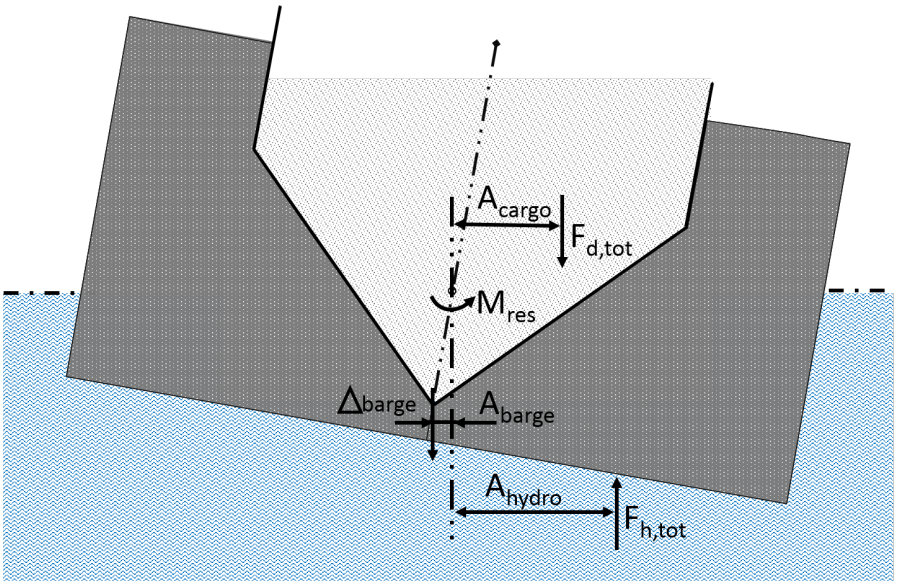

Figure 3.9: Restoring moment acting on the SHB.

The restoring moment that acts on the barge, M_{res}, can be expressed using three contributions. First there is the total buoyancy force that acts on the barge times the accompanying lever arm with respect to the center of flotation of the barge. The second contribution is the moment that results from the cargo weight times its lever arm. Then there is the contribution due to the barge its own combine weight again times its lever arm. Figure 3.9 shows the different contributions to the restoring moment that acts on the barge. The relation used to obtain the restoring moment in Matlab is:

$$M_{res} = \overline{A_{hydro}} \cdot F_{h,tot} - \overline{A_{cargo}} \cdot F_{d,tot} + \overline{A_{barge}} \cdot \Delta_{barge} \tag{3.11}$$

In which $\overline{A_{hydro}}$ is the horizontal distance between the CoF and the point of engagement of the buoyancy force. $\overline{A_{cargo}}$ is the horizontal distance between the CoF and the center of gravity of the cargo. $\overline{A_{barge}}$ is the lever arm of the barge its weight to the center of flotation. Note that the lever arms of the restoring moment are vectors, they have components in both the y' and z'-direction.

3.1.4. Hydraulic cylinder & hinge forces

After that all loads and forces that act on the SHB are determined and their accompanying lever arms are found using the barge geometry as well. The resulting forces in the hinges and the hydraulic cylinders can be determined. These forces are found using the equilibrium of forces and moments around the hinges, which are found by adding up the different excitations that act on the half-hulls of the barge.

First the moments around the hinges for both the port and starboard side of the barge are determined. Note that the restoring moment that was determined in section 3.1.3 is subtracted from the starboard side moment.

$$\begin{aligned} M_{op,s} = &- F_{h,s,side} \cdot a_{1,s} + F_{h,s,in,1} \cdot a_{1,s,in,1} + F_{h,s,in,2} \cdot a_{1,s,in,2} + F_{h,s,bot} \cdot b_{1,s} + F_{d,s,side} \cdot a_{2,s,side} \\ &+ F_{d,s,bot} \cdot \sin\theta_u \cdot a_{2,s,bot} - F_{d,s,bot} \cdot \cos\theta_u \cdot b_{2,s} - \frac{1}{2} \triangle_{SHB} \cdot \cos\theta_r \cdot b_{3,s} + \frac{1}{2} \triangle_{SHB} \cdot \sin\theta_r a_{4,s} \\ &+ F_{t,s,side} \cdot \frac{1}{2} B_{hop} + F_{t,s,bot} \cdot \left(H_{hinge} - H_{bot}\right) \cdot \cos\theta_u - M_{res} \end{aligned} \tag{3.12}$$

$$\begin{aligned} M_{op,p} = &- F_{h,p,side} \cdot a_{1,p} + F_{h,p,in,1} \cdot a_{1,p,in,1} + F_{h,p,in,2} \cdot a_{1,p,in,2} + F_{h,p,bot} \cdot b_{1,p} + F_{d,p,side} \cdot a_{2,p,side} \\ &+ F_{d,p,bot} \cdot \sin\theta_u \cdot a_{2,p,bot} - F_{d,p,bot} \cdot \cos\theta_u \cdot b_{2,p} - \frac{1}{2} \triangle_{SHB} \cdot \cos\theta_r \cdot b_{3,p} - \frac{1}{2} \triangle_{SHB} \cdot \sin\theta_r \cdot a_{4,p} \\ &- F_{t,p,side} \cdot \frac{1}{2} B_{hop} - F_{t,p,bot} \cdot \left(H_{hinge} - H_{bot}\right) \cdot \cos\theta_u \end{aligned} \tag{3.13}$$

The lever arms that are used in the equations are shown in figure 3.10. For clarity only the lever arms on the port-side are shown. On the starboard side, the used forces are shown again.

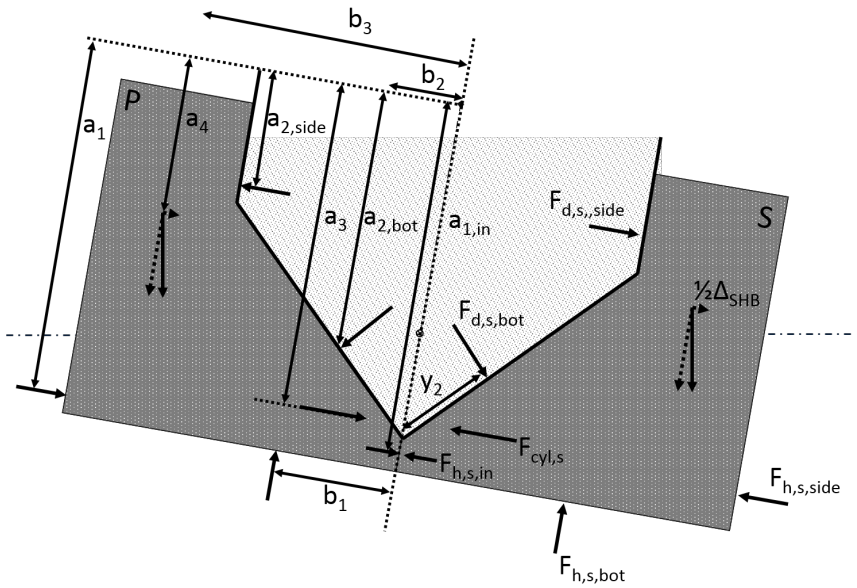

Figure 3.10: Lever arms for the opening moment.

Using the obtained moments around the hinges, the required forces in the hydraulic cylinders to keep the barge closed or under a steady opening angle can be determined. These forces follow directly from the moments:

$$F_{cyl,s} = \frac{M_{op,s}}{n_{cyl} \cdot h_{cyl}} \tag{3.14}$$

$$F_{cyl,p} = \frac{M_{op,p}}{n_{cyl} \cdot h_{cyl}} \tag{3.15}$$

Using the obtained moments, the forces in the bottom chocks can be determined as well. These forces partially depend on the pre-tension in the hydraulic cylinders $F_{cyl,pre}$:

$$F_B = \frac{n_{cyl} \cdot h_{cyl} \cdot F_{cyl,pre} - M_{op}}{n_B \cdot h_{hge}} \tag{3.16}$$

Here, M_{op} is either the starboard or port-side opening moment on the barge. Note that the pre-tension in the hydraulic cylinder only exists when the barge is closed. In this situation the superfluous capacity the hydraulic cylinder has on top of the required force that is needed to keep the barge closed, is used to pull the half-hulls together. As a result, a force in the bottom chocks exists.

When the barge is opened, the hydraulic cylinders only delivers the force that is needed to maintain the static opening angle. In case that the hydraulic cylinder force would deviate from this required force, the half-hulls would either start to open further or start to close. In the opened situation the bottom chock force is equal to zero, when the barge is opened the bottom chock do not touch so no force exists.

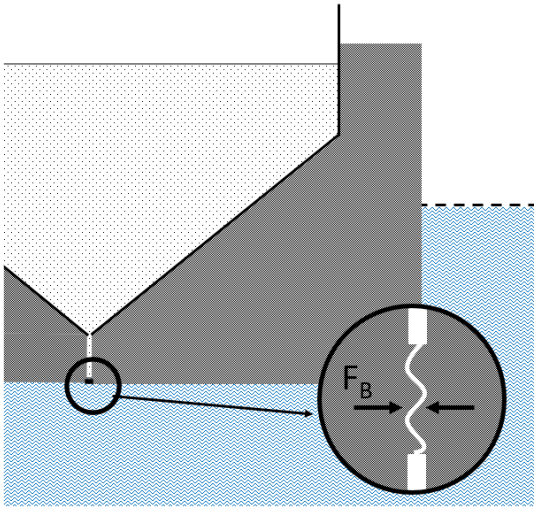

Figure 3.11: The bottom chocks of the SHB

Next the hinge forces in the y'-direction are obtained for both half-hulls using the equilibrium of forces that exist over the hinges in the y'-direction:

$$F_{hge,y',s} = \frac{1}{n_{hge}} \Big(F_{h,s,side} - F_{h,s,in,1} - F_{h,s,in,2} - F_{d,s,side} - F_{d,s,bot} \cdot \sin\theta_u - \frac{1}{2} \triangle_{SHB} \cdot \sin\theta_r - F_{t,s,bot} \cdot \cos\theta_u + n_{cyl} \cdot F_{cyl,pre} - n_B \cdot F_{B,s} \Big) \tag{3.17}$$

$$F_{hge,y',p} = \frac{1}{n_{hge}} \Big(F_{h,p,side} - F_{h,p,in,2} - F_{h,p,in,2} - F_{d,p,side} - F_{d,p,bot} \cdot \sin\theta_u + \frac{1}{2} \triangle_{SHB} \cdot \sin\theta_r + F_{t,s,bot} \cdot \cos\theta_u + n_{cyl} \cdot F_{cyl,pre} - n_B \cdot F_{B,p} \Big) \tag{3.18}$$

Finally, using the equilibrium of forces over the hinges in the z'-direction, the z' forces in the hinges can be obtained as well:

$$F_{hge,z',s} = \frac{1}{n_{hge}} \left(F_{h,s,bot} - F_{d,s,bot} \cdot \cos\theta_u - \frac{1}{2} \triangle_{SHB} \cdot \cos\theta_r + F_{t,s,bot} \cdot \cos\theta_u + F_{t,s,side} \right) \tag{3.19}$$

$$F_{hge,z',p} = \frac{1}{n_{hge}} \left(-F_{h,p,bot} + F_{d,p,bot} \cdot \cos\theta_u + \frac{1}{2} \triangle_{SHB} \cdot \cos\theta_r + F_{t,p,bot} \cdot \cos\theta_u + F_{t,p,side} \right) \tag{3.20}$$

When the barge is floating in an upright position, the buoyancy each half-hull should be equal to the weight of it. Besides, since the barge is modelled to be fully symmetric, the forces on each side of the barge should be in equilibrium as well for the upright situation. As a result, for the upright position only, the hinge forces in the z'-direction should be equal to zero for that situation.

The model was checked on its reliability by comparing the numerically values of some of the variables obtained with it with those found using hand calculations. A more detailed review of the reliability check of the described model is given in appendix A. In the next sections the Matlab model is used to simulate the SHB in the situations of interest for the chapter.

3.2. The effect of roll

Now that the Matlab model is defined and validated, the hinge and hydraulic cylinder forces can be determined for the situations of interest. The first effect that is considered in the model is the effect of roll of the barge on the forces in the hinges and hydraulic cylinders.

The first calculations that are made using the Matlab model concern a closed hopper barge, $3800m^3$, fully filled with a cargo of density $\rho_c = 1450\frac{kg}{m^3}$ which is assumed to behave like a fully liquid cargo. For this loading condition the barge has an initial mean draught of roughly $T_0 = 5.8m$. The simulations are run for roll angles upto 25 deg. Journee (Journee & Massie, 2001) states that the RMS angle of roll for light working conditions is not allowed to exceed 6 deg. Therefore, a maximum roll angle of 25 deg seems a reasonable upper limit for the simulations for now.

3.2.1. Cargo forces

In the model first the cargo forces on the hopper are determined. Figure 3.12 displays the ship bound cargo forces that act on the hopper walls for both the y'- and z'-direction. Figure 3.13 clarifies the direction in which the resulting cargo forces work.

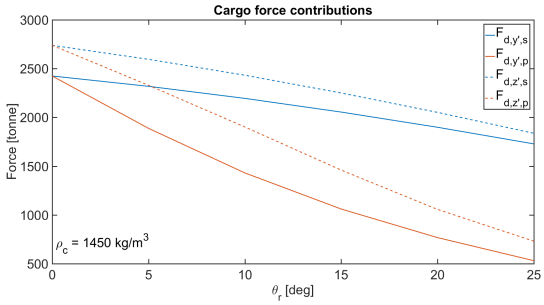

Figure 3.12: Cargo forces acting on the hopper walls.

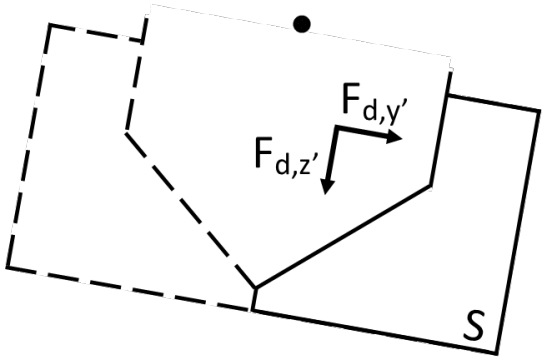

Figure 3.13: Orientation of the cargo forces on the hopper walls

In the figure it is shown that the cargo forces both in the y'- and z'-direction decrease. Since a liquid cargo is considered during the simulations, cargo will flow out of the hopper into the sea. As a result the total amount of cargo that is present in the hopper, decreases for increasing angles of roll. This explains why the overall weight of the cargo decreases during the simulations. Apart from this, the figure also shows a growing difference in hopper forces in between the two half-hulls. Since the liquid cargo is able to move freely through the hopper, one can expect that when the barge rolls, the cargo will flow to the lowest half hull causing a difference in the cargo forces for both half-hulls.

When the cargo forces in the y'-direction are considered, the tendency of the cargo to move to lower half hull causes the resulting cargo forces on this half hull to exceed those that act on the upper half hull. Since, again, cargo is expected to flow out of the hopper as well, a decrease of the sum of the y'-forces can be expected as well just as it was for the z'- cargo forces as well. This decrease in the overall y' cargo forces is clearly shown by the results from the model as well.

3.2.2. Hydrostatic forces

Next, the hydro-static forces that result from the pressures that load the outer walls of the barge are determined. The resulting ship-bound forces are shown figure 3.14. Figure 3.15 shows the expected directions of the forces that result from the hydrostatic excitation of the rolling barge.

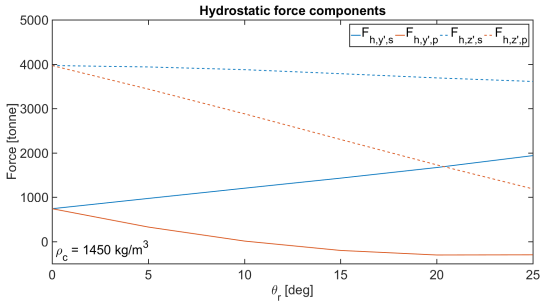

Figure 3.14: Hydro-static forces acting on the hopper walls.

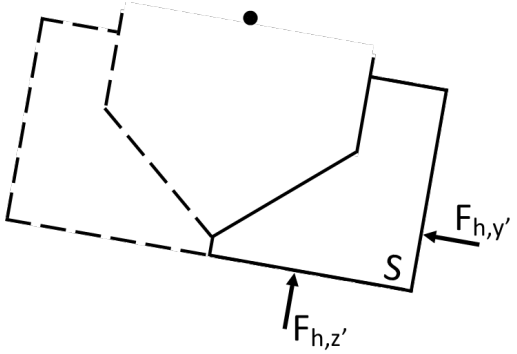

Figure 3.15: Orientation of the hydrostatic forces on the hull.

Figure 3.17 shows that in correspondence with the decreasing cargo loads, the hydro-static forces that act on the barge decrease as well. Due to the loss of cargo, the total weight of the barge will become less, causing the required displaced volume of the barge to drop as well. As a result the draught of the barge decreases causing both the hydrostatic pressures acting on the hull in all directions to decrease.

Due to the starboard orientated roll motion, the displaced volume of the starboard side will increase, while the displaced volume of the port side will decrease. Remember that the changes in displaced volumes for both the half-hulls are in equilibrium due to the equality of the immersed and emerged wedges of the barge.

Furthermore, the roll motion causes the side walls of the lower half-hull to be submerged further, while the side walls of the upper half-hull will be lifted out of the water. This change in wall heights is in equilibrium due to the symmetry of the system. As a result differences in the hydro-static pressures in the y'-direction are expected, which is shown in the figure.

3.2.3. Resulting hinge and hydraulic cylinder forces

Using the determined loads that were mentioned, the Matlab model is used to calculate the hinge and hydraulic cylinder forces that result from them. For the barge that was described at the start of this section, the resulting y' and z' hinge forces are shown in figures 3.17 and 3.20. The required cylinder forces are shown in figure 3.16.

First the resulting forces needed in the hydraulic cylinder to keep the barge closed are determined. Figure 3.16 shows that for an increasing angle of roll, the resulting forces in the hydraulic cylinders decrease. Secondly the graph displays that the forces for the port and starboard side are in equilibrium for the entire range of roll angles.

When the barge is in a rolling motion, the upper half-hull is lifted out of the water and starts to lean on the lower half-hull. This causes both of the half-hulls to be pushed together due to the upper half-hull weight that starts to develop a component in the y'-direction. Besides, since a liquid cargo is concerned, the cargo forces that cause an opening moment decrease. Lastly, the hydrostatic forces on the lower half-hull side increase due to the growing wetted surface area on its side wall. As a result, the forces needed in the hydraulic cylinders to keep the barge closed decrease.

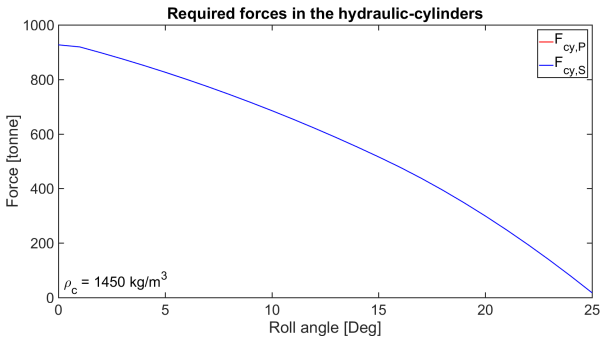

Figure 3.16: Resulting required cylinder forces.

It was mentioned that the forces for both half-hulls appear to be in equilibrium. This behaviour can be seen as a requirement of the static model rather than a result from it. The barge in the model is assumed to be in a static equilibrium, as a result it does not have a velocity or acceleration. This means that the resulting forces for both half-hulls have to be in equilibrium, otherwise the half-hull with the highest force would push the other one with a motion as a result. Since the hinges and hydraulic cylinder are the only components attaching the half-hulls to each other, the equilibrium of forces over them should follow from the exciting forces that work on them.

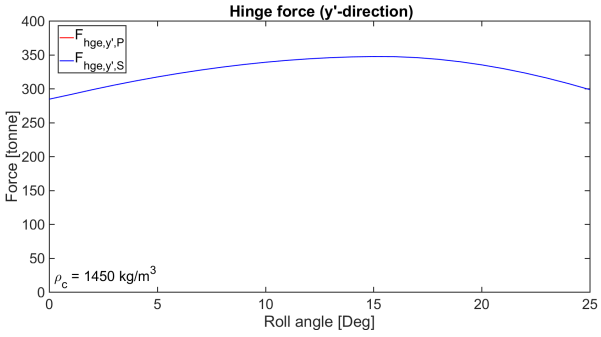

Figure 3.17: Resulting hinge forces (y'-direction).

Next the hinge forces are considered. For the resulting hinge forces in the y'-direction , figure 3.17 shows that they first increase and later on decrease again. To describe this behaviour, the combination of the effects of the exciting loads that are included in the y' hinge forces have to be explained. First, the cargo inside the hopper causes a negative force contribution to the y' hinge forces. Due to the outflow of cargo, the cargo height in the hopper decreases causing the y' cargo forces to decrease for an increasing roll angle. As a result, when only the effect of the cargo is considered, the hinge forces would increase.

Next there are the hydrostatic loads on the outer walls of the barge, which have a positive contribution to the hinge forces. When the weight of the cargo becomes lower due to outflow, the draught of the barge decreases causing the hydrostatic forces to decrease as well. However, due to the angle of roll, the wetted surfaces of the lower half-hull will increase and that of the upper half-hull will decrease. The combined effect of the decreasing draught and the effect due to the roll angle causes the hydro-static forces on the lower half-hull to increase, while the hydrostatic forces on the upper half-hull decrease.

Due to the angle of roll, the required hydraulic cylinder forces decrease. The cylinder force that is included in the calculation of the hinge force however stays constant since this is the pre-tension in the cylinder. Since the bottom chock forces are dependent on the surplus cylinder force that is put on the barge over the required cylinder force, they increase when the required cylinder force decreases. Due to the negative effect of the bottom chock forces on the hinge reactions, these will decrease.

Finally , for an increasing angle of roll the y'- component of the SHB empty-weight starts to increase. The weight effect on the hinge force in the y'-direction is positive for the upper half-hull and negative for the lower half-hull.

When all the mentioned effects are combined, the effect captured in figure 3.17 is the result. Figures 3.18 and 3.19 display the described components for both of the half-hulls. The forces that are shown in the figure are the combined force contributions of the hydrostatic, cargo, weight, cylinder and bottom chock forces. For example, F_d is the combined force that results from the cargo pressures on both the bottom and side walls of the hopper in the y'- hinge direction.

Note how the pre-tension in the hydraulic cylinder forces influences the found forces. When the pre-tension in the hydraulic cylinders would be disregarded, the resulting hinge forces in the y'-direction would turn out to be much lower.

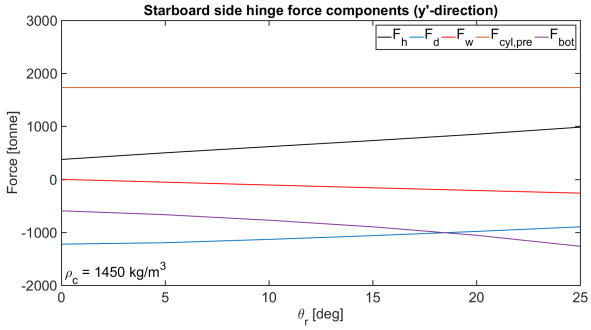

Figure 3.18: Hinge force components on the starboard side (y'-direction)

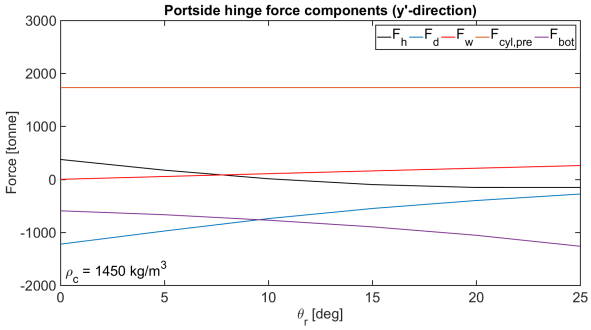

Figure 3.19: Hinge force components on the portside (y'-direction)

The last results from the Matlab calculations are those giving the resulting z' hinge forces of the SHB model. Note that, just as for the other resulting forces, for the z' hinge forces the condition of equality for both half-hulls is met again.

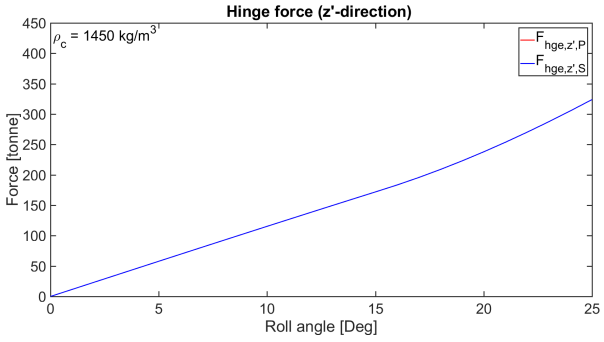

Figure 3.20: Resulting hinge forces (z'-direction).

The resulting z' hinge forces increase for an increasing angle of roll. Due to the increasing angle of roll, the upper half-hull of the barge is lifted out of the water, causing the hydrostatic contribution to the z' hinge force for the upper half-hull to decrease. According to the relation for the z' hinge force given in formula 3.20, this causes the z' hinge force of the upper half-hull to decrease.

From the mentioned behaviour, it can be argued that in fact the weight of the upper half-hull has to be supported by buoyancy that is generated with the lower half-hull. Since the hinge is the only connection between the two half-hulls that can account for the z'-force, the z'-hinge force increases.

3.2.4. Conclusions on the effect of roll

When the roll angle of the barge grows, the hydraulic cylinder forces decrease. Again, since the upper half-hull is lifted out of the water, its weight causes a closing moment around the hinge arrangement. Together with the decreasing moment due to the cargo and the increasing hydrostatic moment that acts on the lower half-hull, the force required in the cylinders to keep the barge closed decreases. The highest response for the hydraulic cylinders is therefore found for the situation in which the barge is in a perfect upright position, so when the weight of the half-hull does not cause an additional added moment to the moment equilibrium.

The hydraulic cylinders that are installed on the split hopper barge in this model, prove to have a capacity that exceeds the required force that is needed . Due to this over capacity, the hydraulic cylinders pull the half-hulls together with a certain pre-tension. This tension causes a force in the bottom chocks for the closed condition only, i.e. the half-hulls are pulled together. The combined effect of the hydraulic cylinder force and that of the force in the bottom chocks dominates the response that is found for the hinge forces in the y'-direction. Under influence of the forces in the cylinders and bottom chocks, the hinge force in the y'-direction increases slightly for an increasing angle of roll.

The z' hinge forces increase when the SHB is rolling . This can be explained best by the added weight that has to be supported by the lower half-hull when the upper half-hull is lifted out of the water due to the increasing angle of roll. As a result, the weight of the upper half-hull has to be supported by the hinges, causing an increase in the ship bound z'-forces.

3.3. The effect cargo density

Using the same model with the same barge dimensions as in paragraph 3.2, the influence of cargoes with different densities on the forces in the hinges and hydraulic cylinders of the SHB can be obtained. According to the earlier described sliding law by Bureau Veritas, different kinds of cargo will react differently to the motions of the barge and thus will have a different effect on the barge loads as well. For instance the amount of outflow over the coaming is taken to be different for the different densities. To determine this effect, the barge was again considered under the same range of roll angles, yet now loaded with all different types of cargo (liquid, sliding & solid). Note that it is assumed that a cargo of $\rho_c = 1450 kg/m^3$ is fully liquid. As a result the sliding law that is used in de model becomes:

- Liquid cargo for $\rho_c \leq 1450$ $[\frac{kg}{m^3}]$

  $\theta_c = \theta_r$

- Sliding cargo for $1450 < \rho_c < 2000$ $[\frac{kg}{m^3}]$

  $\theta_c = \frac{2000-\rho_c}{600}\theta_r$

- Solid cargo for $\rho_c \geq 2000$ $[\frac{kg}{m^3}]$

  $\theta_c = 0$

To be able to compare the different types of loading conditions with each other, the initial conditions of the barge have to be kept equal for each simulation. To account for this, the barge was assumed to have a maximum initial draught of 5.8 m. By doing so, the initial cargo volume and cargo height differ for each cargo type. However, the initial cargo weight and therefore the initial displaced volume of the barge are equal for all different types of cargo. As a result, almost all exciting forces that act on the barge are equal for each loading situation. Only the y'-force due to the cargo differs for each situation. By creating a constant starting point for the simulations, a clear and direct observation can be made for the differences that occur due to the different types of cargo under the growing angles of roll.

Table 3.1: Cargo input for the roll model.

Cargo regime	Density $[\frac{kg}{m^3}]$	Filling percentage [%]	Initial Volume $[m^3]$
Liquid	1450	100	3778
Sliding	1600	90.6	3424
Solid	2200	65.9	2490

Table 3.1 displays cargo conditions that were considered in the simulations. Note how the initial volume of the cargo decreases for an increasing cargo density as a result of the maximum initial draft.

3.3.1. Resulting hinge and hydraulic cylinder forces for multiple types of cargo

Using the mentioned input, the model is run for the same range of rolling angles up to 25 deg. Just as was done in the previous section. First, the hydraulic cylinder forces for the barge loaded with different types of cargo are show in figure 3.21.

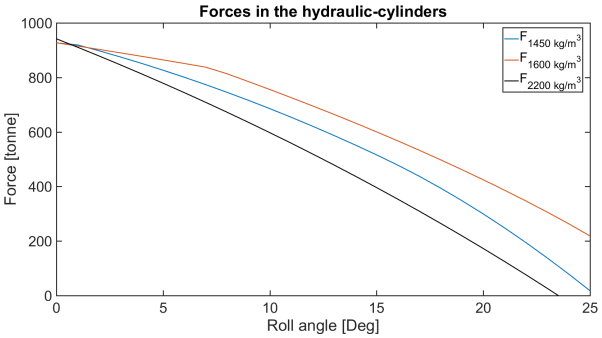

Figure 3.21: Required cylinder forces for three types of cargo.

For an increasing angle of roll, the required hydraulic cylinder force that is necessary to keep the barge closed decreases due to the resting of the upper half-hull on the lower half-hull. For the solid cargoes this effect is the biggest, since than also the weight of the cargo causes a closing moment that pushes the two half-hulls towards each other. The effect is the smallest for sliding cargoes. Since the cargo does slide trough the hopper, but does not flow out in the extent that the liquid cargo does, the total load in the hopper will remain high. Besides, due to the sliding of it, most of the cargo will be located in the lower half-hull. As a result, the cargo will not cause a closing moment such as the solid cargo does, neither will its effect decrease under the influence of outflow instead it will cause an opening moment acting on the lower half-hull causing the relative high required hydraulic cylinder forces.

Although the required cylinder forces remain high for the sliding cargoes, the most limiting condition is found in the upright position. Due to the equality in initial conditions the hydraulic cylinder force is equal for all load cases in this position.

Next the hinge forces are considered. The resulting y'- and z'- hinge forces for all load conditions are shown in figures 3.22 & 3.23.

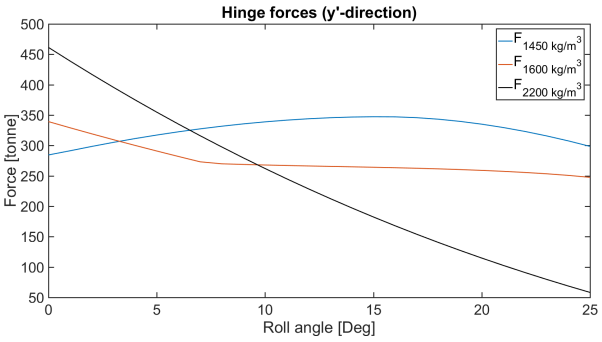

Figure 3.22: Hinge forces for three types of cargo (y'-direction).

From figure 3.22 the observation can be made that although the initial conditions of the barge were kept constant, a difference in hinge forces is found for the different types of cargo from the start. The presence of the initial differences can be explained using the changing initial loading height of the cargo in the hopper. Due to the higher initial cargo height of the lighter cargoes, the resulting y'-forces on the hopper walls are found to be high in comparison with those of the heavier and thus lower cargoes. Meanwhile, the hydro-static forces, the hydraulic cylinder contribution and the weight contribution to the hinge force in the y'-direction are all equal. As a result and since the cargo loads in the y'-direction work in the opposite direction of the hinge forces in the y'-direction, the initial hinge forces in the y'-direction for the cargoes with a large initial cargo height are low.

For cargoes that result in less or no outflow, the hinge forces seemingly decrease more than those of the barges that are filled with cargoes that do flow out. Since the cargo pressures on the hopper walls have a negative contribution to the hinge forces, the remaining of the cargo in the hopper causes the negative cargo contribution to the hinge forces to remains quite stable. As a result the y' hinge forces decrease more rapidly for non or hardly outflowing cargoes.

Figure 3.22 shows that the most limiting condition is found for a $0\,deg$ angle of roll, for a barge loaded with a heavy and thus solid cargo. For a larger angle of roll, the liquid cargoes become limiting.

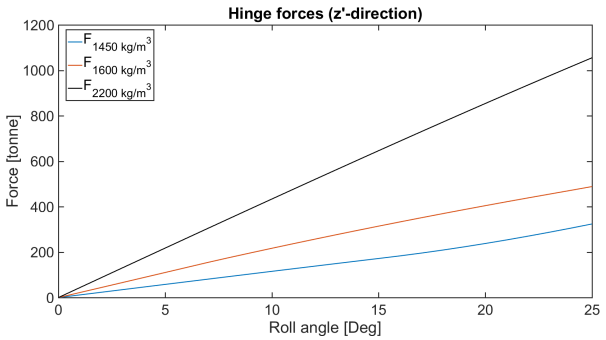

Figure 3.23: Hinge forces for three types of cargo (z'-direction).

Figure 3.23 shows the z' hinge forces of the barge loaded with different types of cargo. Initially the resulting z' hinge forces are equal for all cargo conditions. Note how for an increasing roll angle the z' hinge forces increase. Again, the found increase can be explained by the weight of the upper half-hull that has to be supported by the lower half-hull. Note that for the heavier cargo types the mentioned effect seems to cause larger loads on the hinge. This is a result from the additional amount of cargo that stays in the upper half-hull during the roll motion. While for liquid cargoes eventually all cargo has either flown out of the hopper or is completely located in the lower half-hull, heavier cargoes do not slide or flow out that easily, making that more of it stays located in the upper half-hull. Ultimately the result is that a barge loaded with a heavy cargo develops the highest z' hinge forces and therefore causes the limiting condition.

3.3.2. Conclusions on the effect of the cargo density

Based on the simulations that were done for the SHB model filled with different types of cargo, multiple conclusions can be drawn. First it is evident that changing the type of cargo from liquid to sliding or solid does have an effect on the hinge and cylinder forces of the SHB.

When the hydraulic cylinder forces are of concern, it was found that cargoes of a sliding type will dominate them for growing roll angles. This was due to the fact that for the sliding cargo the highest concentration of loads in the down slope half-hull were found, resulting in a high opening moment around the hinges. The largest force that is found for the hydraulic cylinders is that in the upright position of the barge, were the required cylinder forces are equal for all cargo types. Do note, that the available force in the hydraulic cylinders is much higher than the force required in them. Based on the quasi-static results, the reactions in the hydraulic cylinders are therefore no cause of concern.

From the obtained results concerning the forces in the hinges, it was found that the highest response is found in the z'-direction for a barge loaded with a heavy solid cargo under a high angle of roll. Due to the weight that is supported by the hinges in this situation, this load becomes the biggest. For the loads in the y'-hinge direction, the responses are dominated by both the solid and liquid cargoes. The high initial forces due to the solid cargo dominate for low angles of roll, while for the freely moving liquid cargo the found forces become high for large angles of roll. The pre-tension that exists in the hydraulic cylinders was found to have a large influence on the hinge responses in the y'-direction.

When different types of cargo are regarded, the response due to liquid and solid cargoes proves to cause the most governing load cases.

3.4. The effect of opening the barge

Now that the behaviour of the barge for a rolling motion in a closed condition was determined, the effect of a rolling motion of a barge in an opened configuration is considered. Figure 3.24 shows the opened barge experiencing a rolling motion.

To simulate this condition using the Matlab model some alterations to the original model have to be made. First of all an assumption about the outflow of cargo has to be made. In the model it is assumed that no cargo will flow out of the hopper although it is opened. To do so, an additional floor section is defined to be located in between both of the half-hulls, that prevents the cargo from flowing out of the hopper.

On the additional floor section, forces due to the cargo and forces due to the buoyancy of the barge will act. Since the floor section is assumed to be fixed to the barge, these forces will have to be taken into account in the summation of the forces and moment of the barge as well. An illustration of the opened barge together with the additional forces that act on the added floor sections is given in figure 3.24.

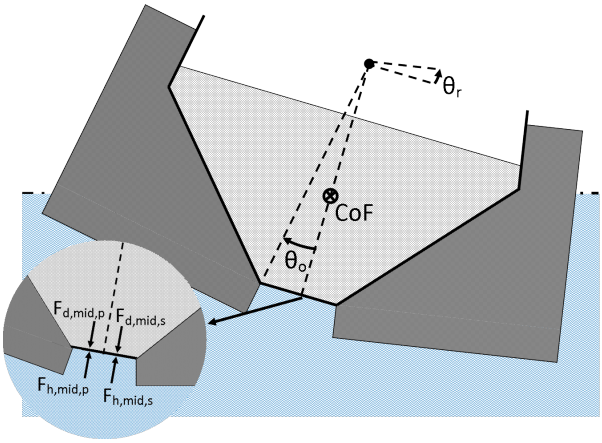

Figure 3.24: The opened split hopper barge.

Although, the cargo is not expected to leave the hopper through to the gap in between the two half-hulls, it will settle deeper in the hopper due to the new hopper lay-out. The opening of the barge and the presence of the additional floor board result in additional hopper space that is added to the barge. This means that when the barge is loaded with the same volume of cargo, the initial cargo height in the opened barge will be lower than that in the closed barge. Note that no volume is added to the barge, the barge can never be loaded with more cargo than it can hold in a closed condition. The opened barge has to be loaded with the same amount of cargo that would have been loaded into it when it was considered in a closed condition.

Due to the opening of the barge, the underwater geometry of the barge changes from a symmetric beam to a multi-angled complex body. As a result, the assumption that the barge will rotate around a steady center of flotation in the center of its initial water line is no longer valid. However, in order to keep the model as simple as possible, the resulting shift of the center of flotation is not taken into account. By neglecting the shift, the barge is no longer expected to be in an equilibrium. As a result, the forces that are found for both half-hulls will no longer be in equilibrium as well. The resulting forces in the hinges and hydraulic cylinders that are found with the model for both of the half-hulls will not be equal as a result. Since, this model is only used to get familiar with the possible effects of opening the barge, the inaccuracy that was just described is not expected to have large consequences. For the resulting hinge and cylinder forces the mean value taken from both half-hull results is considered as the resulting force.

3.4.1. Resulting hinge and hydraulic cylinder forces for the open barge

Figure 3.25 shows the resulting hydraulic cylinder forces for the SHB loaded with a cargo of $\rho_c = 1450 \frac{kg}{m^3}$ when it simulated for opening angles of $0, 5, 10$ and 15 degrees. The figure clearly shows the effect that outflow of the cargo over the coaming of the hopper has on the forces needed in the hydraulic cylinders. When the barge opens, the initial cargo height will be lower due to the change in hopper lay-out. As a result, a higher angle of roll is needed for the cargo to reach the top of the coaming and thus start to flow out over it. The cargo pressures on the hopper walls will therefore remain high for a larger amount of roll angles causing a higher resulting forces needed in the hydraulic cylinders for these roll angles. As a result, the hydraulic cylinder forces increase for the barge in an opened configuration.

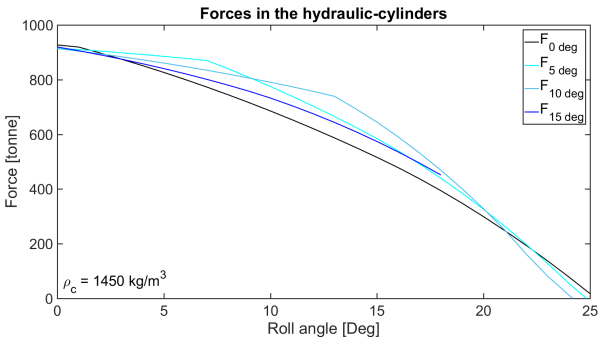

Figure 3.25: Hydraulic cylinder forces for a opened SHB.

From section 3.3 it is know that when cargo flows out of the hopper, the cylinder forces drop. So it is expected that when the SHB is opened the cargo forces on the hopper will decrease fast. As a result, a drop in hydraulic cylinder forces is expected as well.

Even for the barge with an opening angle of 15 deg, the barge will keep rotating around the same center of flotation. At this angle of roll however, the upper half-hull of the barge is lifted out of the water in such an extent that its side wall will no longer be in touch with the water. This causes unrealistic forces in the hinge and hydraulic cylinders. These unrealistic results are therefore left from the results in order to obtain clean and clear graphs.

For a real SHB, the center of flotation of the barge will shift in position causing the barge remain more stable in the water. For the real situation the forces are therefore expected to follow the shown trends for the high angles of roll as well.

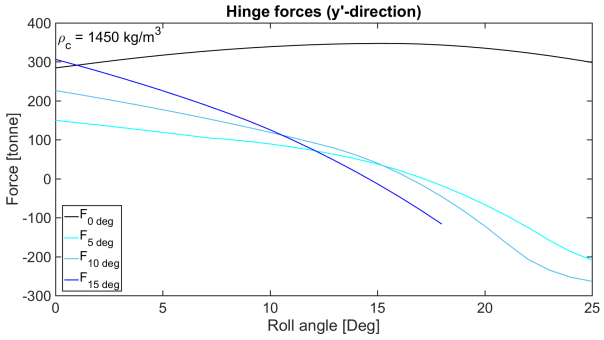

Figure 3.26: Hinge forces for a opened SHB (y'-direction).

In figure 3.26, the resulting y'-direction hinge forces of the barge in a opened configuration with a liquid cargo, $\rho_c = 1450 \frac{kg}{m^3}$, is shown. When the barge is opened, the working force that acts in the hydraulic cylinders is the force that is needed to keep the opening angle constant. This cylinder force is therefore no longer equal to the pre-tension in the cylinders but is now equal to the hydraulic cylinder force that was shown in figure 3.25. As a result, the contribution of the cylinder force to the hinge force in the y'-direction decreases. Although the other force contribution to the hinge forces do grow, the lower tension in the hydraulic cylinders causes the resulting y'-direction hinge forces to be lower than those that were obtained for the barge in a closed configuration.

When discharge of the cargo would have been taken into account, the hinge forces are expected to turn out lower. Since the amount of cargo inside the hopper will decrease rapidly after the initial opening of the barge, the forces that excite the barge decrease resulting in lower hinge forces.

Figure 3.27 shows the resulting z' hinge forces for the barge under several opening angles. For an increasing opening angle of the barge under an growing roll angle, the found z' hinge forces increases slightly compared to those of a closed barge.

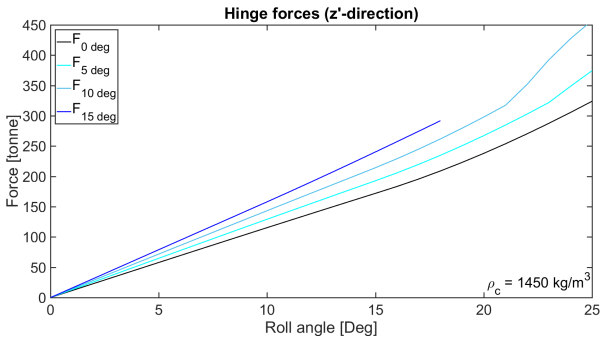

Figure 3.27: Hinge forces for a opened SHB (z'-direction).

Due to the geometry of the opened barge, its initial draught will decrease. As a result, the increasing roll angle will cause the upper half-hull to be lifted out of the water faster. This causes the amount of weight that has to be accounted for by the buoyancy force on the lower half-hull to increase more rapidly. Besides, cargo is expected to be flowing out later, causing the amount of weight inside the hopper to increase compared to the situation of the closed barge. In section 3.2 the effect of the weight of the upper half-hull hanging on the lower half-hull and the weight of the cargo were found to cause an increases in z' hinge forces. Therefore, in the opened conditions when these effects are stronger, the z' hinge forces will become bigger as a result.

Note that when the effect of the cargo discharge was taken in to account. The weight of the cargo inside the hopper would decreases fast. This causes the draught of the barge to decrease. When the draught of the barge is small, the effect of the weight of the upper half-hull hanging on the lower half-hull will become larger. As a result, the z' hinge forces are expected to become higher than that was predicted using the model.

3.4.2. Conclusions on the effect of opening the barge

From the simulations that were run with the opened SHB in a quasi-static equilibrium, it was learned that the complexity of the shape of the opened barge makes it difficult to obtain proper results for the opened configuration using the static Matlab approach.

The obtained resulting hydraulic cylinder forces showed that the outflow of cargo over the coaming has a significant and clearly visible effect on the resulting required forces in the hydraulic cylinders. Again, the found forces are the highest for the upright position and do not approach the installed capacity of the cylinders by far.

From the determined hinge forces in the y'-direction it was learned that the lack of pretension in the hydraulic cylinders and due to the resulting absence of the bottom chock forces as well, the y' orientated hinge forces decrease on the moment that the barge is opened. Although the lower initial height of the cargo for an increasing opening angle has an increasing effect on the resulting y'-forces in the hinge, the forces that were obtained for the closed barge are not exceeded.

For the z' hinge forces, the delayed outflow of the cargo for the opened condition without discharge, causes the total combined weight of the barge and cargo to increase with respect to the closed condition. As a result, the weight the hinges have to bear in the z' direction when the barge is in a increasing angle of roll increases. Evidently, the forces become the biggest for the opening angle where the least cargo flows over the coaming, in the simulations that are discussed in this section that is for 15 degrees of opening.

One important side note on the results that were shown and discussed in this section, is that the situation where discharge of the cargo is not assumed to happen although the barge is opened ,is very conservative. Knowing that the loss of cargo causes the hinge and cylinder forces to decrease causes that it can be expected that once the barge is opened and cargo is flowing out of it, the resulting forces in the hinges and cylinders will decrease fast.

3.5. The effect of discharge

Section 3.4 showed the results from the quasi-static model that was used to describe the effect of the opened barge geometry on the resulting forces in the hinges and hydraulic cylinders of the SHB for multiple angles of roll. In this conservative model, the outflow of cargo due to the opening of the barge was neglected based on the knowledge that the forces of interest would only decrease when the amount of cargo in the hopper becomes less. The conclusion that was drawn from the model is that the outflow of cargo would cause the resulting forces in the hinges and cylinders of the barge to decrease rapidly, making the closed barge load case more governing.

For the steady states of the barge before and after the discharge of the cargo, it is reasonable to state that the drawn conclusion is correct. However, in the calculations done to get to this conclusion, no attempt was made to capture the effect that the out-flowing cargo has on the resulting forces in the hinges and cylinders. Since the outflow of the cargo is a dynamic process, the dynamic response of the barge could potentially cause additional forces that were not captured nor predicted using the static model. As a result, it could be possible that although the opening of the barge itself does not directly lead to an increase in forces in the hinges and cylinders, the resulting cargo flow causes a dynamic response that does. Therefore, the dynamic effect of outflow of cargo from the hopper should be studied in more detail before drawing the final conclusion about the effect of opening the barge.

To study the dynamic discharge behaviour of the SHB, a new Matlab model was constructed in which the barge is considered in a opened condition with a static opening angle. The barge is only expected to move in the heave direction and no external roll moment will be applied. The cargo in the hopper flows through the gap in the bottom at a fixed speed having a steady volume flow in the hopper as a result.

In the model two types of outflow will be considered. First there is the standard outflow of cargo, where the cargo surface moves uniformly down through the hopper until all cargo has flown out of it. Secondly, there is the situation in which the cargo is expected to disappear from the bottom up. This situation is meant to approximate the real life situation where internal friction in the cargo causes it develop a bridge over the opening in the hopper floor supporting the cargo on top of the bridge, resisting it from flowing out of the hopper. As a result, in this situation, the cargo remains positioned high in the hopper until the internal friction is overcome. The second situation will be simulated by keeping the initial cargo surface fixed in top of the hopper, while the bottom level of the cargo moves up through the hopper. Figures 3.28 and 3.29 show both situations that were modelled.

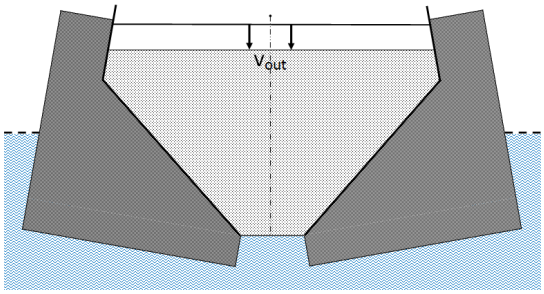

Figure 3.28: Discharge model with downward cargo motion.

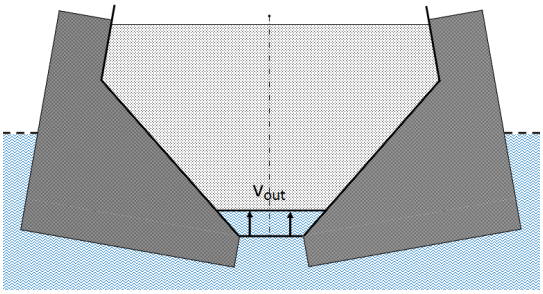

Figure 3.29: Discharge of crumbeling cargo

Note that in both situations water will start to flow into the hopper upto the water line when the amount of cargo in the hopper is decreasing. For the first situation, water is first assumed to be pushed away by the moving cargo and will therefore only start flowing in after all cargo has flown out of the hopper. In the second situation the water will fill up the space in between the bottom of the cargo and the hopper floor directly when the space is present.

3.5.1. Theory

To find the resulting forces in the hinges and hydraulic cylinders for the dynamic outflow of cargo, the same principle as in section 3.1.2 is used . Again, the forces that result from the pressures that excite the barge and hopper walls will be used to find an equilibrium of forces and moments around the hinges, from which the resulting forces follow. For this situation these forces that act on each half-hull are shown in figure 3.30. Note that since the barge is only modelled to react to the outflow of the cargo in the heave direction, the behaviour of both of the half-hulls will be identical. As a result the forces that follow from both half-hulls will be equal as well. Therefore in this model only one half-hull has to be modelled in order to describe the behaviour of the entire barge.

The forces that excite the hopper walls due to the presence of the cargo in the hopper result from the orientation of the cargo in the hopper at a certain moment in time. The state of the cargo can be calculated using the fixed flow velocity through the gap in the bottom of the hopper, which has a steady volume flow in the hopper as a result. Using this, the amount of cargo in the hopper can be determined for each time step which can be used to find the cargo wall heights. Remember that these heights do no longer only depend on the amount of cargo in the hopper but also on the way the cargo is expected to flow out of the hopper. When a crumbling cargo is concerned, the hopper wall height will start to decrease in a bottom up direction, while for the normal outflow of cargo the hopper wall heights will start to decrease at the top of the hopper first.

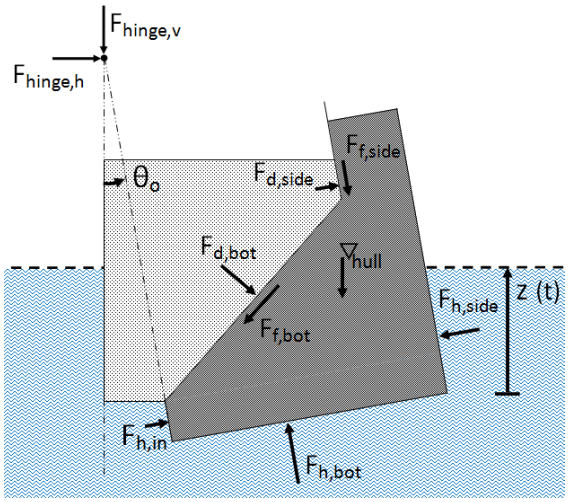

Figure 3.30: Exciting forces during cargo outflow.

Now that the barge is no longer considered in a static equilibrium, the submerged outer wall heights do no longer follow directly from the necessary displaced volume that is needed to keep the barge afloat. Instead the submerged outer wall heights will now oscillate around their static equilibrium due to the velocity and acceleration that the barge experiences over time. To find the submerged wall heights the equation of motion for the barge has to be solved for each time step. The general equation of motion for the entire barge, as it is stated in the offshore hydromechanics book by Journee (Journee & Massie, 2001), for a heave motion is given by:

$$(M+a)\cdot\ddot{z}+b\cdot\dot{z}+c\cdot z=0 \tag{3.21}$$

In which:

M is the combined mass of the barge + cargo $[kg]$.

a is the added mass $[kg]$.

b is the damping coefficient in the chosen direction $[\frac{Ns}{m}]$.

c is the restoring spring coefficient $[\frac{N}{m}]$

z is the vertical submerged depth of the outer side wall of the barge $[m]$

Mass

The mass that is used in the given equation is the combined mass of the entire barge and all the cargo together. For the calculations it has to be kept in mind that the weight of the cargo that is felt by the barge in not only decreasing over time, it is no longer equal to the gravitational weight of the cargo as well. If the weight of the cargo would act entirely on the barge, the cargo would be fully supported, preventing it from flowing out of the hopper. Instead, for the discharge situation , the only weight of the cargo that excites the barge is that that either follows directly form the cargo pressures on the hopper walls or from the friction and cohesion that the cargo has with the hopper walls. The weight of the barge can then be found using the following relation:

$$W = 2 \cdot W_c(t) + \triangle_{SHB} \tag{3.22}$$

Where W_c is the weight of the cargo that is supported by one half-hull. This weight follows from the summation of forces:

$$W_c(t) = -F_{d,side}(t) \cdot \sin\theta_o + F_{d,bot}(t) \cdot \sin(\theta_l - \theta_o) + F_{f,side}(t) \cdot \cos\theta_o + F_{f,bot}(t) \cdot \sin(\theta_l - \theta_u) \tag{3.23}$$

The mass of the barge, M, is then of course the weight divided by the gravitational acceleration.

Next the added mass coefficient has to be determined. The value of this coefficient can be found using the following equation for the inertia coefficient:

$$C_M = 1 + C_a \tag{3.24}$$

Here C_M is the inertia coefficient and C_a is the added mass coefficient of the vessel. Journee (Journee & Massie, 2001) states that a typical value for the inertia coefficient is 2. This value for the inertia coefficient results in a standard added mass coefficient of $C_a = a = 1$.

Damping

To make sure the behaviour of the barge in the model is stable and to assure that it eventually converges to a steady state, some damping has to be added to the model. Usually damping of a vessel is caused by several phenomena including: radiation of surface waves, vortex shedding, separation phenomena and drag of the vessels body with the water. All these contributions to the damping will be included later on. For now, since the damping is only intended to stabilize the behaviour of the build model, the damping of the barge will be estimated using some drag.

To do so, the damping of the barge will be approximated by taking the resulting damping force, $b \cdot \dot{z}$, equal to the drag of the bottom floor of the barge multiplied by some factor to create a suitable damping. The drag of the bottom of the barge can be found by using the second part of Morissons equation (Journee & Massie, 2001), which is given by:

$$b \cdot \dot{z} = \frac{1}{2} \rho_s \cdot C_d \cdot A_{bot} \cdot \dot{z} \cdot |\dot{z}| \tag{3.25}$$

C_d is the drag coefficient, that is chosen to be equal to $C_d = 2$ for this model. This value is based on the drag coefficient of a non-smooth cube in a turbulent flow. A_{bot} is the area of the barge bottom. In the model the area that is used to determine the drag force is that of the bottom area perpendicular to the heave direction.

Force term

The spring term of the barge model is equal to the buoyancy force that acts on the barge during its motions. This force can be found using:

$$c \cdot z = \rho_s \cdot g \cdot V_{disp} \tag{3.26}$$

Where V_{disp} is the displaced volume of the barge. Due to the outflow of cargo from the hopper the combined weight of the barge and the cargo decreases each time step. As a result, the displaced volume of the barge has becomes a time dependant variable, that has to be determined for each time step during the simulation.

The equation of motion of the barge experiencing outflow of cargo is solved in Matlab using a ordinary differential equation (ODE) solver. Since some of the variables in the equation are time dependent, a fixed time step ode-solver is used. Using the barge its position for each moment in time the required submerged outer wall heights necessary for the calculation of the hydrostatic forces are determined.

Since the cargo was assumed to flow out of the barge at a fixed rate, the amount of cargo in the hopper is only depended on the time. As a result, for the calculation of the cargo pressures in the hopper, the oscillations of the barge do not play a role.

Using the obtained hydrostatic and cargo forces, the resulting forces in the hinges and the hydraulic cylinder of the barge can be determined according to the same relations that were introduced in section 3.1.4. The results and accompanying conclusions are presented in the section 3.5.2 and 3.5.3.

3.5.2. Standard outflow

Comparison with static Matlab model

Figure 3.31 shows the resulting forces in the hinges and the hydraulic cylinders for the SHB model opened with an angle of 10 deg. At $t = 0\,sec$ the barge is filled with $2490m^3$ of cargo with density $\rho_c = 2200\frac{kg}{m^3}$. The cargo flows downwards trough the bottom opening in the hopper at a constant speed of $v_{out} = 0.2\frac{m}{s}$. The cargo in the figure does not experience any friction with the hopper walls, nor does it have any cohesive strength $(\mu = 0; c = 0)$. In this particular simulation forces that act on the floor section in-between both of the half-hulls were taken into consideration. Although this is actually not possible when the cargo is flowing out of the hopper, this was done to create a situation that could be compared and related to the earlier found results from the static opened barge model in section 3.4.

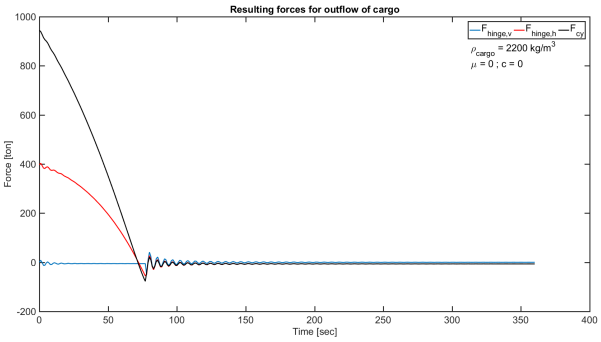

Figure 3.31: Resulting forces for the outflow of a solid cargo (floor panels included).

The initial values that are shown in the graph, do match with those that were found earlier for this specific type of cargo in a barge with the same opening angle using the static model. When the outflow of the cargo starts a small oscillation can be seen in the resulting forces, this comes from the immediate start of the outflow of the cargo instead of the slow and steady start that will occur in practise.

After all cargo has flown out of the hopper, a small jump can be seen in the resulting forces before they damp out to their steady state value. This small jump and the oscillations that follow from it are the result from the rapid inflow of sea water after the last bit of cargo has flown out of the hopper. In the model, when the cargo is still flowing, the momentum that the cargo has due to its velocity will prevent seawater from flowing into the hopper. The cargo is effectively assumed to push the water out of the opening although the cargo level is already below the waterline. Then when all cargo has flown out of the hopper, the 'resistance' against the inflow of the seawater immediately stops. As a result the barge directly fills up with water up to its water line causing a small jump in draught resulting in a jump in resulting forces as well. Following from that, the resulting forces in the hinges and cylinder will start oscillating until the barge its motions dampen out when it reach its steady state position.

In real, the last phase of the discharge cycle will evidently result in a much smoother behaviour of the barge. The moment that the cargo level becomes low, water will already start to mix with the cargo that is still left in the hopper. As a result, the transitions of cargo to water in the hopper occurs already before the hopper is empty. Therefore, the forces will dampen out to their equilibrium position instead of making a jump due to the violent inflow of seawater. For the resulting forces in the hinges and cylinder this would mean that they will smoothly come to their final value instead of showing the oscillations that are predicted using the model.

Finally, when the barge is empty all forces approach zero. Since the barge is not experiencing any roll motion and is not excited by waves, wind or current either, the empty barge will be in complete equilibrium with the hydrostatic forces that act on it when it comes to rest. As a result, in this ideal model, the forces that result in the hinges and cylinder will be close to zero. In practise there will always be some motion or excitation left, the resulting hinge and cylinder forces will therefore never damp out to the steady state equilibrium that is shown in the graphs.

Realistic discharge

Now that the general behaviour of the barge for out-flowing cargo is known, and the simulation results have proven to agree with the earlier preformed static calculations. The model is run for a more realistic situation where the additional floor panels in between the two half-hulls are left.

Figure 3.32 shows the resulting forces in the hinges and hydraulic cylinder for the outflow of a solid cargo without friction or cohesion. Due to the absence of the bottom floor sections , the only weight of the cargo that if felt by the barge is that that pushes on the bottom and side hopper walls. This causes the resulting forces in the hinges and hydraulic cylinders to turn out lower as was predicted before. Despite the drop in forces, the found trends that are shown in the graph still show the same behaviour for the resulting forces. When the cargo leaves the hopper, the forces in both the hinges and the cylinders decreases, eventually finding an equilibrium close to zero tonnes. The drop in forces occurs quite smoothly and does not show any signs of sudden increases besides that due to the rapid inflow of seawater after the cargo has flown out.

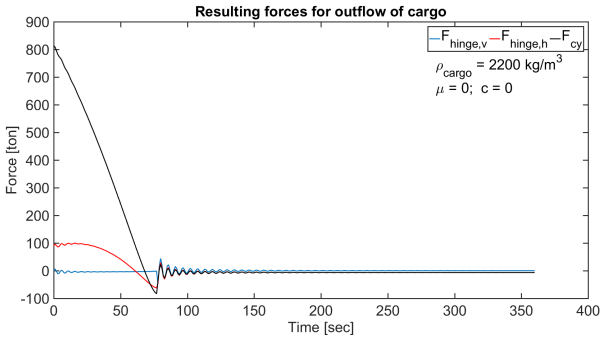

Figure 3.32: Resulting forces for the outflow of a solid cargo.

The next step is to determine the influence that friction and cohesion of the cargo have on the resulting forces in the hinges and hydraulic cylinders during the outflow of cargo. Figure 3.33 and 3.34 show the resulting forces in the hinges and hydraulic cylinders of the SHB for a solid cargo with friction only and for a solid cargo with friction and cohesion. The value for the friction coefficient for the friction only simulation is based on that of a sandy soil (A. Kolijl, 2016). For the combined friction and cohesion simulation, the values of the friction coefficient and the cohesive strength resemble a clayey soil (A. Kolijl, 2016).

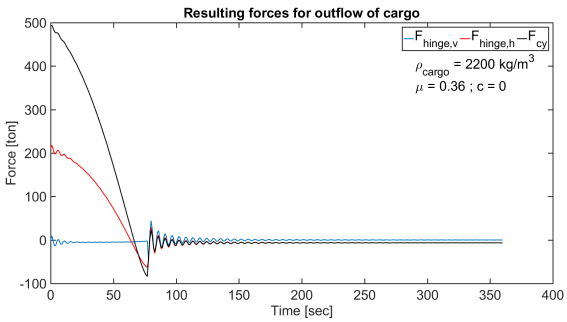

Figure 3.33: Effect of outflow of solid cargo with friction

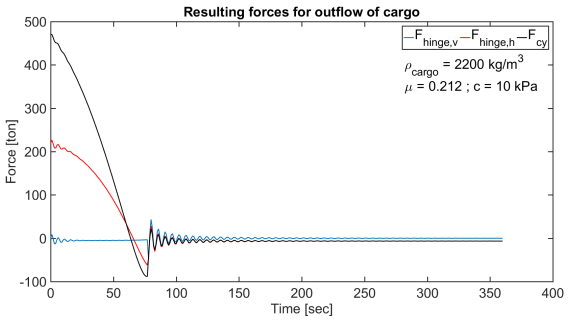

Figure 3.34: Effect of outflow of solid cargo with friction and cohesion

From the graphs it is learned that both friction and cohesion cause the necessary hydraulic cylinder force to decrease. When there is friction or cohesion of the cargo to the hopper wall, this causes a force along the wall in the direction of the motion of the cargo (figure 3.30). Due to its direction, the frictional force that acts on the hopper walls causes a closing moment around the hinges. As a result, the force required in the hydraulic cylinder to maintain a stationary opening angle becomes lower.

The y'- hinge force on the other hand increases for both situations compared to the load case displayed in figure 3.32. Due to the angle of the hopper walls, the frictional force that act along them does work in both the z'- as well as in the y'- hinge direction. Due to the direction of the frictional forces, the friction contribution in the y'-direction causes an increase in forces compared to the friction- and cohesion-less situation. Although the determined forces do increase, the resulting forces that were found do not exceed the forces that were found with the static open barge model nor do they approach the y'-orientated hinge forces that were found for the closed barge.

The z' hinge forces are again found to be equal to or in the vicinity of zero. Since the discharging barge is only considered in an upright position, where all processes and forces are completely equal for both half-hulls it is evident that no forces should occur in the z' hinge direction. The buoyancy and the weight of the barge are in equilibrium at all time, and are equal for both half-hulls of the barge. The result is that no force is passed through the hinges in the z'- hinge direction. Just as for the cylinder and y'-forces small oscillations in the z'-forces are found due to the inflow of water.

3.5.3. Inverse outflow

Next the extreme situation of outflow, where cargo is expected to form bridges in the hopper due to bottom up crumbling is simulated. Figures 3.35 and 3.36 show the resulting forces in the hinges and hydraulic cylinder for a discharging barge with crumbling cargo. Again the left figure shows the situation for a cargo with only friction with the hopper walls, the right graph displays the resulting forces for a cargo with friction and cohesion. Again the chosen values are based on sandy soil (l) and on clayey soil (r). For this type of outflow, the cargo speed is reduced to $0.05\frac{m}{s}$ since for the higher outflow speed the discharge occurs too fast. A fast outflow causes large dynamic motion amplitudes in the behaviour of the barge which would overshadow the effects due to the outflow of the cargo.

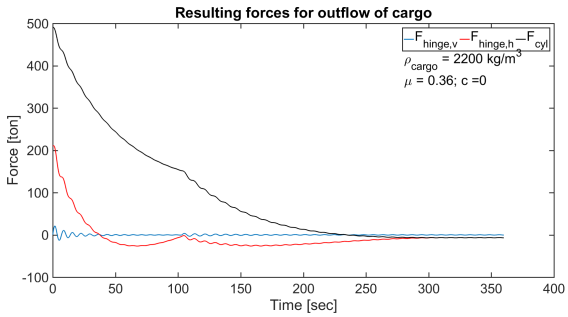

Figure 3.35: Effect of inverse outflow of solid cargo with friction

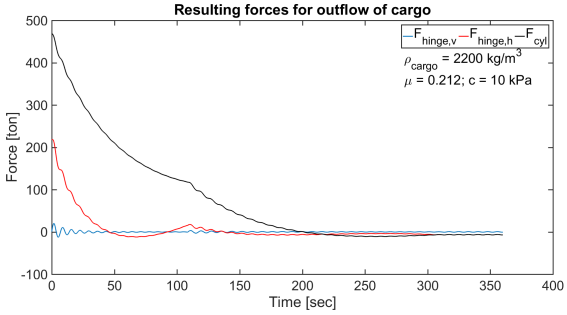

Figure 3.36: Effect of inverse outflow of solid cargo with friction and cohesion

For the crumbling cargo model, the initial values that are found for the resulting forces match the found forces for the normally out-flowing barge. Since the initial state of the barge and the cargo is equal for both types of outflow, this is a logical consequence rather than an outcome. The found resulting forces decrease due to the outflow of the cargo again, making the initial condition the most severe. Do note that for the crumbling type of cargo, the forces decrease relatively fast compared to the normal outflow. This faster decrease is the result of the decrease of the lever arms of the cargo with respect to the hinges. Due to this decrease the opening moment that the cargo causes around the hinges decreases , eventually leading to lower forces in the hinges as well.

Note that the fast decay of the cylinder forces even causes the y'-orientated hinge forces to become negative. Since the cargo is now moving upwards, the horizontal cargo pressures will remain high for a longer period, since the cargo forces now work mainly on the hoppers upper side walls. This in combination with the fast decrease in hydraulic cylinder forces causes that the sum of the forces in the y'-direction as it was determined in section 3.1.4 becomes negative, causing the y'-orientated hinge forces to become negative as well.

From the graphs, it can be seen that the process of crumbling of the cargo causes a stepwise decrease of forces. This is a direct result from the way that the displaced volume of the barge was modelled in Matlab. According to Archimedes principle, the barge has to displace a certain amount of water to create the buoyancy force that is needed to keep itself afloat. In the Matlab model, this displaced volume is taken to be equal to the submerged volume of both the barge and its cargo. In other words, the cargo that is present underneath the waterline does also contribute to the displaced volume of the barge.

In the first model, where the cargo surface moves down until all cargo has flown out of the hopper, the cargo that is still present seals the empty hopper space from the water, creating a large and steady added amount of displaced volume to the barge model up to the moment that the last cargo has flown out of the hopper. As a result of the sudden inflow of water after that, the small threshold was observed in the resulting forces on the moment the barge sank back into the water into it final equilibrium position (t=150s).

In the second model however, the cargo does not seal the hopper off from the seawater, causing the water to flow in freely directly after the crumbling has started. Due to this inflow of water and the ongoing loss of submerged cargo volume, the barge in the model raises out of the water due to the loss in weight only to sink back a little as result of the loss of available submerged volume at each time step. The resulting draught over time does therefore show a step-by-step decrease to the empty draught. This step-by-step decrease in draught causes little impulses in the forces that act on the barge for each time step, which causes the oscillating behaviour that is shown in the graphs.

The moment that the cargo loses it last contact with the water, the found forces show a small peak, after which the resulting forces smoothly decay to their steady state value. As a result from the assumed steady volume flow of the cargo, a constant volume of cargo is removed from the hopper each time step. Since this begins in the v-shaped part of the hopper and this is narrow at the bottom, the initial loss in cargo height per time step is large. Since the submerged cargo is expected to participate in the displaced volume of the barge, the rapid loss in height causes a rapid loss in added displaced volume by the cargo as well. When the cargo moves up to the wider part of the hopper, the loss in height per time step becomes smaller as well as the loss in displaced volume. Following from that the barge will start to stabilize just as the resulting forces in the hinges and hydraulic cylinders.

The moment the cargo loses its last contact with the water, suddenly all displaced volume needed to generate the required buoyancy has to result from the submerged volumes of the barge only. This will cause the barge to sink faster again, just as it did in the beginning of the simulation, causing the resulting force to decrease fast again as well. Since the barge is basically stabilizing up to the moment that the cargo losses its final contact with the water, and the barge starts to accelerate again after this point, the small peak in the resulting forces is found.

3.5.4. Conclusions on the effects of discharge

In accordance with the conclusions drawn after section 3.4, a final conclusion about the effects of opening the SHB is drawn using the information that is obtained using the model on the outflow of cargo that is discussed in this section.

From the results in this section, in agreement with the earlier stated expectations, it becomes clear that the resulting forces in the hinges and hydraulic cylinders of the SHB decrease when cargo is discharged. The determined forces decrease rapidly after the cargo starts flowing out of the hopper and reach a steady state at a force level more or less equal to zero tonnes.

When friction and cohesion are included in the outflow model, it can be seen that the added forces to the hopper walls result in an additional closing moment which results in a decrease in the required hydraulic cylinder forces. The direction of these forces also causes the y'-directed hinge forces to increase slightly. This increase however, does not cause the obtained hinge forces to exceed the forces that were found for the quasi-static closed barge that was simulated earlier on in this chapter.

When an inverse outflow of the cargo is considered, in which the cargo crumbles down bottom-up instead of flowing uniformly down through it, the conclusion can be made that this positively influences the decrease of resulting forces in the cylinders and hinges. The decrease in forces occurs at a faster rate, the hinge force in the y'-direction even becomes negative under the influence of the rapidly decreasing cylinder forces and the higher cargo forces that act on the upper hopper walls for this situation.

The z' hinge forces are found to be equal to zero, since the model is only concerned with a discharging SHB that is floating in a upright position. From section 3.4 however, it is known that the z' hinge forces do increase when roll angles are considered. The increase in z' hinge forces though will not be as significant as it was for the closed barge, since the total weight that has to be transferred trough the hinges in the z'-direction will decrease under influence of the outflow of the cargo.

For the opened situation of the barge, it is found that the reactions in the hinges and cylinders do not exceed those found for the closed barge. Based on the results from section 3.5, the results from section 3.4 are found to be very conservative. Discharge of the cargo results in a decrease of the forces, friction and cohesion of the cargo with the hopper walls during discharge do not result in an increase of the reactions as well. Ultimately, the closed barge load case proves to be a more governing one that the opened load case.

3.6. The influence of environmental forces

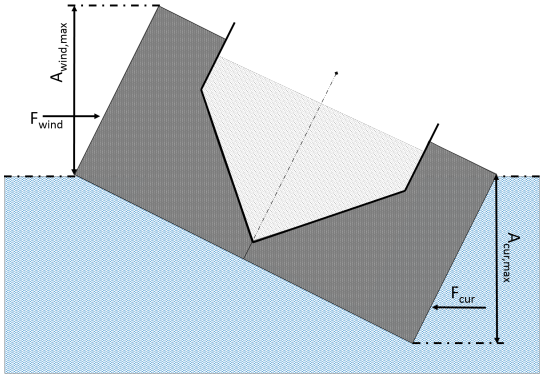

Figure 3.37: Wind & current forces on the split hopper barge.

In the model for the SHB no exciting forces due to the wind or current were included. It was assumed that these forces are not large enough to cause any major effect on the static response of the barges hinges and hydraulic cylinders. To make sure this assumption is valid, both the wind and current contributions to the exciting loads that act on the SHB were determined each for one extreme situation. In case the determined forces are found to be insignificant for these situations, the assumption that they will not have a significant contribution to the summation of exciting forces that act on the SHB is considered to be valid.

The forces that act on the barge due to the wind and current are the result of the drag that the wind and water flow have along the body of the barge. The resulting forces that act on the body of the barge are therefore drag forces. To determine the drag forces caused by the wind and the current the following relations are used:

$$F_{wind} = \frac{1}{2} \cdot \rho_{air} \cdot C_d \cdot H_{wall} \cdot L_{wall} \cdot u_{wind} \cdot |u_{wind}| \tag{3.27}$$

$$F_{cur} = \frac{1}{2} \cdot \rho_s \cdot C_d \cdot H_{wall} \cdot L_{wall} \cdot u_{cur} \cdot |u_{cur}| \tag{3.28}$$

The resulting forces for the wind and current are expected to be the highest when they act perpendicular to the largest possible area of the barge. For the current, the largest area it can work on is the submerged side wall of the barge. This area is the biggest when the barge is considered to have lost all of its free-board, meaning that the entire outer wall of the barge is submerged in the sea.

For the wind force, the largest area is also found on the side wall of the barge. For the wind however, the largest area is obtained when this outer wall of the barge is fully emerged from the water. Both the extreme situation for the wind and the current drag force are shown in figure 3.37.

For the calculations of the wind and current drag force on the outer walls of the barge, the same barge dimensions were used as in the Matlab model. The barge is assumed to be fixed in its position, although the exciting forces work on it. The drag coefficient of the barge is assumed to be the same as that of a cube in a flow, C_d = 1.05, for both the wind and current calculation. For the wind a relatively high wind speed of $U_{wind} = 21 \frac{m}{s}$ is taken, for the current a speed of $u_{cur} = 2knots$ is used in the calculation.

The resulting drag forces that excite the barge due to the presence of wind and current are than found to be equal to $F_{wind} \approx 32t$ & $F_{cur} \approx 16t$. When these environmental forces are compared with the other exciting forces that act on the barge (+1000t), it is found that they are much smaller. Therefore, completely in line with the earlier made assumption, the forces due to the wind and current drag on the body of the SHB model are not large enough to have a significant contribution to the summed exciting loads that act on the barge in the quasi-static equilibrium.

3.7. Chapter summary

In section 3.1 the quasi-static Matlab model of the SHB is defined. In section 3.2 it is used to study the effect of roll on the hinge and cylinder reactions. The results show that roll in general causes the resulting forces to decrease. Only the z' hinge forces increases due to the additional weight that has to be supported by the hinges due to the lifting of the upper half-hull out of the water. Furthermore, it is learned that the required forces in the hydraulic cylinders and the bottom chock forces that result from the pre-tension in the hydraulic cylinders, have a significant effect on the y'-orientated reactions that are found in the hinges. A high hydraulic cylinder force is found to result in a high hinge reaction in the y'-direction.

In section 3.3, the quasi-static SHB model is used to study the influence that the cargo density has on the resulting forces in the hinges and cylinders. Both a solid, liquid and a sliding cargo were considered. For the hydraulic cylinders it is found that cargoes of a sliding type will dominate the responses for increasing angles of roll. The highest required cylinder force however occurs in an upright position and is equal for all types of cargo as long as the barge kept at an equal draught.

With regards to the hinge forces, first it is found that the solid and liquid cargo types yield the highest forces in the hinges for the y'-direction. For the z'-orientated hinge forces, it is found that the mentioned supported weight effect due to the upper half-hull that is supported by the lower one is most severe for the solid cargoes. Since no cargo flows out of the hopper for the solid cargo, the highest weight has to be supported by the hinges. As a result, the z' hinge forces for the solid cargo type become the highest.

Sections 3.4 and 3.5 are used to find the combined effect of opening the barge together with the outflow of cargo. From these sections it is found that the forces in the hinges and hydraulic cylinders decrease when cargo starts to flow out of the hopper. When this outflow would not occur, the open configuration of the barge together with an angle of roll results in an increase of the forces in the hydraulic cylinders and in the hinges in the z'-direction. However, since neglecting the outflow of cargo is found to be very conservative an increase in forces for the opening of the barge is not expected.

Since the bottom chocks do not work in the opened situation, the hydraulic cylinders can only load the barge with the force necessary to counteract the opening moment around the hinges. This force is low compared to the cylinder force that acts on the closed barge. As a result, the y' hinge forces turn out to be lower for the opened situation. When friction and cohesion of the cargo with the hopper wall during the outflow is taken into account, the resulting y'-orientated hinge forces do increase slightly. However, the forces that are found for the closed barge are still not exceeded. Friction and cohesion do also result in a closing moment around the hinges, hence the required hydraulic cylinder forces decrease. The conclusion is drawn that for the static barge, opening it does not lead to an increase in hinge and/or cylinder forces. The closed barge proves to be the most governing load case as a result.

Finally, section 3.6 is used to show that neglecting the effects due to the wind and the current on the barge is valid. The forces are determined for one extreme situation, which already shows that the force contributions due to the wind and the current do not play a significant role in the quasi-static barge model.

4

Modelling the dynamics

This chapter will present the method that is used for finding the workability limits of the SHB in a dynamic environment. First the general steps of the method are introduced after which the theory behind them is explained. Special attention is given to adjustments that are required to deal with a SHB that is carrying a liquid cargo. To study the limits of a split hopper barge that operates in an irregular sea, expanding the quasi-static method that was presented in chapter 3 is not preferred. For finding the forces that result from a dynamic sea environment, the diffraction and potential equations of the barge have to be solved. This is better done using an existing software tool, the method that is presented in this chapter is based on Ansys AQWA.

4.1. Model method

To conclude on the workability limits of the SHB, the hinge and hydraulic cylinder forces have to be found again. In chapter 3 it was learned that these forces result from the splitting forces that act in the splitting plane of the SHB. To obtain these splitting forces for a SHB that is excited in a dynamic sea environment, Ansys AQWA is used.

Ansys AQWA is a commonly used software package to determine the effects of wind, wave and current on offshore and marine structures. According to the AQWA user manual ("AQWA User Manual", 2012):

> *AQWA simulates the linearized hydrodynamic fluid wave loading on floating or fixed rigid bodies. This is accomplished by employing three-dimensional radiation/diffraction theory and/or Morrisons's equation in regular waves in the frequency domain.*

In the method that is proposed, the results from the standard AQWA simulations are used as input for the AQWA GS environment, which is capable of determining the splitting forces that act in an user define splitting plane of the investigated structure. Since it are the splitting forces that are of interest, a method that is based on the Ansys AQWA software tool is the most straightforward.

Figure 4.1 shows the flow chart of the method that is proposed to find the workability limits of the SHB. From the top down, first input for the Ansys simulations is generated. The hull of the barge is modelled in Rhino and information on the inertias and mass of the barge is determined using excel calculations.

Using this input, Ansys simulations are run to solve the diffraction and radiation problems of the barge. The model is ran for a variety of regular frequencies to be able to perform a spectral analysis of the results later on. The output from this model is used for Ansys AQWA GS. In AQWA GS, the splitting forces in the splitting plane of the barge are determined. The resulting force RAO's are transferred to Matlab to be processed.

In Matlab, the forces in the hinges and hydraulic cylinders that result from the force amplitudes are determined. Using a spectral analysis the response spectrum of the forces is determined. From this spectrum the maximum responses can be calculated. The mean response of the hinge and cylinder forces is determined and added to these maximum forces in the end to obtain the complete hinge and cylinder reactions.

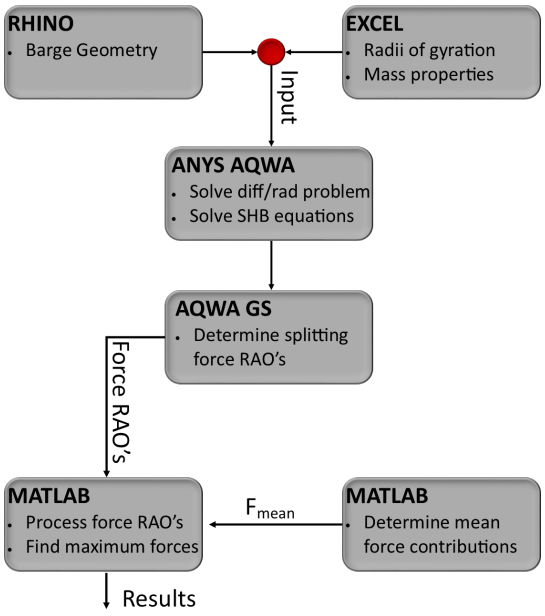

Figure 4.1: Flow chart for the proposed method.

4.2. Model theory

4.2.1. Geometry

For the AQWA simulations, the outer hull geometry of the SHB is required. Based on the lines plan of the barge, this geometry can be built in a 3D CAD software tool. For this research Rhinoceros 5 is used. Since the outer hull geometry of the barge is required, no effort is made to model the inside of the barge in detail. Figure 4.2 gives an impression of the outer hull geometry as it was used.

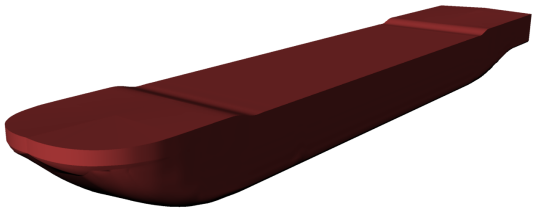

Figure 4.2: The split hopper barge model in Rhino.

In the model of the SHB, exterior details such as skegs, ducts and open spaces are not modelled in detail. By neglecting these parts, the buoyancy of the modelled SHB is not estimated correctly in the simulations. The correction for this is explained later on.

The barge is modelled as a single body, i.e. the two half-hull are modelled rigidly connected without any gap separating them. Modelling the gap is expected to cause interaction problems in the AQWA simulations. To prevent unexplainable effects from occurring, it is better to model the barge in one piece. Besides, for the calculation of the splitting forces in AQWA GS it is not necessary to model the two half-hull separately. AQWA GS can determine these forces for all types of rigid bodies in a user defined splitting plane.

For the Barge model, contrary to the model in chapter 3, its actual dimensions and shapes are used. Furthermore, the dredging draught is already taken into consideration. In the model, the barge its mean waterline corresponds with the z = 0 plane. By doing so the displaced water volume of the model becomes fixed. Since this displacement is the result of the combined weight of the barge and cargo, it can be used to find the mass of the barge. By subtracting the known mass of the cargo from the equivalent mass resulting from the fixed displacement, the mass of the barge including the simplifications that were made to it is obtained.

4.2.2. Mass and inertia

Next to the geometry of the barge, details on its mass properties and radii of gyration are required for the AQWA simulations as well. To determine the required input, first the barge and its cargo are regarded separately. For each its geometry is subdivided into sections that can be described with arbitrary shapes, for which it is easy to find the moments of inertia and the CoG. The obtained results for the individual sections is combined to find the required information for the entire model.

Barge

First the empty barge is considered. The geometry of the barge is subdivided into n sections that can be described by rectangular bodies, figure 4.3. The centre of gravity for each body is assumed to be in the exact centre of it, its mass m_n follows from the barge its mass distribution that was found using the fixed displacement. For each section the mass moment around a fixed point in the global coordinate system can be determined. For the X,Y,Z direction these moment follow from:

$$SM_{n,x} = m_n \cdot \overrightarrow{CoG}_{n,x} \tag{4.1}$$

$$SM_{n,y} = m_n \cdot \overrightarrow{CoG}_{n,y} \tag{4.2}$$

$$SM_{n,z} = m_n \cdot \overrightarrow{CoG}_{n,z} \tag{4.3}$$

Here $\overrightarrow{CoG}_n$ is the distance from the centre of gravity to the origin of the global coordinate system. By adding up the moments of all the sections and dividing it by the total mass of the empty barge, the coordinates of the centre of gravity for the empty barge are found:

$$CoG_{barge} = \frac{\sum_n SM_{n,x,y,z}}{\sum_n m_n} \tag{4.4}$$

Knowing the CoG of the barge, the moments of inertia for it can be determined. The inertia for each subsection of the barge is determined and placed in the barge coordinate system using Steiner's theorem:

$$I_{n,xx,yy,zz} = \frac{1}{12}\left(b_n^2 + h_n^2\right) \cdot m_n + m_n \cdot d_n^2 \tag{4.5}$$

Here, b_n and h_n describe the width and height of each section and d_n is the straight distance from the CoG of the section to the body axes of the barge.

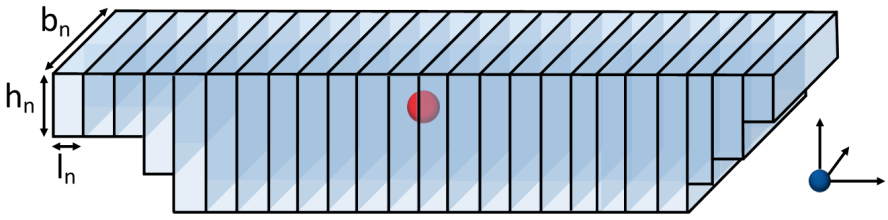

Figure 4.3: Rectangular barge sections.

Cargo

To obtain the required information about the cargo, it is regarded as a solid block. Just as the barge , the cargo is subdivided over its length into j equal sections. To be able to combine the barge and cargo data later on, the amount of longitudinal sections in which the cargo is subdivided is kept equal to the amount of sections that were used for the hopper in the barge calculations.

Due to the shape of the cargo, it is not possible to consider the cargo sections as rectangular bodies directly. Therefore an additional step is required in which each cargo section is divided into r horizontal sections as well. Figure 4.4 shows the subdivided cargo.

To find the centre of gravity for each section j of the cargo, again the mass moments around the origin of the global coordinate system are used:

$$SM_{j,x} = \sum_r m_{j,r} \cdot \overrightarrow{CoG}_{j,r,x} \tag{4.6}$$

$$SM_{j,y} = \sum_r m_{j,r} \cdot \overrightarrow{CoG}_{j,r,y} \tag{4.7}$$

$$SM_{j,z} = \sum_r m_{j,r} \cdot \overrightarrow{CoG}_{j,r,z} \tag{4.8}$$

Where $\overrightarrow{CoG}_{j,r}$ again follows directly from the rectangular geometry of each slice of the cargo section. $m_{j,r}$ is the weight of each slice. This weight follows from the volume of each slice in combination with the cargo density:

$$m_{j,r} = b_{j,r} \cdot h_{j,r} \cdot l_{j,r} \cdot \rho_c \tag{4.9}$$

The centre of gravity of a complete section j is than found using:

$$CoG_j = \frac{SM_{j,x,y,z}}{m_j} \tag{4.10}$$

Here m_j is the weight of the section of cargo that follows from the summations of the weights of the slices from which it was build up. For each section of the cargo the inertia around the combined centre of gravity of the cargo is found using:

$$I_{m,xx,yy,zz} = \sum_j I_{j,xx,yy,zz} + m_j \cdot d_j^2 \tag{4.11}$$

Since all cargo sections are equal, the determined mass and inertia holds for all of them. Only the x-coordinate of the centre of gravity changes per section of cargo. Note that this x-coordinate is equal to the x-coordinate of the hopper section at the same location of the specific section of cargo.

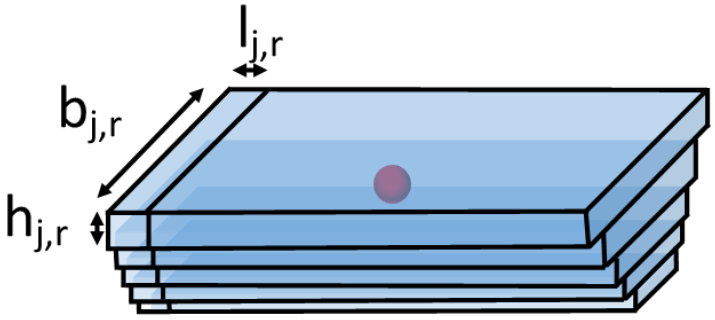

Figure 4.4: Rectangular cargo sections and slices.

Combined inertias

Now that for each section the inertias and CoG for both the cargo and the barge are defined, their contributions can be combined to obtain the inertias and CoG of the barge and cargo together. First the combined CoG is determined. Note that the location of the x-coordinate of each section is always in the middle of the section. For y- and z-coordinate their locations can be found using:

$$CoG_{y,z} = \frac{m_n \cdot CoG_{n,y,z} + m_j \cdot CoG_{j,y,z}}{m_n + m_j} \tag{4.12}$$

The combined inertia from the barge and its cargo can be found by adding up the individual inertia terms per section and by applying Steiner's rule again:

$$I_{xx,yy,zz} = \sum_n \left(I_{n,xx,yy,zz} + I_{j,zz,yy,zz} + m_n \cdot d_n^2 + m_j \cdot d_j^2 \right) \tag{4.13}$$

The radii of gyration are found by dividing the determined inertia in each direction by the mass of the complete barge:

$$k_{xx,yy,zz} = \sqrt{\frac{I_{xx,yy,zz}}{M_{SHB}}} \tag{4.14}$$

Where M_{SHB} is the summation of the masses of all the sections of the barge and the cargo. This mass has to be in equilibrium with the displaced volume of the barge.

4.2.3. AQWA simulation

Using the build geometry, the mass properties and the radii of gyration of the SHB, the Ansys AQWA model can be run. The barge geometry is put into AQWA using the Ansys Spaceclaim environment. In the CoG of the model a point mass with inertia is added. Furthermore, some additional viscous roll damping is added for the roll direction.

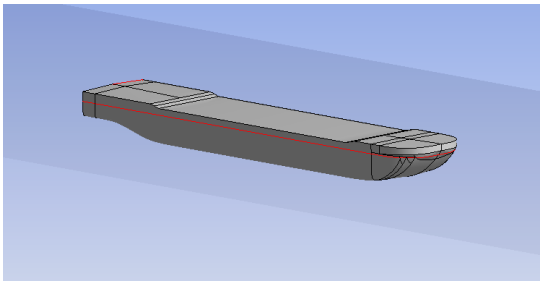

Figure 4.5: Ansys Aqwa model.

Viscous damping of the barge is the damping it experiences due to skin friction, forward speed, etc. This damping is always present but its effect is usually found to be negligible in comparison with the potential damping of a vessel. For a roll motion however, the potential damping is small, the roll damping of the barge is therefore governed by viscous damping. Since AQWA is based on potential theory, viscous effects are not taken into account. This means that the roll damping of the model is small, causing extreme roll responses around the natural roll frequency. Based of some Seaway data that is available, the roll damping of the barge is iteratively tuned to get its roll response amplitude in the same order of magnitude.

Effectively Ansys AQWA is used to solve the equation of motions of the barge in the frequency domain. These equations of motion follow from:

$$\mathbf{M}_{SHB}\ddot{x}(t) = \sum \mathbf{F}_{exc}(t) \tag{4.15}$$

Here, $\mathbf{M}_{SHB}$ is the mass matrix of the SHB, $\ddot{x}(t)$ is a vector containing the accelerations of the barge in all 6 directions. $\mathbf{F}_{exc}(t)$ are the exciting forces that act on the SHB. For the simulations in AQWA, no difference is made between the mass of the empty barge and the rigid mass of the cargo. This rigid/static mass of the cargo is therefore included in $\mathbf{M}_{SHB}$.

According to Journee (Journee & Massie, 2001), the force vector is build up from two different force contributions. Knowing, the excitation due to waves and the hydro-mechanic excitation:

$$\mathbf{F}_{exc}(t) = \mathbf{F}_{w}(t) + \mathbf{F}_{hm}(t) \tag{4.16}$$

The latter contributions consists of a static and dynamic part. The static part, $\mathbf{F}_{hm,stat}$, can be described using a stiffness matrix, $\mathbf{C}_{SHB}$, that is in phase with the displacement, $x(t)$, of the barge. The dynamic contribution, $\mathbf{F}_{hm,dyn}$ is described using an added mass and added damping matrix. The added mass matrix, $\mathbf{A}_{SHB}$ is in phase with the acceleration, $\ddot{x}(t)$ of the barge. The added damping matrix, $\mathbf{B}_{SHB}$, is in phase with the velocity, $\dot{x}(t)$, of the SHB. The hydromechanic force can then be written as:

$$\begin{aligned} \mathbf{F}_{hm}(t) &= \mathbf{F}_{hm,stat}(t) + \mathbf{F}_{hm,dyn}(t) \\ &= -\mathbf{C}_{SHB}x(t) - \mathbf{A}_{SHB}\ddot{x}(t) - \mathbf{B}_{SHB}\dot{x}(t) \end{aligned} \tag{4.17}$$

The complete equation of motion for the SHB is found by substituting equation 4.16 and 4.17 into equation 4.15:

$$(\mathbf{M}_{SHB} + \mathbf{A}_{SHB})\,\ddot{x}(t) + \mathbf{B}_{SHB}\dot{x}(t) + \mathbf{C}_{SHB}x(t) = \mathbf{F}_w(t) \tag{4.18}$$

To obtain the equations for the frequency domain, the following relations for $x(t)$ and $\mathbf{F}_w(t)$ are used:

$$x(t) = \Re\left[\hat{x}e^{i\omega t}\right] \tag{4.19}$$

$$\mathbf{F}_w(t) = \Re\left[\hat{F}e^{i\omega t}\right] \tag{4.20}$$

Using these relations the equations of motion for the SHB as they are solved by Ansys AQWA in the frequency domain are found to be equal to:

$$\left[-\omega^2(\mathbf{M}_{SHB} + \mathbf{A}_{SHB}) + i\omega\mathbf{B}_{SHB} + \mathbf{C}_{SHB}\right]\hat{x} = \hat{\mathbf{F}}(\omega) \tag{4.21}$$

The model is simulated in AQWA for multiple regular wave frequencies. The solution of the program is used to obtain the splitting forces in Ansys AQWA GS.

4.2.4. Splitting forces in AQWA GS

Using the solved equations of motion of the SHB that follow from the simulation in Ansys AQWA, Ansys AQWA GS can be run. Using AQWA GS, the splitting forces that exist in the splitting plane of the SHB can be obtained. For a 3D dynamic model of the barge the splitting forces in all 6 DoF have to be found, knowing:

- Fx The splitting force in the x-direction
- Fy The splitting force in the y-direction
- Fz The splitting force in the z-direction
- Rx The moment around the x-axis
- Ry The moment around the y-axis
- Rz The moment around the z-axis

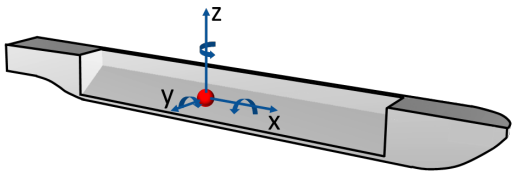

Figure 4.6: Splitting forces in the splitting plane of the SHB.

The orientation of these splitting forces in the in the splitting plane of the split hopper barge is shown in figure 4.6.

When these forces are known, the forces that result in the hinges and hydraulic cylinders can be obtained using simple forces equilibria in the 6 DoF. The splitting forces acting in the splitting plane of the SHB can be found by adding up all the force contributions around a single point X_Q, that is located in the splitting plane of the model. This point X_Q is indicated in figure 4.6 by the red dot. In the summations of the force contributions, only the forces acting on one half-hull are considered.

The first force that is considered is the contribution due to the external hydrostatic forces that work on the barge. The resulting force and moment are defined in the AQWA theory manual by ("AQWA Theory Manual", 2013):

$$\vec{F}_f(\omega) = \int_S (-p(\omega) \cdot \vec{n}) dS \tag{4.22}$$

$$\vec{M}_f(\omega) = \int_S \left[\left(\vec{X} - \vec{X}_Q \right) \times \left(-p(\omega) \cdot \vec{n} \right) \right] dS \tag{4.23}$$

Where S is the surface of the half-hull below the waterline and ω is the incoming wave frequency. $p(\omega)$ is the summation of the hydrostatic and hydrodynamic pressures, $\vec{n}$ is the normal vector of the hull surface pointing in the direction of the fluid field.

The gravitational contribution to the force and moment around point X_Q follow from:

$$\vec{F}_g(\omega) = \sum_j \left[(0,0,-m_j g) - \vec{\theta}(\omega) \times (0,0,-m_j g) \right] \tag{4.24}$$

$$\vec{M}_g(\omega) = \sum_j \left[\left(\vec{X}_j - \vec{X}_Q \right) \times \left[(0,0,-m_j g) - \vec{\theta}(\omega) \times (0,0,-m_j g) \right] \right] \tag{4.25}$$

In which $\vec{\theta}$ is the rotational motion response of the barge and m_j is its mass at the location X_j within the boundary box of the half-hull. Finally, the inertial contribution can be found using:

$$\vec{F}_m(\omega) = \omega^2 \sum_j m_j \left(u_j(\omega), v_j(\omega), w_j(\omega) \right) \tag{4.26}$$

$$\vec{M}_m(\omega) = \omega^2 \sum_j \{ m_j \left(\vec{X}_j - \vec{X}_Q \right) \times \left(u_j(\omega), v_j(\omega), w_j(\omega) \right) \} \tag{4.27}$$

here, $u_j, v_j \& w_j$ are the motion responses of the half-hull at location X_j

By summing up all the mentioned components at the location of the splitting point on the splitting plane, AQWA finds the resulting splitting forces that act in this plane. These forces are then returned as frequency dependent force RAO's.

4.2.5. Process data

After the splitting forces are determined, the forces in the hinges and hydraulic cylinders that result from them can be found. To find the dynamic forces, first the splitting force amplitudes are used to obtain the harmonic force responses per regular wave frequency.

According to the Ansys theory manual ("AQWA Theory Manual", 2013) the harmonic splitting forces in the time domain per regular wave frequency follow from:

$$p(t) = a_p \cos(-\omega t + \alpha + \vartheta) \tag{4.28}$$

Where a_p is the force RAO, α is the wave phase angle relative to the global coordinate system in radians and ϑ is the phase angle of the force RAO with respect to the wave. $p(t)$ is the harmonic splitting force. Using this relation the harmonic forces for all six degrees of freedom are obtained. Using these harmonic forces, the resulting forces in the hinges and hydraulic cylinders can be computed using simple force equilibria. The resulting forces that are of interest in this research are shown in figure 4.7.

The static force contributions that are used are obtained using a modified version of the Matlab model that was made in chapter 3. In the model the barge is only considered in an upright position ($\theta_r = 0 deg$).

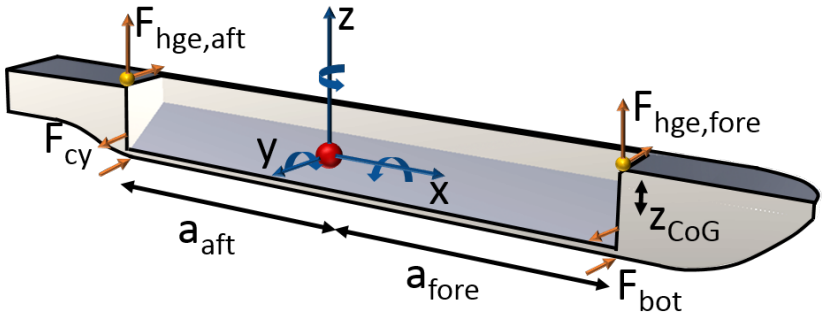

Figure 4.7: Resulting forces in the splitting plane of the SHB.

Vertical hinge forces

Using the harmonic splitting forces, first the vertical components of the hinge forces are determined. From figure 4.6 it is clear that the two vertical hinge force contributions have to account for the total force FZ that works in the splitting plane:

$$FZ(t) = F_{hge,z,fore}(t) + F_{hge,z,aft}(t) \tag{4.29}$$

Furthermore, the vertical hinge force contributions are solely accountable for the moment around the y-axes:

$$RY(t) = -F_{hge,z,fore}(t) \cdot a_{fore} + F_{hge,z,aft}(t) \cdot a_{aft} \tag{4.30}$$

In which a_{fore} & a_{aft} are arms of the hinge forces with respect to the longitudinal location of the splitting forces. The resulting vertical hinge forces are then found using:

$$F_{hge,z,fore}(t) = \frac{RY(t) - FZ(t) \cdot a_{aft}}{-(a_{fore} + a_{aft})} + F_{hge,z,stat} \tag{4.31}$$

$$F_{hge,z,aft}(t) = FZ(t) - F_{hge,z,fore}(t) + F_{hge,z,stat} \tag{4.32}$$

Where $F_{hge,z,stat}$ is the mean contribution to the vertical hinge force.

Cylinder forces & bottom chock forces

Next the hydraulic cylinder forces are determined. The hydraulic cylinders are again assumed to be the only components that are capable of resisting the opening moment that exists around the hinges of the barge. This opening moment is defined by:

$$M_{op}(t) = RX(t) + FY(t) \cdot z_{CoG} + M_{op,stat} \tag{4.33}$$

In which z_{CoG} is the vertical distance between the location of the splitting forces and the hinges. $M_{op,stat}$ is the static opening moment around the hinges that is determined using the approach of chapter 3 again.

The required hydraulic cylinder forces are than found by:

$$F_{cyl,req}(t) = \frac{M_{open}(t)}{n_{cyl} \cdot h_{cyl}} \tag{4.34}$$

Note that it is still assumed that the forces in the hydraulic cylinder is equal for both the fore and aft cylinders. This comes from the fact that there is only one equation for the opening moment of the barge and thus only one unknown variable can be determined using it.

Using the cylinder forces the bottom chock forces can be determined. Just as in chapter 3 these forces result from the difference between the installed hydraulic cylinder capacity and the required hydraulic cylinder capacity.

$$F_{bot}(t) = \frac{\left(F_{cyl,pre} - F_{cyl,req}(t)\right)}{h_{hge}} \tag{4.35}$$

In which, $F_{cyl,pre}$ is again the installed hydraulic cylinder capacity and h_{hge} is the lever arm of the bottom chocks with respect to the hinges.

Horizontal hinge forces

Using the hydraulic cylinder and bottom chock force the horizontal contributions to the hinge forces can be obtained. To do so, first the horizontal forces that have to act in the plane of the hinges and hydraulic cylinders are determined for both the fore and aft of the barge. These forces are described by:

$$FY_{fore}(t) = F_{hge,y,fore}(t) + F_{bot,fore}(t) - F_{cyl,inst,fore} + F_{hge,y,stat} \tag{4.36}$$

$$FY_{aft}(t) = F_{hge,y,aft}(t) + F_{bot,aft}(t) - F_{cyl,inst,aft} + F_{hge,y,stat} \tag{4.37}$$

The horizontal forces are found using the following equations:

$$FY(t) = FY_{fore}(t) + FY_{aft}(t) \tag{4.38}$$

$$RZ(t) = FY_{fore}(t) \cdot a_{fore} - FY_{aft}(t) \cdot a_{aft} \tag{4.39}$$

The horizontal forces in the planes of the cylinders, chocks and hinges than become:

$$FY_{fore}(t) = \frac{RZ(t) + FY(t) \cdot a_{aft}}{a_{fore} + a_{aft}} \tag{4.40}$$

$$FY_{aft} = FY - FY_{fore} \tag{4.41}$$

Using these forces, the horizontal contributions to the hinge forces become:

$$F_{hge,y,fore}(t) = FY_{fore}(t) - F_{bot,fore}(t) + F_{cyl,inst,fore} - F_{hge,y,stat} \tag{4.42}$$

$$F_{hge,y,aft}(t) = FY_{aft}(t) - F_{bot,aft}(t) + F_{cyl,inst,aft} - F_{hge,y,stat} \tag{4.43}$$

To obtain the total hinge forces of the SHB the vertical and horizontal forces have to be combined. This is done for both the fore and aft hinge using:

$$F_{hge}(t) = \sqrt{F^2_{hge,z}(t) + F^2_{hge,y}(t)} \tag{4.44}$$

4.2.6. Spectral analysis

The forces that were found in sections 4.2.5 to 4.2.5 are still the time dependent harmonic forces for regular frequencies per meter wave height. To find the force response spectra from them, first the force RAO's in the hinges, hydraulic cylinders are required. These RAO's for the forces, TF_F, are found by combining the amplitudes of the responses per regular wave frequency. So for each regular force that was computed, the amplitude is determined. These amplitudes are than combined to form the required force RAO's.

By doing the above for both the hinge and cylinder the forces for all the considered wave directions, the force amplitudes in the hinges and hydraulic cylinder per wave direction are obtained. Using them, the energy spectra of the resulting forces be found using:

$$S_F(\omega) = |TF_F(\omega)|^2 S_\omega(\omega) \tag{4.45}$$

The spectral moments for such an energy spectrum can then be determined using:

$$m_n = \int_\omega \omega^n |S_F(\omega)|^2 d\omega \tag{4.46}$$

Using these moments, the maximum resulting dynamic forces in the hinges and hydraulic cylinders in irregular seas can be determined from:

$$F_{max,dyn} = 2 \cdot \sqrt{m_0} \cdot \sqrt{\frac{1}{2} \cdot \log\left(\frac{D_{storm}}{T_z}\right)} \tag{4.47}$$

Where the mean zero crossing period is defined by:

$$T_z = 2 \cdot \pi \cdot \sqrt{\frac{m_o}{m_2}} \tag{4.48}$$

To obtain the complete forces that act in the hinges and hydraulic cylinders, the average component to them has to be added. This average component follows from the mean of the regular resulting forces that were used to obtain the force RAO's.

$$F_{max} = F_{max,dyn} + F_{avg} \tag{4.49}$$

The maximum resulting forces for multiple wave directions, periods and for different significant wave heights can then be compared to the design limits of the hinges and hydraulic cylinders of the split hopper barge. Using this comparison conclusions on the technical limits of the SHB in the simulated conditions can be drawn.

4.3. Adaptations for liquid cargo

The simulations using the approach that was shown above do not take the movements of the cargo inside the hopper into account. To be able to draw conclusions about the hinge and cylinder-forces for the situation where the SHB is carrying a non-solid cargo, the approach that was shown has to be expanded.

To simplify the presented problem of moving cargoes, the method is only adjusted for liquid cargo motions in the hopper. In appendix C the coupled equations of motions for the barge and its liquid cargo are determined. From them it was found that the effect that the liquid cargo has on the system can be captured by an additional added mass matrix and by a loss in stiffness that can be described by a loss in metacentric height (i.e. the stability lever arms of the barge decrease in size).

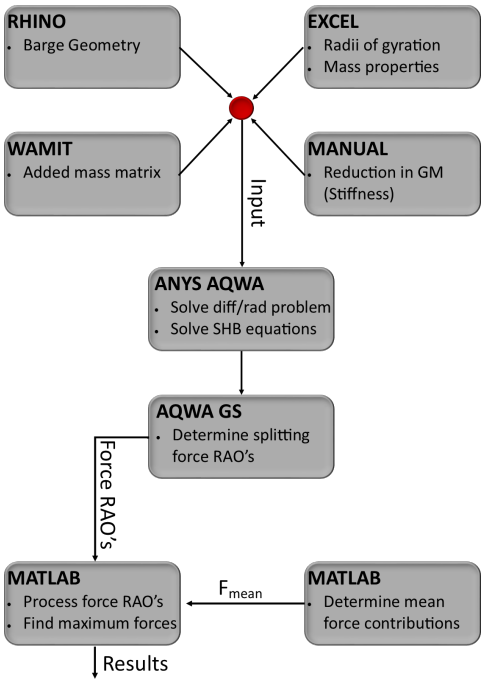

Figure 4.8: Flow chart for the proposed method adjusted for liquid cargoes.

The additional added mass is estimated using a WAMIT simulation of a SHB with and without liquid cargo. It was found that the natural frequencies of the hopper with a liquid cargo do not correspond with the relevant frequencies in the wave spectrum. As a result, the effect of a liquid cargo on the behaviour of the SHB was found to be linear. Based on the differences between the added mass plots of both, an estimation is made on the added mass that has to be added to the AQWA simulations. The loss in metacentric heights follows directly from a relation given in the hydromechanics book by Journee (Journee & Massie, 2001).

Based on the knowledge that is presented in appendix C, the proposed method that was described in section 4.2 can be adjusted for the SHB that is loaded with a liquid cargo. A flow diagram for the adjusted method is shown in figure 4.8. By accounting for the motions of the liquid cargo in the SHB, the method required to determine the maximum reactions in the hinges and cylinders of the SHB in irregular waves is obtained.

5

Results

In this chapter, the forces that result in the hinges and hydraulic cylinders of one type of split hopper barge in irregular seas are determined. The method for determining the forces in the hinges and hydraulic cylinders of a SHB that was shown in chapter 4 is used. The maximum hinge and hydraulic cylinder forces are determined for one type of SHB. The method is used for both a SHB is carrying a solid as well as a liquid cargo. The maximum forces that are obtained using the calculations are compared to the design limits of the hinges and hydraulic cylinders that can be determined using the Bureau Veritas relations that where shown in chapter 2.

In the first section of this chapter the general input that is used for the simulations/calculations is explained. Details on the used SHB are given, as well as some details on the simulation/ calculations. In section 5.2 and 5.3, the details on the simulations with a SHB carrying a solid and a liquid cargo are given. The relevant results obtained using the simulations are discussed as well.

5.1. Input

For the simulations and calculations that are shown in this chapter a model of the Terraferre 501/502 SHB was build. The TF501/502 is a pushed SHB, in the simulations however the pusher tug is not included. Some general design details on the TF501/502 SHB itself are given in table 5.1.

Terraferre 501/502 details:	
Length	94.30m
Breath	16.45m
Draugth [full]	5.8m
Length hopper	58.52m
Breath hopper	12.04m
Volume hopper	about $3800m^3$

Table 5.1: Terraferre 501/502 details.

Using the mass and inertia calculations shown in section 4.2.2, the centre of gravity and radii of gyration of the barge model are found. The total mass of the barge is estimated based on the actual displacement that the model has due to its fixed draught. In the AQWA simulations the mass of the model is taken into consideration using a point mass in the determined CoG of the barge. For the splitting force analysis, the mass and inertia of the system is divided equally over the two half-hulls.

In chapter 4 it was already mentioned that due to the linearization of the equations of the barge in Ansys, the viscous effects to the damping of the barge are not automatically included in the simulations. Since this causes a large overestimation of the roll motion amplitude of the barge, viscous damping has to be added by hand to the model. Using Seaway data, the viscous damping of the model in Ansys is iteratively tuned. The motions amplitudes of the model are therefore in the expected order of magnitude.

The barge in Ansys is subjected to 15 different wave angles varying between $-\pi$ and π. Using a mesh size between $0.75m$ and $1.4m$, a maximum frequency of $2.6\frac{rad}{s}$ could be simulated. A range 48 different wave frequencies where selected with regular wave frequencies between $0.05\frac{rad}{s}$ and $2.4\frac{rad}{s}$.

Using these settings the TF501 SHB model was run, and the splitting forces where obtained using the AQWA GS environment. The data from the obtained RAO's was processed using Matlab and a mean force contribution was added. The mean force contributions that are added to the dynamic hinge and cylinder forces are determined for a rectangular barge with an equal draught and equivalent displaced volume as the TF501/502.

The response spectrum of the obtained resulting hinge and hydraulic cylinder forces is found using a JONSWAP spectrum with a peak enhancement factor of $\gamma = 3.3$. From this response spectrum the maximum resulting forces are determined and are compared to the design limits of the barge. The maximum resulting forces are determined for significant waves heights varying between 2.5 and 3.5 m and for an extreme duration of 3 hours. Significant wave period within a range of 3 to 15 seconds are used for the spectral analysis. The results for a significant wave height of $H_s = 3.0m$ are shown and explained, the end results for the wave heights $H_s = 2.5m$ and $H_s = 3.5m$ are put in appendix D.

5.2. Results for solid cargo

First, the barge carrying a solid cargo of $\rho_c = 2200 \frac{kg}{m^3}$ is considered. The results that were found for the simulations with it are presented. In the first section, the splitting force RAO's that were obtained using Ansys are shown and shortly described. The results for the hydraulic cylinder, vertical hinge and horizontal hinge forces will be explained afterwards. Ultimately, the horizontal and vertical hinge forces are combined to conclude on the total hinge force.

5.2.1. Splitting force RAO's

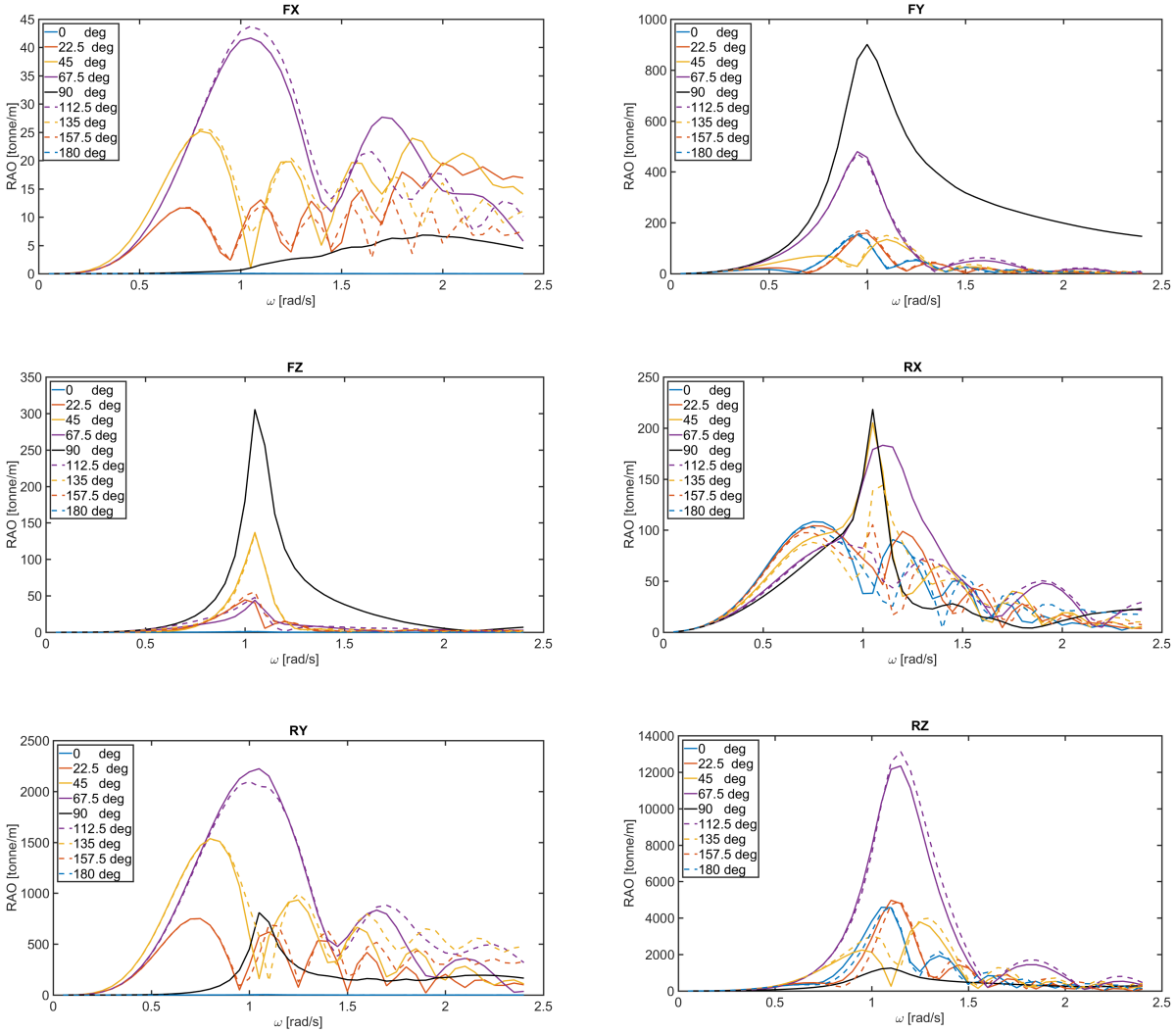

Figure 5.1: Splitting force RAO's.

Figure 5.1 shows the splitting force RAO's that are obtained using Ansys AQWA GS for the SHB carrying a solid cargo. The RAO's are shown for all the wave directions that where simulated in Ansys. Note that for the different force amplitudes, different wave directions result in the highest response. Since the splitting forces follow from the solution of the equation of motions in Ansys, their effects can be described using the four major components of the equations of motion of the barge knowing:

- Inertial forces
- Damping forces (Radiated waves)
- Static forces (Hydrostatic changes)
- Exciting forces (Diffracted waves, incident waves)

The explanation for the obtained forces is found to be the same causes for each considered direction. Therefore, to keep from making the explanation of the shown splitting forces to complex or elaborate, the splitting force components for only one direction are shown. For the y-direction splitting force, FY, the force contribution amplitudes and resulting splitting forces RAO's for following (l) and beam waves (r) are shown in figures 5.2 and 5.3.

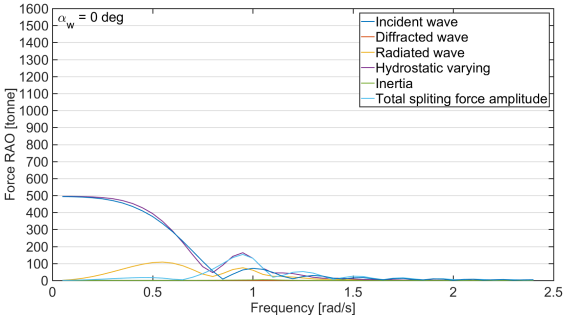

Figure 5.2: Y-direction splitting force components for following waves .

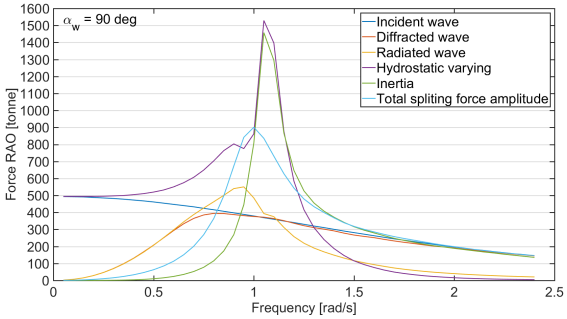

Figure 5.3: Y-direction splitting force components for beam waves.

The figures show that for low frequency waves, the different wave headings do not result in differences of the force components. For these low frequencies the wave lengths are long compared to the barge length. As a result, the barge will react to the resulting waves like it would to tidal variations of the water elevation. Accelerations and velocities are low, only a change in hydrostatic forces is the result. Thus only static splitting force components are found.

When a large wave frequency is considered, the waves become shorter. Eventually the wave length compared to that of the barge will be in such a range that the incident and diffracted wave excitations result in a more dynamic reaction of the SHB. For the 0 deg wave heading however, the waves move in the positive x-direction (stern to bow). Therefore, the barge its surge and pitch motion will be excited the most. The reactions of the barge in the sway and roll direction, that have a large effect on FY, will remain small. As a result the resulting splitting force in the y-direction remains small as well.

For the 90 deg. wave heading, the excitation of the barge occurs in the exact direction of the FY-splitting force. As a result, when the wave length are short enough to excite the barge dynamically, the accelerations and motions that result in the y-direction are large. For this wave heading, a maximum acceleration of 0.6 m/s^2 is obtained. The resulting large accelerations, motions and displacements of the barge result in an increase of the inertial, damping and stiffness forces in it. The largest force contributions are found for frequencies near the natural roll frequency of the SHB. When than the different force contributions are added up, the splitting force that results will be large as well. For a wave frequency of approximately 1 rad/s the splitting force that results for beam waves is 6 times higher than that for a 0 deg. wave heading.

When the wave frequencies increase even further, the waves eventually become too short to excite the barge. The resulting motions and displacement of the barge become small. Only some diffracted wave forces will result in some inertial forces. In the case that really high wave frequencies will be considered, all splitting force component will approach zero.

Based on the motion, velocity and acceleration of the barge in combination with the incoming wave angle, the large differences in the splitting forces and moments can be explained. For surge, pitch and yaw the splitting forces are found to be the largest for 67.5 or 112.5 deg. wave headings. For sway, heave and roll beam waves result in the highest forces. Due to the large differences that are found for the splitting forces and moments of the barge for different wave headings, the differences in the resulting forces in the hinges and hydraulic cylinders can be expected to be large as well.

5.2.2. Hydraulic cylinder forces

To determine the required hydraulic cylinder forces, the splitting force RAO's are read into Matlab. Following the approach from chapter 4, they are used to find the harmonic splitting forces and moments per regular wave frequency first. Using these, the harmonic opening moment that acts on the barge can be determined for each regular frequency. By adding the mean opening moment to the harmonic one, the complete opening moment per regular wave frequency is found. Using this, the required harmonic cylinder forces can be determined, again first per regular wave frequency.

To illustrate the components that are added in Matlab, figure 5.4 shows the dynamic and average moment contributions to the opening moment that act around the hinges of the SHB for regular beam waves, ($\alpha_w = 90 deg$), with a regular frequency of $\omega = 1.05 rad/s$. Note that the dynamic contribution to the opening moment, in blue, oscillates with the considered frequency around a mean zero value. The average contribution, in red, has a static value that corresponds to the found value for the opening moment in chapter 3 for a zero angle of roll ($\theta_r = 0 deg$). For different regular wave frequencies the amplitudes that are found for the dynamic moment contribution obviously differ. Around the natural frequencies of the barge, the found amplitudes are the highest.

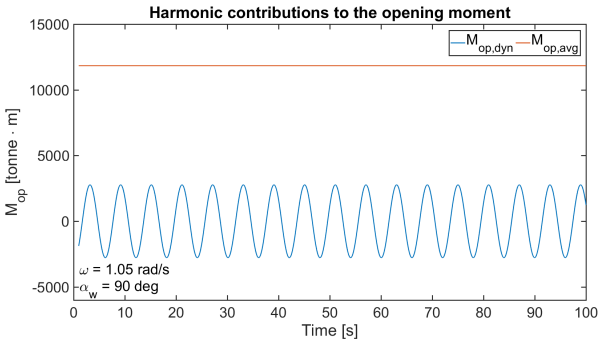

Figure 5.4: Dynamic and average contribution to the opening moment.

Following equations 4.33 and 4.34, the two force contributions are first added together to obtain the harmonic opening moment per regular wave frequency. From this, the hydraulic cylinder force can be obtained. For each regular wave frequency the force amplitude is determined. The different amplitudes are than combined to find the force RAO's of the cylinder forces that are to be used to determine the force response spectrum. The above is done for all the wave directions that where considered in the AQWA simulations, thus for each wave direction a separate RAO is found.

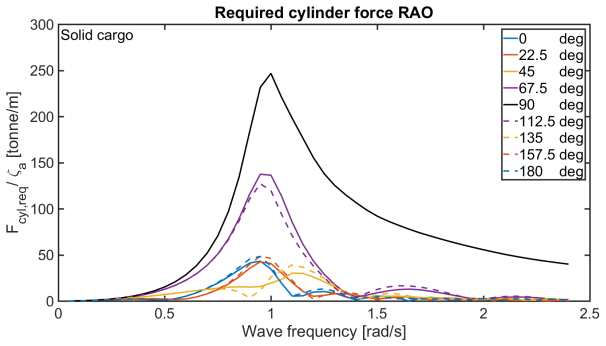

Figure 5.5: Hydraulic cylinder force RAO's.

Figure 5.5 shows the obtained force RAO's for the hydraulic cylinder forces. In the figure the RAO's for the wave directions $\alpha_w = 0 deg$ up to $\alpha_w = 180 deg$ are shown. The static force contribution that was obtained for the hydraulic cylinder forces is equal to 930 $tonne$.

The figure shows that the highest amplitudes are found for beam waves. From the splitting force RAO's that are shown in section 5.2.1 it was found that in beam waves the splitting moment around the x-axes, RX, is excited the most. Furthermore, the horizontal splitting force, FY, was found to be 6 times higher for beam waves compared to following waves. Since the RX-moment and the FY-force ultimately result in the dynamic opening moment of the barge, the required hydraulic cylinder forces that are found for this wave direction are the highest. As a result, the regular forces in the hydraulic cylinders will exceed those found for the other wave directions. For the resulting forces for beam waves a dynamic amplification factor, DAF, of 1.26 is found.

For the lowest and highest wave frequencies that are considered, the amplitudes that are found tend to zero. For these regular wave frequencies, the barge is found to be hardly excited by the waves. The low frequencies result in long waves, causing the barge to react like a fishing bobber. The high frequency waves are to short to excite the barge at all. The forces that result for these situations will be static ones, the dynamic force amplitudes are zero as a result.

Using the found force RAO's for the required hydraulic cylinder force, the response spectra of the hydraulic cylinder forces can be determined. For this calculation shown in equation 4.45, a JONSWAP spectrum is used. From the obtained response spectrum, the maximum expected required hydraulic cylinder forces for a 3 hour extreme can be determined using equations 4.46 to 4.48. To them the static/average force component is added to obtain the full required hydraulic cylinder forces.

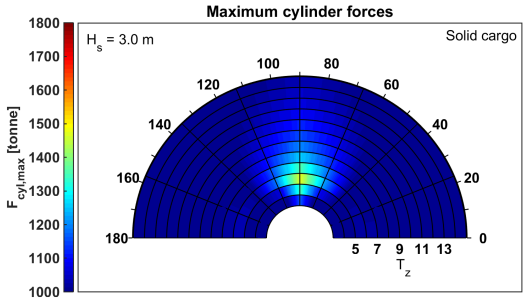

Figure 5.6: Maximum required hydraulic cylinder forces for a 3 hour storm.

Figure 5.6 shows the maximum required hydraulic cylinder forces that where found for the SHB carrying a solid cargo. In the figure the maximum forces for mean zero crossing periods varying between $T_z = 3s$ and $T_z = 15s$ are shown for wave directions varying between 0 and $180\,deg$. The figure shows that beam waves, $\alpha_w = 90\,deg$, result in the highest required hydraulic cylinder forces for the chosen conditions. The absolute peak, $F_{cy,req} = 1475\,tonne$, is found for a period of $T_z \approx 5s$. Do note that this period is close to the natural periods that where found for the SHB. For all wave directions the maximum forces are found for this period as a result.

In the shown graph, the cylinder limits of the TF501 SHB are not exceeded. In appendix D, the results obtained for irregular seas with $H_s = 2.5m$ & $3.5m$ are shown as well. There it is found that even for seas with a significant wave height of 3.5m the limits of the hydraulic cylinders for the SHB with solid cargo are not exceeded.

5.2.3. Vertical hinge forces

Using the harmonic forces that result from the splitting force RAO's, the vertical hinge force contributions are obtained as well. Figures 5.7 and 5.8 show the harmonic and average vertical hinge forces of the barge at a single regular frequency of $\omega = 1.05 rad/s$ for a beam wave, $\alpha_w = 90 deg$.

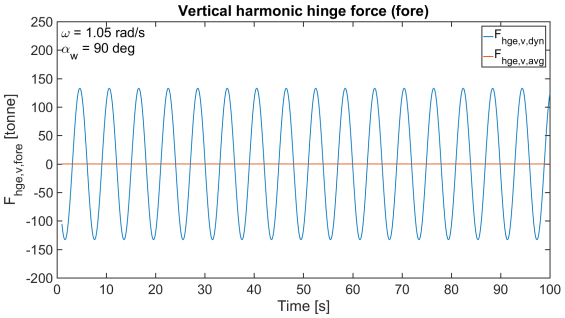

Figure 5.7: Harmonic force contributions to the vertical hinge force (fore).

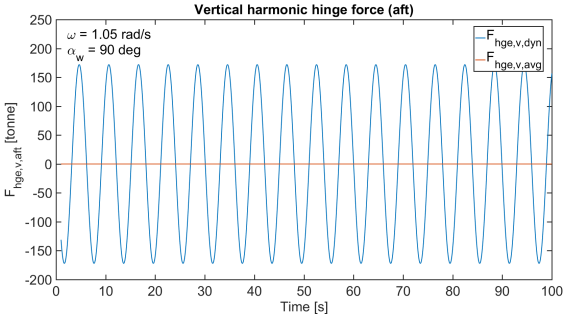

Figure 5.8: Harmonic force contributions to the vertical hinge force (aft).

In the figures it is shown that the mean contributions to the vertical hinge forces are equal to zero. In chapter 3 it was already found that this is the result from the equilibrium that exists between the weight and buoyancy of the barge. The dynamic vertical hinge force contributions are found to oscillate harmonically and shows amplitudes of approximately 130 tonnes for the fore hinge and 170 tonnes for the aft hinge. The difference that is found between the two vertical hinge forces comes from the non-symmetry of the SHB. As a result, the lever arm of the forward hinge is slightly larger compared to the aft hinge.

Just as was done for the hydraulic cylinder forces, the amplitudes that are found for the regular vertical hinge forces are combined to form the force RAO's. Figures 5.9 and 5.10 show these for the vertical hinge forces on the bow and the stern of the SHB for all considered wave directions.

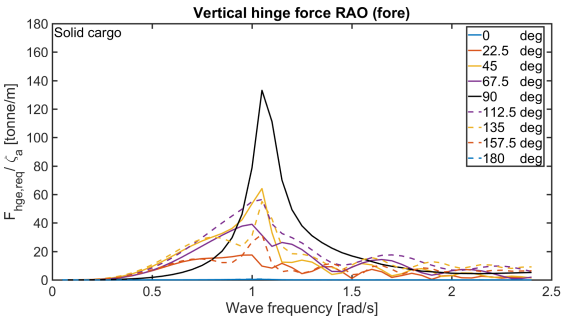

Figure 5.9: Vertical hinge force RAO's (fore)

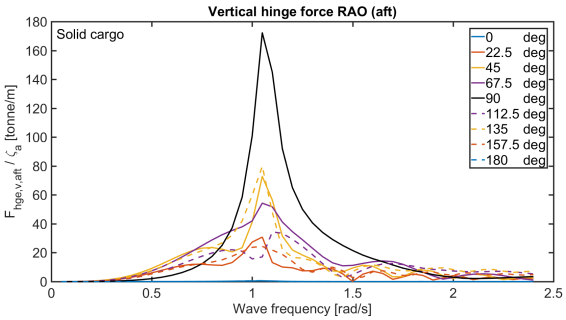

Figure 5.10: Vertical hinge force RAO's (aft)

Again, beam waves result in the highest regular forces. From the figures it is clear that the peak amplitude for both the vertical hinge forces is found at a frequency of $\omega = 1.05 rad/s$. An absolute maximum peak is found for the aft vertical hinge. Just as for the required cylinder forces, low regular wave frequencies cause the force amplitudes in the hinges to tend towards the average forces that where determined. Note that the DAF for the vertical hinge forces is infinite since the mean force contribution is zero.

The shown RAO's for the vertical hinge forces are not directly used to obtain a resulting force spectra. For the comparison with the design loads, it is more useful to obtain the combined hinge forces. The RAO's are purely shown to illustrate the effects that play a role in the combined hinge forces.

5.2.4. Horizontal hinge forces

For the horizontal hinge forces, the harmonic forces per regular wave frequency consist of four force contributions. First there is the dynamic horizontal force, FY, that results from the splitting forces, than there is the average force contribution, $F_{hge,h,avg}$. Furthermore, the bottom chock, F_{bot} and cylinder forces, $F_{cy,pre}$, have to be taken into account. Figure 5.11 shows the horizontal hinge force contributions for the fore hinge of the SHB. Again the regular force components are shown for a single frequency and wave direction, $\omega = 1.05\ rad/s$ and $\alpha_w = 90\ deg$. Only the fore hinge components are shown since it was found that the force contributions in the aft hinge are the same.

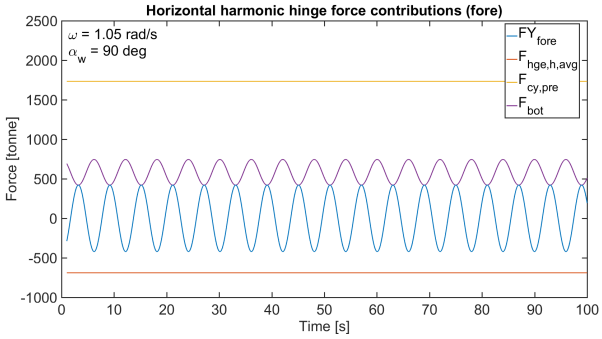

Figure 5.11: Harmonic horizontal hinge force contributions (fore).

In the shown figure the average force contributions to the horizontal hinge forces are found to be negative. The average forces that are shown in the figure result from the static pressures of both the cargo and the water on the hopper walls. In chapter 3 is was found that the forces that result from the cargo pressures exceed those resulting from the hydrostatic pressures. Since the average hinge forces solely rely on these two components and since the cargo forces are negatively included in the calculations of them, negative force contributions are found.

The bottom chock forces are found to be exactly 90 degrees out of phase with the harmonic horizontal force contributions. Since these forces result from the difference between the installed and required hydraulic cylinder force, it has a maximum when this force is low and a minimum when the required cylinder force is high. As a result there is 90 degree phase shift between the required cylinder force and the bottom chock force. The required hydraulic cylinder force and the dynamic horizontal force contribution to the hinge forces both follow from the splitting forces that are present in the splitting plane of the barge. Since these forces are in phase with each other, the bottom chock force is out of phase with the dynamic horizontal force FY.

By summing up the shown components, the horizontal hinge forces per regular frequency are found. This is done for all regular frequencies and for all wave directions. Using the amplitudes of the determined regular forces per frequency, the force RAO's for the horizontal hinge forces are found. Figure 5.12 shows the obtained RAO's for all wave direction for the fore hinge. The RAO's for the aft hinge were found to be similar and are therefore not shown. The static force contribution to the hinge forces of the SHB carrying a solid cargo is determined as well and is found to be equal to 461 tonne.

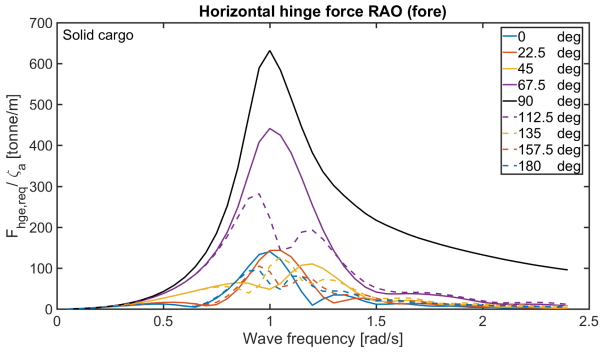

Figure 5.12: Horizontal hinge force RAO's (fore)

The found RAO's show that just as for the cylinder and vertical hinge forces, beam waves result in the highest regular horizontal hinge forces. However, the differences between the different wave angles are found to be smaller compared to the differences found for the vertical hinges, for beam waves a DAF of 2.3 is found. Compared to the vertical hinge forces the difference between the fore and aft hinge force amplitudes is lower as well, only a difference of 2% is obtained. The force contribution that is being influenced by the lever arms of the hinges is now found to be small compared to the other force contributions. As a result, the differences due to the non-symmetry of the barge do not show in a large extend.

Just as for the vertical hinge force RAO's, the ones for the horizontal hinge forces are not used to find a force response spectra as well. Again, they are only shown to give an insight in the different aspects that cause the eventual results.

5.2.5. Resulting hinge forces

For the research it is of more value to determine the combined hinge forces that follow form the vertical and horizontal hinge forces. To obtain these combined resulting hinge forces, already the regular forces found for both the horizontal and vertical hinge forces are combined using relation 4.44. By doing so, for each regular wave frequency the harmonic hinge forces of the barge are found. Just as is done for the cylinder forces, for each regular hinge force its amplitude can be determined. The amplitudes of all the regular forces are than combined to find the different force RAO's for the different wave directions. The obtained force RAO's for the combined hinge forces of a SHB carrying a solid cargo are shown in figures 5.13 and 5.14 for both the fore and aft hinge of the barge. The static force contribution to the hinge forces is equal to that of the horizontal hinge forces, $F_{hge,stat} = 461\ t$, since the static vertical force is zero.

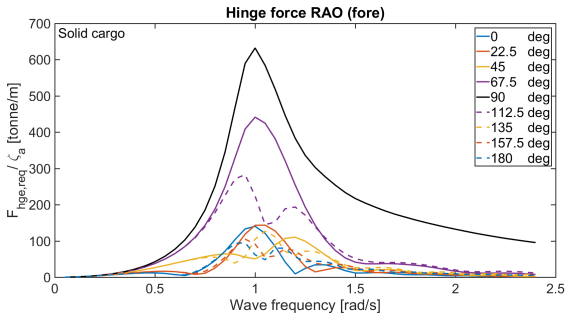

Figure 5.13: Hinge force RAO's (fore)

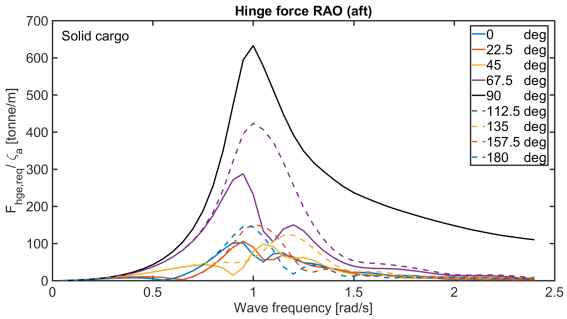

Figure 5.14: Hinge force RAO's (aft)

Note that the obtained force RAO's found for the combined hinge forces resemble the ones found for the horizontal hinge forces. Since the vertical hinge force maxima are small compared to those of the horizontal hinge forces, the contribution to the combined hinge forces is small as well. For beam waves a DAF of 2.3 is found. For low and high frequencies the amplitudes again tend to zero.

The shown force RAO's are used to determine the hinge force response spectrum. Using this spectrum, the maximum dynamic hinge forces can be determined. To them, the static term is added. The obtained combined maximum hinge forces for the SHB carrying a solid cargo for a significant wave height of $H_s = 3.0m$ in a 3 hours extreme are shown in figures 5.15 and 5.16 .

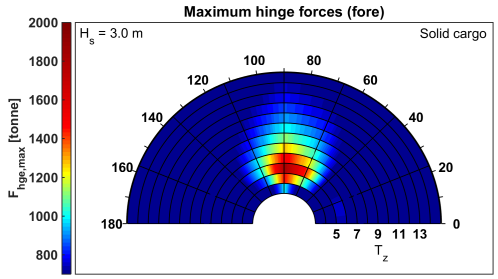

Figure 5.15: Maximum hinge force (fore)

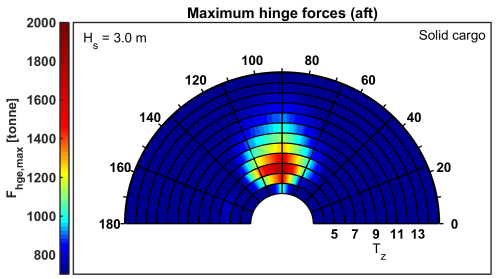

Figure 5.16: Maximum hinge force (aft)

Just as for the hydraulic cylinder forces, it is found that beam waves cause the highest resulting forces in the hinges. For wave periods approximately equal to $T_z = 5s$ the found forces are the highest. An absolute maximum is found for the aft hinge force, here a peak force of approximately 1850t is observed. In the resulting forces for the hinges of the SHB slight differences are found between the fore and aft hinge forces. However, for the absolute peak force, ($\alpha_w = 90$ & $T_z \approx 5\ sec$), the difference is negligible.

In a 3 hrs. extreme with a significant wave height of $H_s = 3.0m$, the design limits of the hinges of the Terraferre 501 SHB carrying a solid cargo are found to be exceeded. For beam waves with a period of $T_z \approx 5\ s$ the limits of the hinges are too low. Just as was found for the hydraulic cylinder forces however, the peak of the resulting forces is found to be narrow. For other wave directions and periods the design limits of the hinges are adequate. Note that outside of the mentioned area that results in the maximum responses, the forces are low. In appendix D the forces that result for the same storm duration but with significant wave heights of $H_s = 2.5m$ & $3.5m$ are shown. From the response forces it is found that the excitations even for a significant wave height of 3.5 m remain focussed in narrow area of combinations of wave directions and periods.

5.3. Results for liquid cargo

Next to the SHB carrying a solid cargo, one carrying a liquid cargo is considered as well. The results for the SHB carrying a liquid cargo of $\rho_c = 1450 \frac{kg}{m^3}$ are shown in this section. Using the obtained knowledge from appendix C the metacentric height of the barge in the AQWA simulations was adjusted. Furthermore a non-frequency dependent added mass matrix was added based on the differences in added mass that where found using AQWA. As a result from the made changes to account for the presence of liquid cargo, the natural frequencies of the barge are expected to change with respect of those of the barge with a solid cargo. Note that besides the stability lever arm and the added mass, the model of the liquid cargo SHB is equal to that of the solid cargo SHB.

5.3.1. Splitting force RAO's

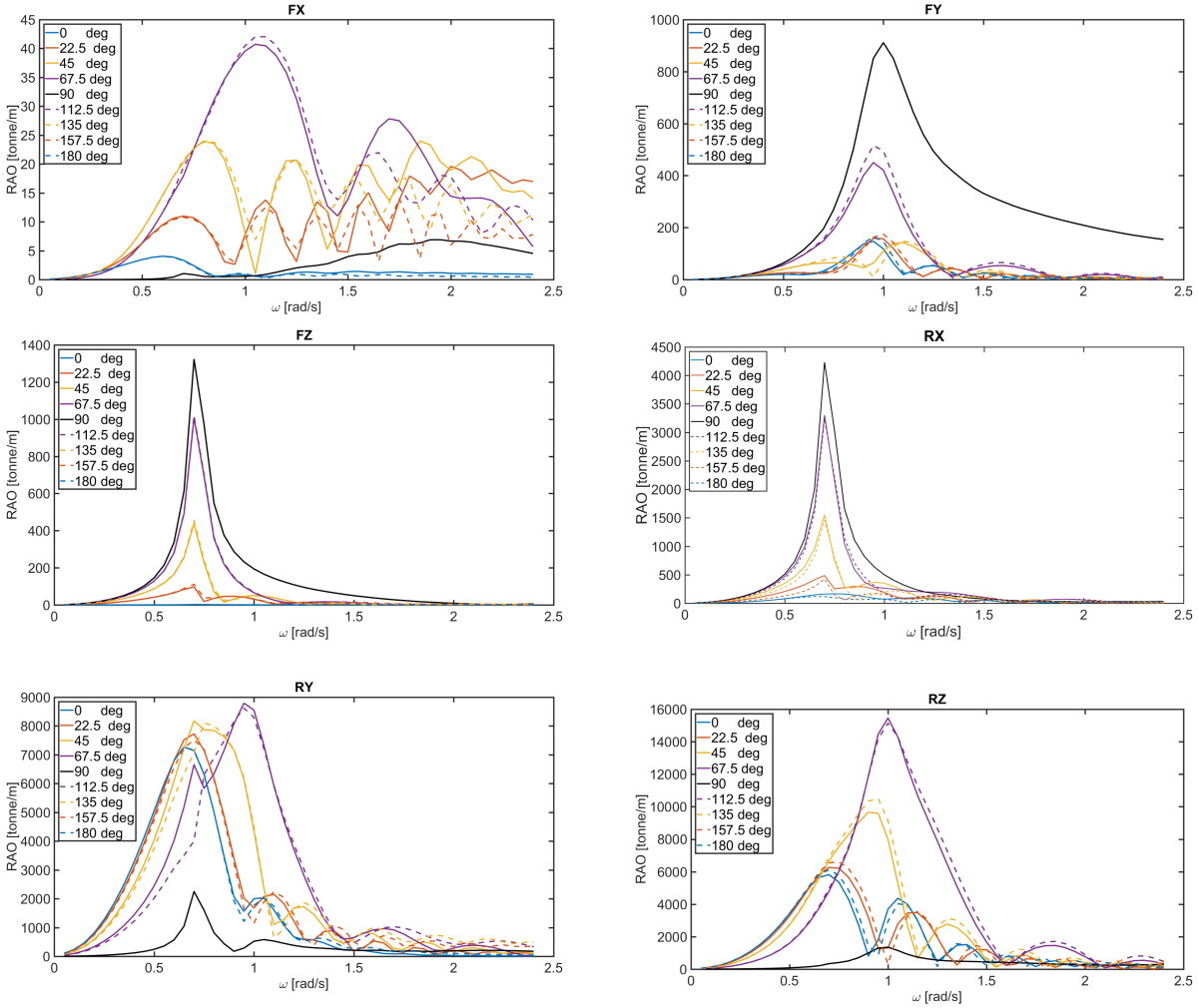

Figure 5.17: Splitting force RAO's.

Figure 5.17 shows the splitting force RAO's that are obtained using Ansys AQWA GS for the SHB carrying a liquid cargo. Again multiple wave directions varying between 0 and 180 deg are considered. Just as for the solid cargo barge, for the different force amplitudes, different wave directions result in the highest responses. Since the same principles of accelerations and resulting wave forces hold, no large differences in the dominance of the different wave directions are found.

What the force RAO's do show though, is the effect of the destabilization of the barge. From the WAMIT calculations in appendix C it was already found that for the motions of the barge which are affected by the motions of the liquid cargo, the resonance frequencies decrease. This effect was found to be the strongest for the sway, roll and yaw motions. In the force RAO's that are shown the decrease in resonance frequencies is found as well. For the force RAO's, the peak frequencies that are found for the vertical splitting force, Fz, as well as the RX and RZ splitting moments change noticeably. However, not all directions that are being influenced compare to the barges motions that were affected by the liquid cargo. The splitting force in the vertical direction for instance shows a decrease in the peak frequency, while the heave motion was found to remain unchanged.

In the discussion of the splitting force RAO's found for the SHB carrying a solid cargo, it was already explained that although the splitting forces are related to the motions of the barge this is not a direct relation. The splitting forces were found to be high when either the acceleration of the combined mass of the barge and its cargo, the forces due to the radiated wave damping or the changes in hydrostatic stiffness are large. Due to the destabilization of the barge the motions of it become more violent, as a result all three mentioned aspects of the splitting force are being influenced. For the vertical splitting force this means that although the heave motions remain the most violent for their initial resonance frequency, the change in the roll motions for instance does cause the accelerations of the mass in the vertical direction to be larger for the lower frequency. As a result, the vertical splitting force can have a maximum for a lower resonance frequency, while the resonance frequency of the heave motion remains unchanged.

Do note that the found splitting force amplitudes in general are high compared to their counterparts that followed for the SHB with a solid cargo. Again, the destabilization of the barge results in large motions. Therefore the aspects that are identified to have an effect on the splitting forces in the splitting plane of the barge are excited more. As a result, the splitting forces in general are larger for the barge carrying a liquid cargo.

5.3.2. Hydraulic cylinder forces

Just as for the SHB carrying a solid cargo, first the hydraulic cylinder forces are considered. Using the splitting force RAO's the harmonic opening moment per wave frequency is determined again. The quasi-static barge model is used to add the mean/average force contribution to this dynamic opening moment in order to obtain the complete harmonic opening moment.

Figure 5.18 shows the two contributions that where found for a wave frequency of $\omega = 1.05 rad/s$ and a wave direction of $\alpha_w = 90 deg$. In the figure the determined mean value of the opening moment is found to be equal to the value that was obtained for $\theta_r = 0 deg$ in chapter 3. The dynamic contribution again oscillates around zero with the chosen regular frequency. Note that the amplitude of the found cylinder forces is 4.5% lower than that that was found for the SHB with solid cargo at this frequency.

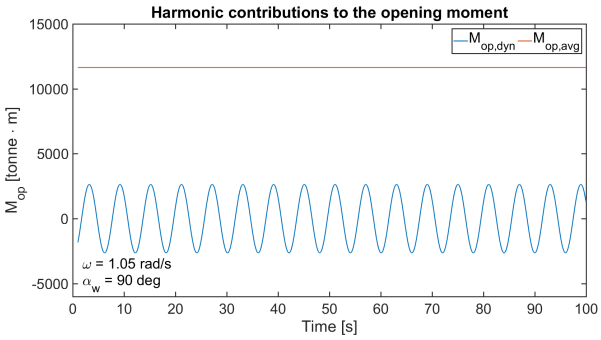

Figure 5.18: Dynamic and average contribution to the opening moment.

Just as was done with the solid cargo model, the amplitudes of the harmonic forces for al considered regular wave frequencies are combined to obtain the force RAO's. Figure 5.19 shows the obtained RAO's for all the considered wave directions. The static contribution to the cylinder forces is found to be equal to that of the solid cargo barge and thus yields $F_{cyl,stat} \approx 930 t$.

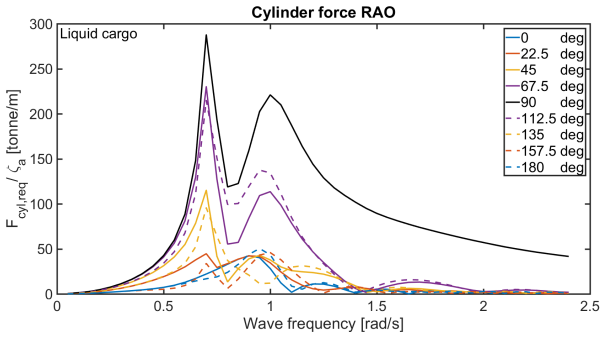

Figure 5.19: Hydraulic cylinder force RAO's.

Following from the destabilization of the SHB and the resulting changes in some of the resonance frequencies of the barge, a second peak is formed at a lower frequency in the transfer functions. Where the barge with a solid/frozen cargo had a single resonance frequency of $\omega \approx 1.0 rad/s$, the barge filled with a liquid cargo experiences high forces at both $\omega \approx 0.7 rad/s$ and $\omega \approx 1.0 rad/s$.

In the calculations of the resulting hinge and cylinder forces, the different splitting forces are combined. For the barge with a solid cargo it was found that the resonance frequencies for the different splitting forces where almost equal, as a result a single force peak was found in the force transfer functions. For the SHB with a liquid cargo however, the liquid cargo effects result in a decrease of the resonance frequencies of the splitting forces in the surge, sway, roll and yaw direction. When the different splitting forces are than combined to form the resulting forces in the hinges and hydraulic cylinders, both the initial as well as the lower resonant frequency will appear. As a result, in the force RAO's for both frequencies a maximum is found.

Beam waves are still found to result in the highest forces. Just as for the SHB with a solid cargo, for low frequencies the forces tend to the mean hydraulic cylinder forces. Do note that in line with the results from chapter 3 the mean required hydraulic cylinder forces for the SHB carrying a liquid and the SHB carrying a solid cargo are equal. The DAF that is found for the barge carrying a liquid cargo is equal to 1.31, which is slightly larger compared to that of the barge with a solid cargo.

When the force RAOs for the solid and liquid cargo barges are compared, the maximum amplitude of the SHB carrying a liquid cargo is found at the lower resonance frequency. The absolute value for the barge with a liquid cargo is found to exceed that of the barge with a solid cargo. An approximate difference for the regular forces is found to be 10%.

The shown force RAOs are used in combination with the JONSWAP wave spectrum to find the force response spectra of the hydraulic cylinder forces of the SHB carrying a liquid cargo. From these spectra the maximum resulting forces for irregular seas can be found. Figure 5.20 shows the maximum required cylinder forces for the SHB carrying a liquid cargo of $\rho_c = 1450 kg/m^3$. The forces shown are found for a 3 hours extreme with a significant wave height of $H_s = 3.0m$.

Beam waves again result in the absolute maximum hydraulic cylinder forces. However, in comparison with the solid cargo condition the range of mean zero crossing periods for which the resulting forces are high is wider for the barge carrying a liquid cargo. This results from the dual resonance peak that was shown in the force transfer functions. The maximum forces that result from the spectral analysis, now show two mean zero crossing periods for which the resulting forces are the highest. For the SHB carrying a liquid cargo the range of mean zero crossing periods that result in the highest responses is now found between $T_z = 4s$ and $T_z = 9s$. A maximum force of approximately 1470t is found for beam waves with a T_z of approximately 7s. Note that thus the found difference between the maximum resulting forces for the SHB with a solid cargo are marginal.

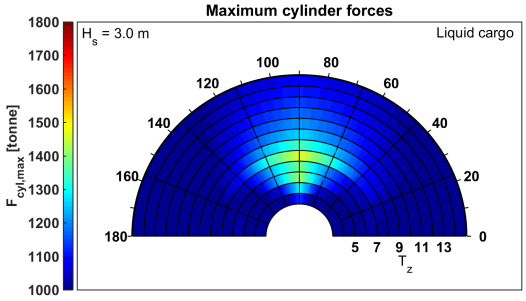

Figure 5.20: Maximum required hydraulic cylinder force for $H_s = 3.0m$.

In general, due to the wider range of wave periods and directions for which the required cylinder forces are high, the cylinder forces for the liquid cargo SHB pose to be of a higher concern. Compared to the barge with the solid cargo, the conditions for which the forces in the cylinders are elevated are met earlier.

For the TF501 SHB, the hydraulic cylinder limits are not found to be exceeded for the liquid cargo condition. For beam waves with periods in the range of $T_z = 4s$ up to $T_z = 8s$ the found forces are the highest. Compared to the situation with a solid cargo, the range of combinations of wave angles and periods for which the required cylinder forces are high is bigger. As a result, the conclusion can be drawn that with respect to the hydraulic cylinder limits, the workability limit of the SHB with a liquid cargo is lower. For the other significant wave height that where considered, the resulting graphs are shown in appendix D.

5.3.3. Vertical hinge forces

Next the vertical hinge forces for the SHB carrying a liquid cargo are considered. First, the harmonic force components per regular wave frequency are determined. Figure 5.21 up to figure 5.24 show the vertical hinge force contributions for beam waves for both the peak frequencies that where found for the required hydraulic cylinder forces ($\omega = 0.7\&1.0 rad/s$).

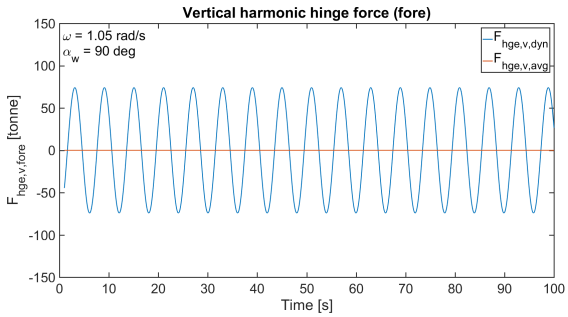

Figure 5.21: Harmonic force contributions to the vertical hinge force (fore).

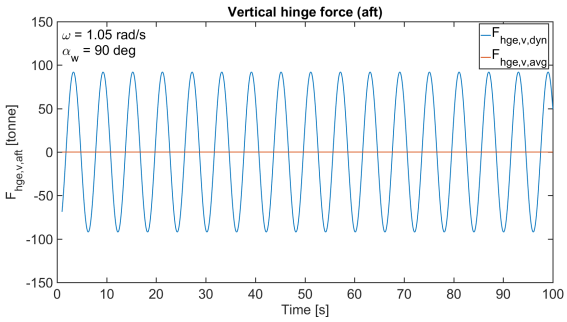

Figure 5.22: Harmonic force contributions to the vertical hinge force (aft).

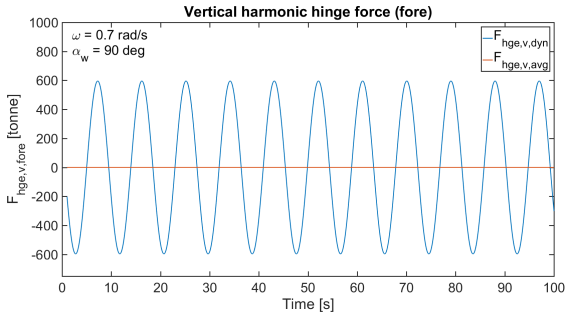

Figure 5.23: Harmonic force contributions to the vertical hinge force (fore).

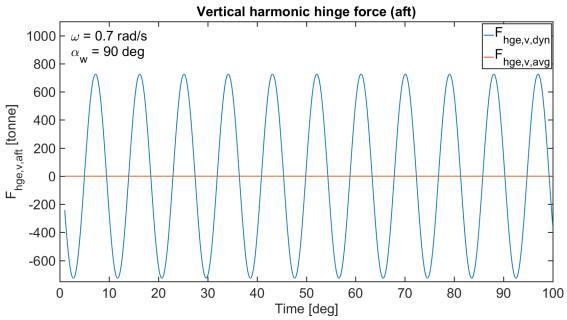

Figure 5.24: Harmonic force contributions to the vertical hinge force (aft).

From the figures with the vertical hinge force contributions, it is found that the static contribution to this forces is again equal to zero. The dynamic contributions oscillate with the chosen frequencies around a zero mean value. Just as for the SHB filled with a solid cargo, it is found that the aft vertical hinge force exceeds that of the fore hinge. For the second frequency that is now considered, the determined forces exceed those of the initial considered wave frequency. The force contributions that are found for $\omega = 0.7 rad/s$ for the SHB with liquid cargo are 4 times higher than the highest force contributions for the SHB with a solid cargo.

From the harmonic resulting forces that follow from the contributions shown, for each considered frequency the amplitudes are taken. From these amplitudes the force RAO's for the vertical hinge forces are once again obtained for all considered wave directions. The resulting functions are shown in figures 5.25 and 5.26 for both the fore and aft hinges. Just as for the barge carrying the solid cargo, the static vertical force component of the forces for the barge with a liquid cargo is equal to zero.

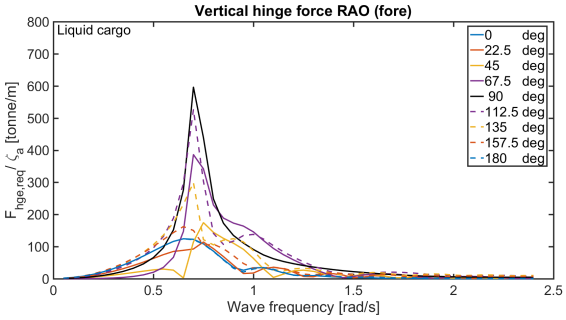

Figure 5.25: Vertical hinge force transfer functions (fore).

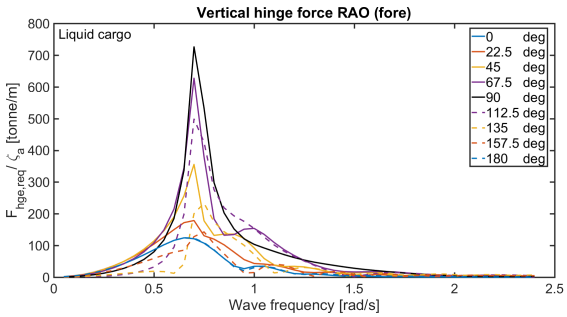

Figure 5.26: Vertical hinge force transfer functions (aft).

The amplitudes of the regular forces show that the peak frequency for the vertical hinge forces decreases when the SHB is carrying a liquid cargo. Again, this is the result from the destabilization of the system due to the presence of liquid cargo. Besides, the regular forces that result in the vertical hinge direction are found to be higher than those that were found for the SHB with a solid cargo. For the splitting forces of the SHB with a liquid cargo, it was already explained that they are high compared to those found for the barge with a solid cargo. The vertical hinge forces are subject to the FZ and RY splitting force and moment, both are found exceed their values of the SHB with a solid cargo. As a direct result, the obtained vertical hinge forces are higher as well.

The differences that are found between the resulting force RAO's for the different wave directions become smaller for the barge that is carrying a liquid cargo. Again beam waves result in the highest regular forces. Just as was found for the SHB with a solid cargo, the aft vertical hinge forces are found to be larger as those of the fore vertical hinge forces. For low and high frequencies, the amplitudes again tend towards the average obtained value.

Just as for the SHB carrying a solid cargo, the force transfer functions are only shown to explain the important effects of the resulting forces. Later on the combined maximum resulting forces for the hinges will be determined and explained.

5.3.4. Horizontal hinge forces

To find the horizontal hinge forces of the SHB with a liquid cargo, first the force contributions per regular frequency are determined again. The found force contributions for both a regular frequency of $\omega = 1.05 rad/s$ and a frequency of $\omega = 0.7 rad/s$ are shown in figures 5.27 and 5.28. Only the components of the fore hinges are shown, since it was found that there is no difference between the fore and the aft.

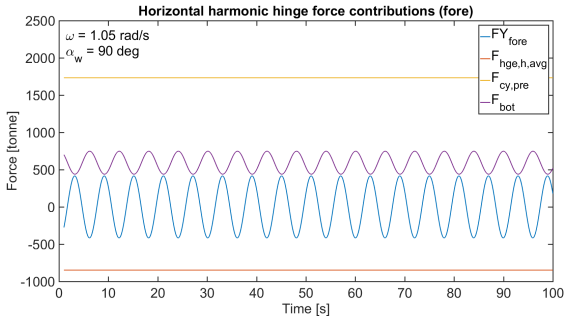

Figure 5.27: Harmonic force contributions to the horizontal hinge force (fore).

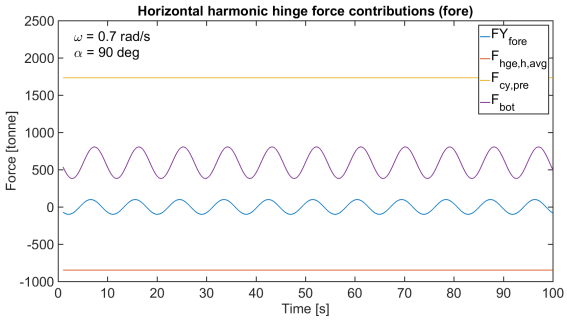

Figure 5.28: Harmonic force contributions to the horizontal hinge force (fore).

The harmonic components to the horizontal hinge forces are mainly subject to the FY and RZ splitting moments. Although RZ has grown significantly due to the presence of liquid cargo in the hopper, its effect does still not compare to the effect of FY that was found to be large due to the large lever arm of this force to the hinge locations. As a result, the harmonic force components to the horizontal hinge forces do not change significantly compared to the solid cargo situation. Besides, since the hydraulic cylinder forces were found to be in the same order of magnitude, the contribution of the bottom chock forces to the horizontal hinge forces does not change significantly as well.

What does change compared to the solid cargo SHB is the average force contribution. For the SHB carrying a liquid cargo a mean force of approximately $290t$ is found. Just as was concluded in chapter 3 the contribution to the average hinge force due to the cargo and hydrostatics is lower for the SHB with liquid cargo. Remember that this was an effect due to the higher elevation of the cargo in the hopper. For the barge that is used a difference between the static hinge forces for the barge with a solid or a liquid cargo is found to be 40%.

After the different components are combined to form the harmonic resulting forces in the horizontal hinge direction per regular wave frequency, for all their amplitudes are taken to find the force RAO's. Figures 5.29 shows the found force RAO's for the SHB with a liquid cargo, again for all considered wave directions.

The RAO's show how the presence of the liquid cargo changes the expected hinge forces for the SHB. For the SHB carrying a liquid cargo, the frequency at which the maximum amplitude is found does not change which is in line with the explanation that this hinge force is mostly affected by the FY splitting force. The height of the found maximum amplitude does decrease. This is found to be an effect of the low average force contribution. The difference between the static and dynamic contributions to the hinge forces does increase for the barge carrying a liquid cargo. A maximum DAF of approximately 3.0 is found.

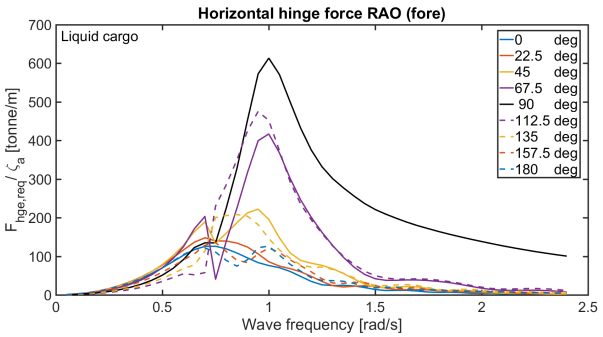

Figure 5.29: Horizontal hinge force RAO's (fore).

Although the resonance frequency of the horizontal hinge force RAO does not change significantly, the RAO's do show some increase around the second resonance frequency. Just as was found for the cylinder forces, this is expected to result in a wider range of mean zero crossing periods for which the resulting hinge forces are elevated.

5.3.5. Resulting hinge forces

Following the approach of chapter 4 the force RAO's for the combined hinge forces are determined based on the amplitudes of the harmonic hinge forces per regular wave frequency. The RAO's that result for a SHB that is carrying a liquid cargo of density $\rho_c = 1450 kg/m^3$ are shown in figures 5.30 and 5.31 for all considered wave directions. The static force contributions to the forces are again equal to those found for the horizontal hinge forces, $F_{hge,stat} = 291t$.

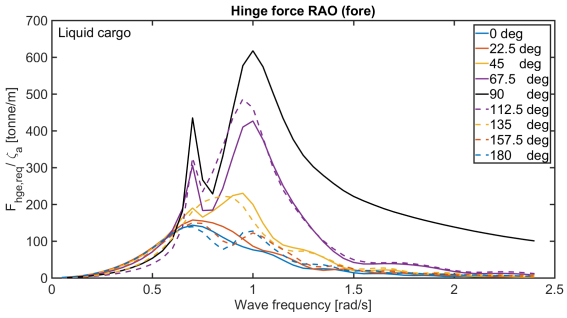

Figure 5.30: Hinge force RAO's (fore).

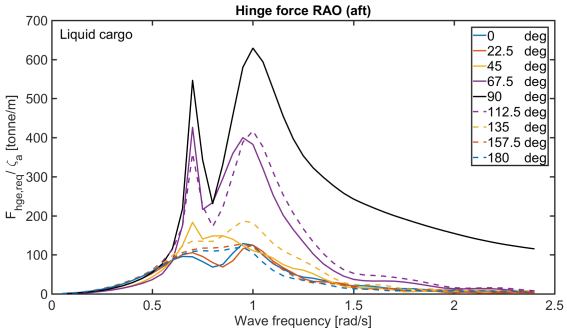

Figure 5.31: Hinge force RAO's (aft).

The figures show that due to the frequency shift of the resonance frequency of the vertical hinge forces, the resulting maxima for the combined regular hinge forces now show two peaks. The first peak follows from the splitting forces and motions that are effected by the presence of liquid cargo. The second peak results from the motions and splitting forces that are not affected by the presence of liquid cargo. The found maximum force amplitudes for the SHB with liquid cargo are low compared to those found for the SHB with a solid cargo. For the maximum amplitude in beam waves a difference of 20% is found. The DAF for the combined hinge forces is equal to 3.1.

Using the obtained RAO's, the response spectra for the combined hinge force can be obtained. From it, the maximum dynamic hinge forces for a SHB carrying a liquid cargo in a 3 hour extreme with a significant wave height of $3.0m$ are determined. To these dynamic forces their static counterparts are added, the combined maximum forces for the chosen conditions are shown in figure 5.32 and figure 5.33.

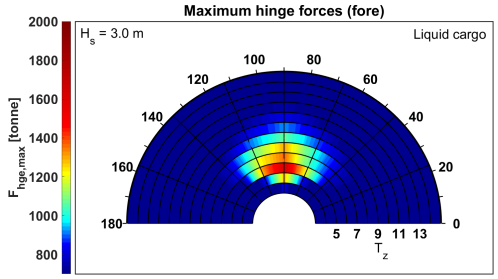

Figure 5.32: Maximum hinge forces (fore).

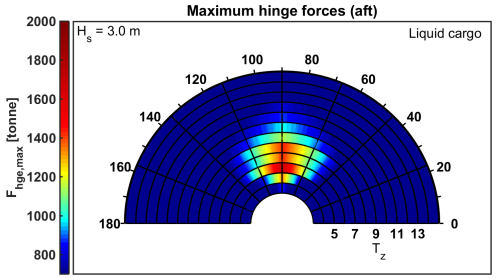

Figure 5.33: Maximum hinge forces (aft).

In the shown plot, again the 90 deg wave direction is found to result in the most significant force responses in the hinges of the SHB. However, compared to the SHB carrying a solid cargo, the hinge forces that are found are low. For both cargo conditions the maximum forces are found for beam waves with a period of $T_z = 5s$. For the barge carrying a liquid cargo the highest resulting force that was found is almost equal to 1700t, which is a decrease of 8% compared to that found for the SHB with a solid cargo.

Due to the lower average force contributions for the SHB carrying a liquid cargo, the resulting forces do not compare to those found for the barge carrying a solid cargo. As a result, the conclusion can be drawn that the hinge limits for a barge carrying a solid cargo are more governing , and therefore of more concern, than those of a barge carrying a liquid cargo.

5.4. Conlcusions on the results

Based on the calculation method that was described in chapter 4, the maximum hinge and hydraulic cylinder forces for one type of SHB where determined. For the Terraferre 501 SHB the maximum resulting forces in its hinges and hydraulic cylinders where obtained for a 3 hours extreme in an irregular sea based on an JONSWAP wave spectrum. The results for a sea state with a significant wave height of 3.0 m where discussed, those for significant wave heights of 2.5 m and 3.5 m are presented in appendix D. The shown results in this chapter are for the SHB carrying either a solid cargo, $\rho_c = 2200 kg/m^3$, or a liquid cargo, $\rho_c = 1450 kg/m^3$.

5.4.1. Hydraulic cylinder forces

In chapter 4 it was found that the dynamic contributions to the hydraulic cylinder forces that are required to keep the barge closed are subject to the FY and RX splitting force and moment. For both of these splitting forces, it was found that they are the highest for beam waves. As a result, for the SHB in irregular waves, it is found that beam waves yield the highest required hydraulic cylinder forces.

When the SHB is carrying a liquid cargo, the system is expected to be destabilized due to the cargo motions. Therefore, some of the natural frequencies of the barge are found to decrease. For the barge with a solid cargo it was found that its natural frequencies are all close to each other. The maximum cylinder forces for a SHB carrying a solid cargo where therefore found in a small frequency range close to $\omega \approx 1.0 rad/s$. Due to the mentioned destabilization, the natural frequencies of the barge carrying a liquid cargo are divided over roughly two frequency ranges, $\omega \approx 0.7 rad/s$ & $\omega \approx 1.0 rad/s$. As a result, the energy in the force response spectrum of the hydraulic cylinder forces is found to be distributed over a wider frequency range. Therefore, the number of combinations of wave directions and periods for which the hydraulic cylinder forces are found to be high is larger for the SHB with a liquid cargo.

For the Terraferre 501 SHB that was considered in the simulations, it was found that the cylinder capacities are not exceeded for the chosen sea conditions. For beam waves, the maximum force was found to be equal to 1475t for a barge carrying a solid cargo. For the barge carrying a liquid cargo the maximum force is lower, 1400t at $T_z \approx 7s$. However, due to the dual resonance frequency that was found, the range of combinations of wave directions and periods for which the cylinders forces are high was found to be large. For approximate beam waves with mean zero crossing periods of $T_z = 4s$ up to $T_z = 8s$ the forces that were found in the cylinder elevated. Therefore, the conclusion can be drawn that for the TF501 SHB carrying a liquid cargo the workability limit with respect to the hydraulic cylinder forces is lower than that of the same barge carrying a solid cargo.

5.4.2. Hinge forces

The resulting hinge forces for the SHB depend on both a contribution due to the vertical as well as a contribution due to the horizontal hinge forces. In chapter 4 it was described that the vertical hinge forces are subject to the splitting force and moment FZ and RY. The FZ splitting force is found to have its maximum for beam waves, for the RY moment a maximum is found for wave angles of $\alpha_w \approx 67.5deg$ and $\alpha_w \approx 112.5deg$. Since the lever arm of the FZ splitting force is large, FZ dominates the dynamic contributions to the vertical hinge forces. As a result, it was found that beam waves excite the hinges in the vertical direction the most. Since the hinges are not positioned at an equal length from the midpoint of the barge, the aft hinges forces are found to be higher than those found for the fore hinges.

The horizontal hinge forces were found to be dependent on the FY and RZ splitting force. Besides, the hydraulic cylinder force has an indirect effect through the bottom chock forces that are included. Therefore, the RX splitting moment has an effect on the resulting horizontal hinge forces as well. For the FY and RX splitting force and moment it was already found that they have a maximum for beam waves. The RZ splitting moment is found to have a maximum for the wave directions 67.5 deg. and 112.5 deg. The horizontal hinge forces result from an equilibrium of the moments around the Z-axis of the barge. Since the lever arm of FY is found to be large, this splitting force has the largest influence on the dynamic horizontal hinge force components. The horizontal hinge forces are therefore found to be the largest for beam waves as well. In line with the results from chapter 3 it was found that the average force contribution to the horizontal hinge forces is lower for the barge carrying a liquid cargo. This was found to be a result from the difference in initial loading height of the cargo. A higher loading height results in a lower average force contribution. For the cargo types that where considered in the simulations a difference of 40% was found.

Since both contributions to the hinge forces show a maximum response for beam waves, the combined forces in the hinges are the highest for beam waves as well. For a solid cargo, it was found that the vertical hinge force contributions are low compared to those of the horizontal hinge forces. As a result, the resulting force RAO that was found for the combined hinge forces for the SHB with a solid cargo resembles the one that was found for the horizontal hinge forces. For the SHB with a liquid cargo, not only are the vertical hinge forces found to be bigger due to the destabilization of the barge, it was found that their resonance frequency drops as well. The changes to the horizontal hinge forces were found to be less. Therefore, in the force RAO for the combined hinge forces for the SHB carrying a liquid cargo, the effect of the vertical hinge forces is found to be of more importance.

Using the force RAO's the maximum resulting forces in the hinges where determined for the chosen conditions. For beam waves the determined resulting hinge forces were found to be the highest. The maximum obtained force for the SHB with a solid cargo is 1850t. For the SHB with a liquid cargo the maximum force found is equal to 1700t. Both maximum forces are found in the aft hinge for a wave period of $T_z \approx 5s$. The differences between the force for the SHB with a liquid and a solid cargo are large. Due to the difference in the average force contribution to the horizontal hinge forces, the resulting maximum forces for the barge carrying a solid cargo are the highest.

For the Terraferre 501 SHB, the limits of the hinges are found to be exceeded. The peak for the solid cargo forces was found to be small, for other combinations of wave direction and periods the design limits of the hinges are adequate. The range of combinations of wave directions and periods for which the hinge forces for the SHB carrying a liquid cargo are elevated was again found to be large. For the hinge forces however, the design limits are found to be exceeded sooner for the barge carrying a solid cargo. Therefore the conclusion can be drawn that for the simulated conditions the limits of a SHB with respect to its hinge design limits are of most concern in case a solid cargo is carried.

6

Conclusions and recommendations

The goal of this research is to describe a method that can be used to determine the technical workability limits of a split hopper barge in irregular seas. In the process of finding this method, both an opened and closed SHB are considered. Multiple types of cargo and loading conditions have to be regarded as well. Using the proposed method, the workability limit of at least one type of SHB has to be determined. However, the method that is proposed has to be applicable to multiple types of SHB's.

This chapter is used to present the conclusions that result from the done research. First conclusions on the proposed method for the calculation of the workability limits of the SHB are shown. After that some general remarks on the observations are made with regards to the workability limits of SHB's are given. In the end, recommendations for further research are stated and explained.

6.1. Conclusions

6.1.1. Method for finding the workability limits of a split hopper barge

In line with the intention of this research, a method was proposed to determine the technical workability limits of a split hopper barge in irregular seas. The limits of the barge where assumed to follow from the design limits of the hinges and hydraulic cylinders of the barge. Using the classification regulations stated by Bureau Veritas (Bureau Veritas, 2016), these design forces can be obtained.

In chapter 4 the calculation method for the workability analysis of the SHB in irregular seas was described. Since the resulting forces in the hinges and hydraulic cylinders where found to result from the splitting forces that act in the splitting plane of the barge, the method that was proposed is based on Ansys AQWA. Ansys AQWA cannot only be used to solve the equation of motions of the barge, it can calculate the resulting splitting forces as well. Using the resulting force amplitudes, the dynamic force contributions in the hinges and hydraulic cylinders can be determined. This is done per regular wave frequency.

Using a quasi-static Matlab model that was introduced in chapter 3, the mean force contributions to the hinge and cylinder forces can be found. By adding these components to the harmonic forces that where already determined, the complete resulting harmonic forces in the hinges and hydraulic cylinders of the split hopper barge are obtained. Again, per regular wave frequency. By using the amplitudes of these harmonic forces, a force RAO per wave direction can be made. This RAO can then be used to obtain the force response spectra of the hinge and cylinder forces. From these spectra, the maximum expected forces for a certain sea state and storm duration can be determined. When to them the static force contribution is added, the overall resulting hinge and cylinder forces are found.

Ansys was found to be incapable of simulating the barge with internal free-surface fluid elevations. The effects due to a liquid cargo had to be included in the simulations separately as a result. In appendix C the equations of motions of the barge where studied upon to find a method to include the liquid cargo effects. It was found that to account for a liquid cargo in the barge, the added mass and the stiffness of the solid cargo barge model have to be adjusted. The additional added mass matrix can be found by solving the equations of the barge with a liquid cargo in WAMIT. To account for the change in stiffness of the system, the stability lever arms of the barge in Ansys have to be decreased.

Using the proposed method of chapter 4, the maximum resulting forces in the hinge and hydraulic cylinder of a SHB in a certain sea state for a certain storm duration can be determined. By taking into account the adjustments that have to be made for the barge that carries a liquid cargo, the proposed method can be used for both a SHB carrying a solid and a liquid cargo. The maximum forces that are found can be compared to the design forces of the hinges and hydraulic cylinders. From this comparison a first conclusion can be made on the workability of the barge for the considered situation.

6.1.2. The workability limits of a SHB

In chapter 3 the barge was considered in a quasi-static Matlab model. In this model the barge carrying different types of cargo in both an open and closed configuration was considered under fixed angles of roll. This basic model showed that the required cylinder forces as well as the horizontal hinge forces decrease for an increasing angle of roll. Only the vertical hinge force was found to increase. This is a result from the additional upper half-hull weight that has to be supported when the barge rolls.

Next the barge was considered carrying different types of cargo. From the comparison between the resulting forces for a liquid, sliding and a solid cargo, it was learned that either a liquid or a solid cargo lead to the extreme forces in the hinges and hydraulic cylinder of the SHB. For an opened barge, it was found that the outflow of cargo results in a fast decrease of the expected resulting forces. As a result, a closed SHB carrying a solid or a liquid cargo was found to be of the highest interest.

Using the method that was described in chapter 4 the barge was considered for irregular sea conditions. The results that followed for a Terraferre 501 SHB where presented in chapter 5. The barge was considered in a 3 hour storm with a significant wave height of $3.0m$ for mean zero crossing periods varying between 3 and 15 seconds. The forces where determined for other significant wave heights as well. For $H_s = 2.5m$ and $H_s = 3.5m$ the results are shown in appendix D.

From the result that where shown, it was found that the destabilization that results from the liquid cargo motions leads to two resonance frequencies for the barge. As a result, the range of wave directions and periods for which the resulting forces in the hinges and hydraulic cylinders are considerable was found to be large compared to that of the barge that carries a solid cargo. Beam waves were found to result in the highest forces and thus in the most limiting load case. Especially for mean zero crossing periods that result in excitations close to the barge its natural frequencies, the resulting forces were found to be high.

The highest force responses were found for the barge that is simulated with a solid cargo ($\rho_c = 2200kg/m^3$). For the cylinder forces a maximum of 1475t was found for $T_z \approx 5s$. For the hinges the maximum force that was found is equal to 1850t for $T_z \approx 5s$ as well.

Due to the multiple resonance frequencies for the barge carrying a liquid cargo, $\rho_c = 1450kg/m^3$, the number of combinations of wave directions and periods for which the forces are high is large. Although the required hydraulic cylinder force that was found for the barge carrying a solid cargo is higher, the mentioned effect causes high resulting forces for more combinations of wave directions and periods . For the hinge forces the same effect was identified for the barge with a liquid cargo. However, since the average force contributions to the hinge forces of the SHB carrying a liquid cargo is low, the maximum resulting forces that where found did not compare to those found for the barge with a solid cargo.

The design limits of the considered SHB are exceeded for the conditions that were simulated. For the solid cargo the number of combinations of wave directions and periods for which this happens was found to be small. For both the barge carrying a liquid and a solid cargo the hinge design limits were met. For the barge carrying a solid cargo this was found to occur the soonest, as a result, the conclusion is drawn that the workability limits are limited the most for a SHB carrying a solid cargo in irregular seas.

6.2. Recommendations

In this research, it was assumed that the hydraulic cylinders of the barge are used to pre-load the hinges and bottom chocks. The pre-tension that results was found to have a significant effect on the determined hinge forces. The pre-load was assumed to be equal to the capacity that the cylinders have on top of the required force that they have to deliver to keep the barge closed. Since the pre-tension in the hydraulic cylinders was found to have such a significant influence on the forces that result in the hinges of the SHB, it is wise to verify the existence, use and size of these forces in more detail. Based on the results from this research it is expected that a more educated use of the pre-tension of the hydraulic cylinder could lead to a decrease in wear and tear of the hinges. Furthermore, in situations where the hinge limits are approached or exceeded, the workability limits of the barge can be stretched when the pre-tension in the hydraulic cylinders is lowered. Do note that such an use of the hydraulic cylinder will have an effect on the rigidity of the closed barge. This will decrease when the pre-tension of the hydraulic cylinders is lowered. The effect of this has to be included in the research to the usage of the hydraulic cylinder force.

Throughout the research, the cargo usually carried by the SHB was simplified in a large extent. The cargo was assumed to be homogeneous and to result in equal pressures on the hopper walls in all directions. Furthermore, the effect of friction and cohesion on the motions of the cargo were not considered. A linear relation was used to describe the motions of cargo in the hopper. The cargo however, has a significant effect on the resulting forces that were determined. Therefore, a wider knowledge on the behaviour of different types of dredged cargo is not only expected to be interesting, it would also prove to be a valuable extension to the results that were obtained in this research. Since specific information on the behaviour and effects of dredged materials on cargo hoppers is not widely available, a strong recommendation is made to set up a new research for it. In such a research a set of laboratory tests could be included to gain a better insight on the behaviour of the cargo and that of the vessel carrying it as well. A link or relation to existing knowledge on the behaviour of non-dredging ships carrying liquid or frozen cargo will prove to be very helpful and will be a very strong initial step.

Finally, it has to be mentioned that the method that was described in the research has only be used for one type of split hopper barge so far. To test the functionality of the method as well as to gain more knowledge on the principles of a SHB it would be wise to simulate more types of barges. It is however important to realise that in order to obtain proper results, all mentioned steps from chapter 4 have to be repeated with great care. Do note that it is wise to determine the resulting forces for at least two cargo conditions (liquid & solid) and that this means that the WAMIT calculations of appendix C have to be repeated as well.

References

A. Kolijl. (2016). *Geotechdata.* Retrieved 23-5-2017, from http://www.geotechdata.info/index.html

AQWA theory manual (15th ed.) [Computer software manual]. (2013, November). 275 Technology Drive,15317 PA, Canonsburg.

AQWA user manual (14.5 ed.) [Computer software manual]. (2012, October). 275 Technology Drive,15317 PA, Canonsburg.

Boskalis. (2014, July). *Picture: Split hopper dredger cork and sand at work.*

Bureau Veritas. (2016). *Bureau veritas erules.* Retrieved from http://erules.veristar.com/dy/app/bootstrap.html

Coa, Y., & Zhang, F. (2016, February). Effects of fluid motions in liquid tanks on vessel motions using a simple panel method. *Journal of Offshore Mechanics and Artic Engineerig, 138.*

FKAB. (2011, 8). *Calculation cylinder & deck hinge forces* (Tech. Rep.). Author.

Gom, N., & Grundlehner, G. (2015, April). *Terraferre 503-504: Cylinder forces and hinge forces calculation.* (Tech. Rep.). Boskalis.

Journee, J., & Massie, W. (2001). *Offshore hydromechanics* (First edition ed.). Delft University of Technology.

Latreille, P. J. (1982, July). *Split dredgers and barge: main aspects of their structural strength* (Tech. Rep.). Bureau Veritas.

Newman, J. (2005). *Wave effects on vessels with internal tanks* (Tech. Rep.). University of Oslo.

Reynaerts, C. (2011, December). *Hydrostatische krachten.* (Lecture notes v7.0)

Verruijt, A. (1999). *Soil mechanics.* Delft University Press.

Wamit user manual (v7.2 ed.) [Computer software manual]. (2016). 822 Boylston St. Suite 202, Chestnut Hill MA..

A

Reliability of the quasi-static Matlab model

Before the quasi-static split hopper barge model in Matlab can be used, some credibility has to be given to the calculations it does. Using the relations that were stated by Bureau Veritas (Bureau Veritas, 2016), it is possible to determine and thus validate some of the variables that are determined in the model and eventually lead to the forces in the hinges and the hydraulic cylinders. To prevent the validation process from becoming to laborious, only a few of the more important variables will be checked using the hand calculations. Important parameters that have been determined to check the Matlab model contain:

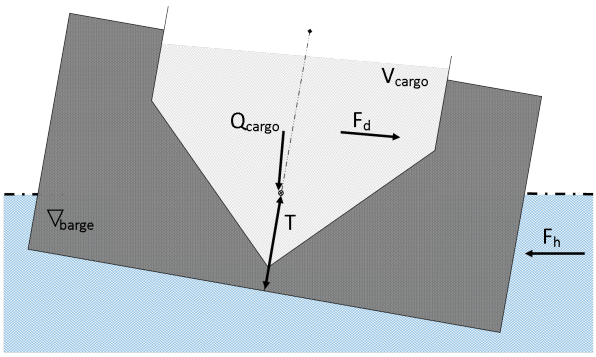

Figure A.1: Parameters that are determined to validate the Matlab model

- The cargo volume and weight
- The resulting earth-bound horizontal cargo load
- The displaced volume of the barge
- The mean draft of the barge
- The earth-bound horizontal hydrostatic forces that act on the hull

Figure A.1 shows the parameters that are calculated by hand and compared to the values that are obtained using the Matlab model.

The parameters were determined for roll angles of a barge fully filled with cargoes of density $1025\frac{kg}{m^3}$, $1600\frac{kg}{m^3}$ and $2000\frac{kg}{m^3}$. By doing so, all cargo regimes are present in the control calculations. As a result, a extensive knowledge on the capabilities of the model is obtained. just as it is done in the Matlab model, the selected variables are determined for multiple angles of roll. In this appendix the results for the angles of $\theta_{roll} = 0\ deg$ and of $\theta_{roll} = 10\ deg$ are shown. The relations that are used for the hand calculations are based on the Bureau Veritas relations that were given in chapter 2.

The results from the reliability calculations that were done for the model used in chapter 3 are included in the tables below. The tables show the results of the hand calculations together with the obtained results from Matlab. First the barge fully filled with a liquid cargo of density $\rho_{cargo} = 1025\frac{kg}{m^3}$. Note that in this situation, according to the sliding law as it is used in chapter 3, the roll angle and the inclination of the cargo surface will be equal $\theta_c = \theta_r$. The determined values are displayed in table A.1.

Secondly the model is checked for a sliding kind of cargo. For this calculation step a sliding cargo with density $\rho_{cargo} = 1600\frac{kg}{m^3}$ is used. The inclination of the cargo surface is now equal to $\theta_c = \frac{2}{3}\theta_r$. The results for the control calculations for the barge loaded with the sliding cargo is displayed in table A.2.

Lastly, The barge is considered loaded with a solid cargo. Fir this situation a cargo density of $\rho_{cargo} = 2000\frac{kg}{m^3}$ was chosen. Using the sliding law the angle of inclination for the cargo surface is found being equal to $\theta_c = 0$. The obtained results are given in table A.3

Table A.1: Calculated values for liquid cargo of density $\rho_{cargo} = 1025\frac{kg}{m^3}$

Cargo volume				
	Variable	Hand calculated	Matlab	Error
	V_0	$3777.9m^3$	$3777.9m^3$	0%
	V_{10}	$3035.2m^3$	$3035.0m^3$	0%
Horizontal cargo force				
	Variable	Hand calculated	Matlab	Error
	$F_{d,0}$	$1713.9t$	$1712.8t$	−0.1%
	$F_{d,10}$	$1229.5t$	$1229.5t$	0%
Cargo weight				
	Variable	Hand calculated	Matlab	Error
	Q_0	$3872.3t$	$3871.3t$	−0.1%
	Q_{10}	$3111.0t$	$3110.9t$	0%
Displaced volume				
	Variable	Hand calculated	Matlab	Error
	∇_0	$5578.3ton$	$5578.3ton$	0%
	∇_{10}	$4816.8ton$	$4816.8ton$	0%
Mean draught				
	Variable	Hand calculated	Matlab	Error
	T_0	$4.27m$	$4.27m$	0%
	T_{10}	$3.69m$	$3.69m$	0%
Hydro-static force				
	Variable	Hand calculated	Matlab	Error
	$F_{h,0}$	$511.2t$	$511.4t$	0%
	$F_{h,10}$	$348.1t$	$348.3t$	0%

Table A.2: Calculated values for sliding cargo of density $\rho_{cargo} = 1600 \frac{kg}{m^3}$

Cargo volume				
	Variable	Hand calculated	Matlab	Error
	V_0	$3777.9 m^3$	$3777.9 m^3$	0%
	V_{10}	$3285.4 m^3$	$3285.4 m^3$	0%
Horizontal cargo force				
	Variable	Hand calculated	Matlab	Error
	$F_{d,0}$	$2675.3 t$	$2675.3 t$	0%
	$F_{d,10}$	$2172.2 t$	$2172.2 t$	0%
Cargo weight				
	Variable	Hand calculated	Matlab	Error
	Q_0	$6044.6 t$	$6043.8 t$	-0.1%
	Q_{10}	$5256.7 t$	$5256.7 t$	0%
Displaced volume				
	Variable	Hand calculated	Matlab	Error
	∇_0	$7750.6 ton$	$7750.6 ton$	0%
	∇_{10}	$6962.6 ton$	$6962.6 ton$	0%
Mean draught				
	Variable	Hand calculated	Matlab	Error
	T_0	$5.93 m$	$5.93 m$	0%
	T_{10}	$5.33 m$	$5.33 m$	0%
Hydro-static force				
	Variable	Hand calculated	Matlab	Error
	$F_{h,0}$	$1091.1 t$	$1093.0 t$	0%
	$F_{h,10}$	$830.8 t$	$831.0 t$	0%

Table A.3: Calculated values for solid cargo of density $\rho_{cargo} = 2000 \frac{kg}{m^3}$

Cargo volume				
	Variable	Hand calculated	Matlab	Error
	V_0	$3777.9 m^3$	$3777.9 m^3$	0%
	V_{10}	$3777.9 m^3$	$3777.9 m^3$	0%
Horizontal cargo force				
	Variable	Hand calculated	Matlab	Error
	$F_{d,0}$	$3344.1 ton$	$3344.1 ton$	0%
	$F_{d,10}$	$3344.1 ton$	$3344.1 ton$	0%
Cargo weight				
	Variable	Hand calculated	Matlab	Error
	Q_0	$7555.8 t$	$7555.8 t$	0%
	Q_{10}	$7555.8 t$	$7555.8 t$	0%
Displaced volume				
	Variable	Hand calculated	Matlab	Error
	∇_0	$9261.7 ton$	$9261.7 ton$	0%
	∇_{10}	$9261.7 ton$	$9261.7 ton$	0%
Mean draught				
	Variable	Hand calculated	Matlab	Error
	T_0	$7.09 m$	$7.09 m$	0%
	T_{10}	$7.09 m$	$7.09 m$	0%
Hydro-static force				
	Variable	Hand calculated	Matlab	Error
	$F_{h,0}$	$1625.8 t$	$1626.4 t$	0%
	$F_{h,10}$	$1576.8 t$	$1577.4 t$	0%

From the tables A.1,A.2 and A.3 no significant deviations were found in the values that were compared. The small deviations that were obtained do most like come from the rounding of of values during the hand calculations. Although the control calculations that are done in this chapter are quite short and do leave room for speculation, they do give the necessary confidence in the Matlab model that is required to use it for the intended calculations.

Note that the actual forces that are of interest in the Matlab model were not checked since this would become to laborious and unreliable. Therefore, great care has to be taken with the obtained result determined using the Matlab model. Although the model seems to work well, the validity of the obtained results has to be checked for each simulation.

B

Cargo friction in the split hopper barge

In section 3.1.2 of chapter 3 perpendicular forces along the hopper walls of the split hopper barge were found. Although these forces are no frictional forces they do show that forces perpendicular to the walls of the hopper do have an influence on the forces that are found in the hinges and hydraulic cylinders of the split hopper barge. This raises the question whether friction inside the cargo and friction of the cargo along the hopper wall could be of interest for this research.

The friction that occurs in and around the cargo in the split hopper barge can be subdivided in two different kinds of friction. First there is the internal friction in the cargo which causes it either to be stable or unstable. Since cargo that is found to be unstable will start to slide, a research to the internal friction could therefore be used to validate the sliding law of Bureau Veritas that is used (Bureau Veritas, 2016). Besides, being able to describe the behaviour of the cargo in more detail would help to describe the cargo motions in the hopper in a more realistic way for the different situations that are of interest in this research.

Next to the internal friction, there exists the friction between the cargo and the hopper walls. This external friction causes the cargo in the hopper to stick to the hopper walls. When cargo is sticky, it will take longer to flow out of the hopper during discharge. Modelling this friction would therefore be helpful in a model that is intended to describe the offloading cycle of the split hopper barge in detail.

B.1. Internal cargo friction

Due to the shape of the individual particles from which a mud or soil is composed, some resistance exists against the sliding of these particles in a opposite direction to each-other. This internal friction that has to be overcome to cause a failure or sliding of the cargo in the hopper can be described using a simple equilibrium of forces over a small element of the cargo as is displayed in figure B.1.

In figure B.1, σ_v and σ_h are the pressures that excite the small element of soil. σ and τ are the normal stress and shear stress that act in the failure plane of the element. Since a failing motion of the particle is expected to have a velocity in the negative direction of τ, the shear stress of the element can be seen as its resistance against failure. When a critical value of the shear stress is exceeded the particle under concideration is expected to fail and will therefor start to slide. The critical shear stress that has to be exceeded to start a failure is defined using the Coulomb failure criterion (Verruijt, 1999) :

$$\tau_{crit} = c + \sigma \cdot \tan\varphi \tag{B.1}$$

In this relation c is the cohesion of the soil between the elements. φ is the angle of internal friction.

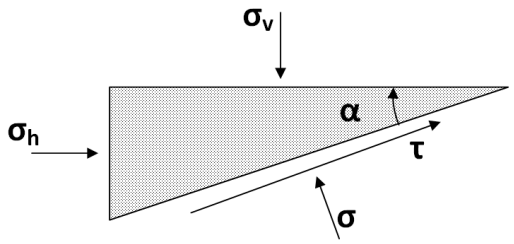

Figure B.1: Equilibrium of forces over a small element of soil

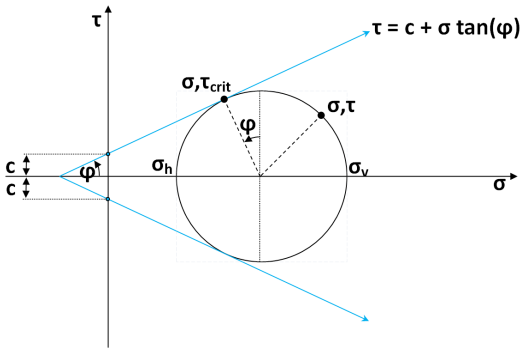

Figure B.2: The Mohr-Coulomb failure criterion

The normal and shear stresses that work on one element can be displayed as a coordinate in a coordinate system. Then, when the element is considered for multiple rotated orientations, for each of the orientations the shear and normal stress components can be determined. When these components are all plotted in the same coordinate system, the circle of Mohr for the element is found. When the Mohr circle plotted together with the failure criterion given by Coulomb, the Mohr-Coulomb failure relation is obtained. Using this criterion the critical orientations of the considered soil can be explained. The Mohr-Coulomb circle for a random particle is shown in figure B.2.

As long as all the coordinates on the Mohr circle are positioned within the boundaries of the Coulomb failure criterion no failure will occur. In case two or more points do cross the criterion lines, failure in that critical direction can be expected for the corresponding soil elements.

Bishops model

To find the relation between the roll angle of the split hopper barge and the angle of inclination of the cargo compared to the hopper, the internal friction of the cargo is used. To be able to describe the stability of the cargo in the split hopper barge in relative ease, the hopper load is considered as a failing slope and its stability can therefore be determined using a slope stability analysis.

In the soil mechanics book of Verruijt (Verruijt, 1999) the slope stability analysis method as it was defined by Bishop is explained. Bishop stated that slopes fail along a circular path that runs through the slope that is considered . When the failing volume, the soil above the failure line, is subdivided into multiple vertical slices, the stability of the slope can be obtained by taking the contribution of each slice to the momentum balance around the midpoint of the circle on which the failure line lies. Than the stability of the slope can be described by a safety factor is defined as the relation between moment that causes the slope to fail and the moment that resists this failure:

$$F = \frac{Strength}{Load} \tag{B.2}$$

Implemented in the failure description of Coulomb this safety factor give the following relation for the shear stress in the individual slice:

$$\tau = \frac{1}{F}\left(c + \sigma \tan\varphi\right) \tag{B.3}$$

From which it is clear that in the case that $F > 1$ the slope is stable and if $F < 1$ the slope is unstable and could possibly fail.

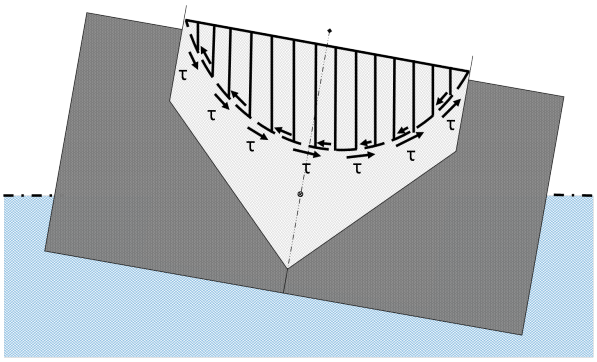

Figure B.3: Bishops slope failure model aplied to the split hopper barge.

Figure B.3 shows the Bishop slope stability model applied to the cargo in the split hopper barge. For the particular case of the split hopper barge however, for the cargoes in which sliding is expected to occur, very little information is available about the cohesion and friction coefficient. For the roll angles under which the split hopper barge is considered, it is known that sand for instance does not slide since it has a high internal friction angle. For clay, it is known that its cohesive strength is far too high to be exceeded by the forces induced in the cargo to cause sliding. The cargo that is expected to move is slurry which is made up from a combination of silt, sand, clay in a mixture of water. Since the exact composition is not known for a cargo with a certain density, estimating the friction and cohesion coefficients would therefore result in very uncertain estimates. This would cause the calculations that are done for the friction to be very inaccurate as well, ultimately giving very little added value to the model of the barge. So although the sliding of the cargo in the hopper is a interesting process ,for now it is decided that it does not fall inside the scope of this research.

B.2. External friction

Besides friction in the cargo itself, there is some friction present in between the cargo and the hopper as well. This friction can be subdivided in two different parts knowing, the static external friction and the dynamic external friction. The static external friction is the friction that has to be over-won in order for the cargo to start sliding over the hopper wall. When the static friction is not over-won, the cargo will remain in position. When the static friction is exceeded, the cargo starts sliding over the wall. During this sliding motion, the cargoes motion is resisted by the dynamic friction. Note that the static friction of the cargo with the hopper wall will always exceed the dynamic friction on the hopper wall, and that the static and dynamic friction do not work simultaneously.

Both the dynamic and static friction are a result from the normal force due to the cargo acting on the hopper wall and can be found using the following relation:

$$F_{fric,stat} = F_{normal} \cdot \tan\delta_{stat} \tag{B.4}$$

$$F_{fric,dyn} = F_{normal} \cdot \tan\delta_{dyn} \tag{B.5}$$

Wherein the δ values are the static and dynamic angles of external friction that exist between the cargo and the hopper wall.

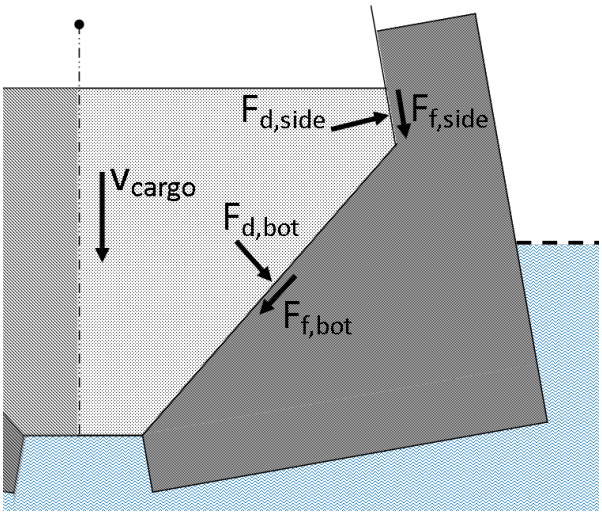

Figure B.4: Dynamic external friction of the cargo acting on the hopper flow during discharge

In a closed condition, the forces due to the friction between the hopper and the cargo do not play a significant role. Since it is the weight of the cargo that works on the barge rather than the friction that transfers the weight of the cargo to it, the friction can be neglected. In the end, the sum of the friction in the vertical direction will be equal to the weight of the cargo anyway.

In a opened condition however, the cargo will start flowing out of the hopper. To do so, first the static friction between the cargo and the hopper walls has to be overcome. Then when the cargo is moving, the barge is no longer excited by the weight of the cargo, but rather is excited by the friction that exists between the hopper walls and the cargo. Therefore, in the opened situation, it is the dynamic friction that will excite the barge. Figure B.4 shows the dynamic external friction that acts on the hopper walls when cargo is flowing out of the hopper.

Since for the external friction the open barge that is discharging its cargo is the most interesting case, it is no longer only the sliding cargo that is of interest. For the discharging barge, all cargo types can be considered. For the sliding cargoes it will again prove to be difficult to find reliable data for the friction and cohesive coefficients and for the liquid cargoes friction and cohesion does not exist. For the solid cargoes such as sand and clay however, good and reliable data is available about the cohesive and frictional coefficients, making it possible to examine the effects of outflow of cargo out of the hopper.

B.3. Conclusions about friction of cargo with the split hopper barge

When the friction of cargo with the split hopper barge is considered. This friction has to be subdivided in internal and external friction.

The internal friction of the cargo will cause it to either remain stable or move in the closed barge. Internal friction and cohesion is therefore the reason for the resistance of a inclined cargo surface for the rolling barge. By defining this internal friction and cohesion the validity of the sliding law as it was presented in chapter 3 can be investigated. However, since there is little to no information available about the friction and cohesion coefficient for the type of cargo for which it is expected to be most likely that sliding occurs, such an question will prove to be a research on its own making it not feasible to do so within the boundaries of this current research.

The external friction is the kind of friction that causes the interaction between the cargo and the hopper when the cargo is flowing out. Since for this situation all cargo types can be considered, the influence of the dynamic external friction can be considered for the types of cargo where information is available about the frictional and cohesive coefficients. The effect of dynamic external friction on the hinge and cylinder forces during the outflow of cargo is determined in section 3.5 of chapter 3.

C

Influence of liquid cargo motions

C.1. Theory

When the SHB moves, the liquid or semi-liquid cargo in its hopper will start moving as well. Doing so, the cargo will perform work on the hopper walls and thereby influences the motion of the SHB, the motion of the cargo and the SHB are thus coupled. To investigate the effect that the coupled motions of the barge and its cargo have on the forces in the hinges and hydraulic cylinders, the model that was presented in chapter 4 has to be adjusted for liquid cargoes. This appendix elaborates on these adjustments and proofs their validity.

To describe the effect of the coupled motions of the barge and its cargo, first their coupled equation of motion have to be found. To do so, first the equation of motion of the barge itself is considered. In chapter 4 the general equation of motion for the SHB was already given in equation 4.21:

$$\left[-\omega^2\left(\mathbf{M}_{SHB}+\mathbf{A}_{SHB}\right)+i\omega\mathbf{B}_{SHB}+\mathbf{C}_{SHB}\right]\hat{x}=\hat{F}(\omega) \tag{C.1}$$

Knowing that the barge and its hopper are rigidly connected to each other, the motions of the hopper can coupled to the motions of the barge using a transformation matrix. The motions of the hopper can then be described by:

$$\hat{x}_{hop}=\mathbf{Q}_{hop}\hat{x} \tag{C.2}$$

Here, $\mathbf{Q}_{hop}$ represents the transformation matrix due to the location of the hopper center of gravity. Using the approach presented by Coa and Zhang (Coa & Zhang, 2016), the static and dynamic force contributions of the tank in a tank fixed frame can then be written as:

$$F_d^{hop}=-\omega^2\mathbf{A}_{hop}(\omega)\mathbf{Q}_{hop}\hat{x}e^{i\omega t} \tag{C.3}$$

$$F_s^{hop}=F^{co}+\mathbf{C}_{hop}\mathbf{Q}_{hop}\hat{x}e^{i\omega t} \tag{C.4}$$

Here, F^{co} is the hydrostatic load on the hopper due to the liquid cargo before it has moved. $\mathbf{C}_{hop}$ is the stiffness due to the cargo. In the hopper load formula, $\mathbf{A}_{hop}(\omega)$ is the overall added mass coefficient for the hopper. In this approach it is assumed that no waves radiate out of the hopper, as a result radiation damping does not occur.

The added mass that is considered for the cargo can be described by two separate parts. First there is the added mass that results from the rigid effects of the cargo, $\widehat{\mathbf{A}}_{hop}$, this is equal to the mass of the frozen cargo. Then there is the added mass that follows from the liquid effects of the cargo in the hopper, $\widetilde{\mathbf{A}}_{hop}(\omega)$. The combined added mass can be written as:

$$\mathbf{A}_{hop}(\omega) = \widehat{\mathbf{A}}_{hop} + \widetilde{\mathbf{A}}_{hop}(\omega) \tag{C.5}$$

The dynamic force contribution of the tank becomes:

$$F_d^{hop} = -\omega^2 \widehat{\mathbf{A}}_{hop}\mathbf{Q}_{hop}\widehat{x}e^{i\omega t} - \omega^2 \widetilde{\mathbf{A}}_{hop}(\omega)\mathbf{Q}_{hop}\widehat{x}e^{i\omega t} \tag{C.6}$$

In the SHB fixed reference frame the equations for the dynamic and static forces of the hopper are:

$$F_d^{SHB} = -\omega^2 \widehat{\mathbf{A}}_{hop}\widehat{x}e^{i\omega t} - \omega^2 \widetilde{\mathbf{A}}_{hop}(\omega)\widehat{x}e^{i\omega t} \tag{C.7}$$

$$F_s^{SHB} = F^{co} + \mathbf{C}_{hop}\mathbf{Q}\widehat{x}e^{i\omega t} \tag{C.8}$$

Implementing these relations into the equation of motion of the SHB (eq. C.1) gives:

$$\left[-\omega^2\left(\mathbf{M}_{SHB} + \mathbf{A}_{SHB} + \widehat{\mathbf{A}}_{hop} + \tilde{\mathbf{A}}_{hop}(\omega)\right) + i\omega\mathbf{B}_{SHB} + \mathbf{C}_{SHB} + \mathbf{C}_{hop}\right]\widehat{x} = \widehat{F}(\omega) \tag{C.9}$$

From the obtained coupled equation of motion for the barge and its cargo, the conclusion can be drawn that the effect of liquid cargo in the hopper can be described by additional added mass and stiffness terms. Since the model that is shown in chapter 4 already includes the weight of the solid/frozen cargo, $\widehat{\mathbf{A}}_{hop}$, it does not have to be determined again. To include the effects of the liquid cargo, only $\tilde{\mathbf{A}}_{hop}(\omega)$ and $\mathbf{C}_{hop}$ have to be found.

C.2. Stiffness

The change in stiffness due to the liquid cargo effect in the hopper is commonly described as a loss in metacentric height. This reduction of GM for the barge is described in the Offshore Hydromechanics book of Journee (Journee & Massie, 2001) and is found using:

$$\begin{aligned} GMx' &= GMx - \overline{GG'} \\ &= GMx - \frac{\rho_{hop} i_{hop}}{\rho_{sea} \nabla} \end{aligned} \tag{C.10}$$

$$\begin{aligned} GMy' &= GMy - \overline{GG'} \\ &= GMx - \frac{\rho_{hop} i_{hop}}{\rho_{sea} \nabla} \end{aligned} \tag{C.11}$$

In these relations i_{hop} is the transverse moment of inertia of the hopper. This moment of inertia is found using:

$$i_{hop} = \frac{1}{12} b_{hop} h_{hop}^3 \tag{C.12}$$

Here, b_{hop} is the width of the hopper and h_{hop} is its height. Do note that b_{hop} and h_{hop} are different for adjustment for GMx and GMy.

The reduction of the metacentric height of the SHB can be implemented into the AQWA model, AQWA itself will than adjust the stiffness matrix of the system. Do note that the change of the stability lever arms of the barge is not the only stiffness effect due to the cargo. The paper of (Coa & Zhang, 2016) shows that a second term of the stiffness has to be taken into account. This term accounts for the hydrostatic (rigid) contributions of the liquid cargo. In the model of chapter 4 this contribution is already taken into account in the Ansys simulations by considering the combined weight of the barge and the cargo. As a result, it does not have to be added separately.

C.3. Added mass

Next to the stiffness, the added mass matrix due to the liquid effects of the cargo in the hopper has to be found. To solve the EOM as it was given in relation 4.21 the software tool WAMIT is used. WAMIT was created at MIT university and is one of the more powerful existing diffraction tools that can cope with potential flow both on the in and outside of a vessel, ("WAMIT User manual", 2016). The equations are solved in the frequency domain for which the main assumption is linearity. As a result, the non-linear sloshing effects that occur in the hopper will not be determined properly by the model. The amplitudes around the natural frequencies of the system have to be considered with care as a result. Furthermore, no viscous damping is included in the simulations, the responses of the SHB in the surge and roll direction will therefore be overestimated as well.

In WAMIT, the SHB is modelled using a predefined ship geometry. Two models will be compared. One model is built without a hopper, here the cargo is assumed to be frozen. In the second model, the hopper is represented by a rectangular closed tank with the same capacity as the actual hopper. In this model the cargo is modelled as a liquid. For both conditions the barge is fully loaded and is therefore considered with its dredging draught. The WAMIT models of barge with and without a tank are shown in figures C.1 and C.2.

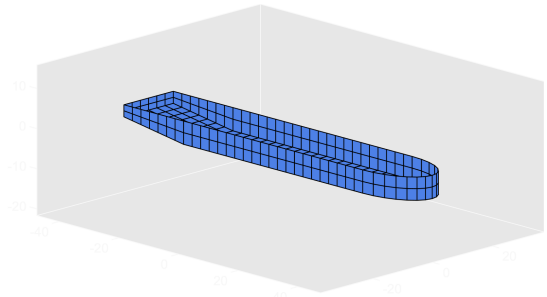

Figure C.1: WAMIT SHB

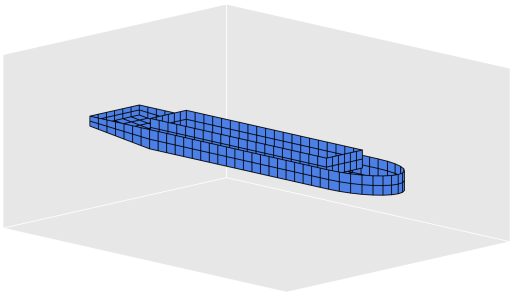

Figure C.2: WAMIT SHB with tank

Using the two shown geometries, first the effect of the liquid cargo on the motion RAO's of the SHB can be determined. Figures C.3 to C.8 show the motion RAO's for the two barges.

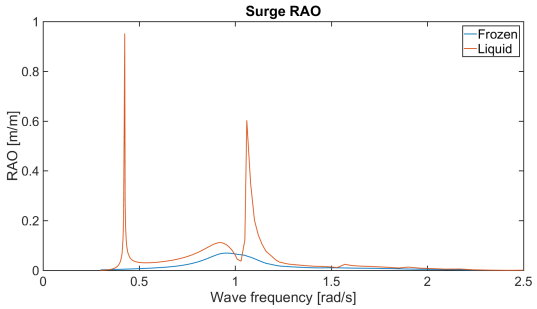

Figure C.3: Surge RAO.

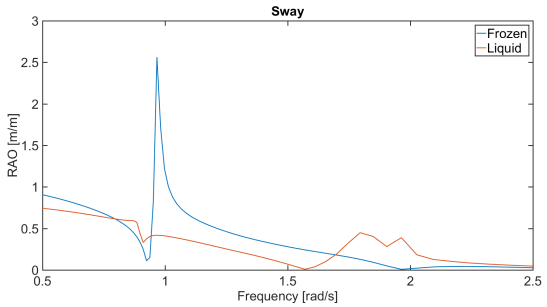

Figure C.4: Sway RAO

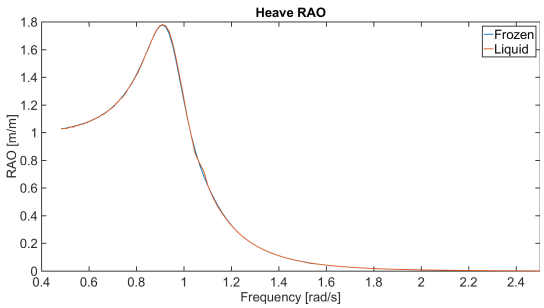

Figure C.5: Heave RAO.

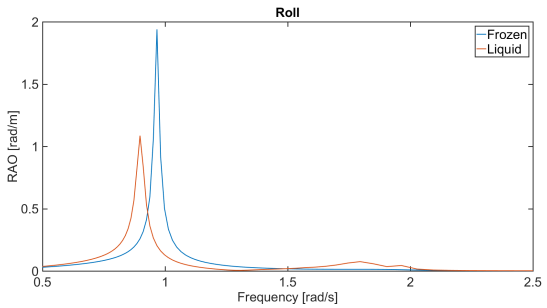

Figure C.6: Roll RAO

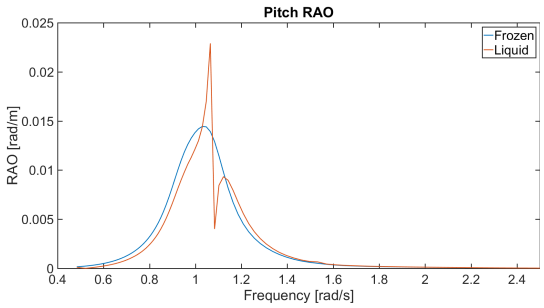

Figure C.7: Pitch RAO.

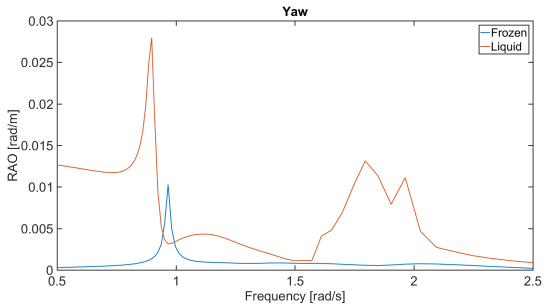

Figure C.8: Yaw RAO

Figures C.3 and C.6 show that due to the lack of viscous damping, the amplitudes of the surge and roll RAO are overestimated as was expected. Note that for surge there is an additional motion peak due to the presence of liquid cargo. This motion peak is found for a low frequency, which is a result from the large length of the cargo hopper. In the other graphs it can be seen that the effects of the liquid cargo on the motions of the SHB are mild. Only in the yaw direction a real increase of the barge's motions is expected around the natural frequency of the hopper. Since the barge in the model is approximately symmetric, the original yaw motions it are quite small. As a result, any effect the hopper has on the yaw motion will pose to be significant.

Note how for the heave direction the motions of the barge with and without liquid cargo are exactly the same. Due to its incompressibility the cargo in the hopper will always behave like a solid one for pure heave. For that same reason the added mass for the liquid cargo in a heave motion is not expected to deviate from that of the solid cargo as well.

For the pitch motion the same reasoning can be used as for the heave RAO. Since pitch is largely influenced by the heave motion of the barge, it is expected that the observed trends form the heave RAO will hold for the pitch RAO as well. However, due to the overestimated surge motions in the model, a large peak is observed in the pitch RAO, near the natural frequency of the barge. Under the assumption that this is indeed an overestimation due to the lack of viscous damping in the surge direction, the motions of the barge for pitch can be said to be the same for a solid and a liquid cargo as well.

Concluding from the shown RAO's, it is expected that the liquid cargo will mainly influence the barge in the surge, sway, roll and yaw direction. The heave and pitch motions are not expected to differ for a barge loaded with a liquid cargo. As a result, the added mass in these directions is not expected to be different as well. For the surge, the difference in added mass will be determined and included in the simulations. However, due to the large overestimation of the surge motions the graphs for it are not clear. For clarity therefore for the further explanation of the liquid cargo effects in this appendix the graphs resulting from the surge motion will not be shown.

To further conclude on the three selected RAO's, a spectral analysis using the shown RAO's is performed to see what the effect of the liquid cargo is energy wise. Figures C.9 to C.14 show the resulting motion energy spectra after analysing the RAO's with a JONSWAP spectrum.

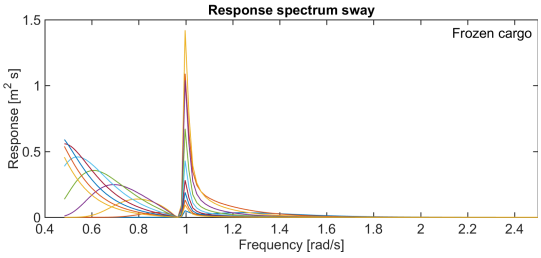

Figure C.9: Response spectrum sway for frozen cargo.

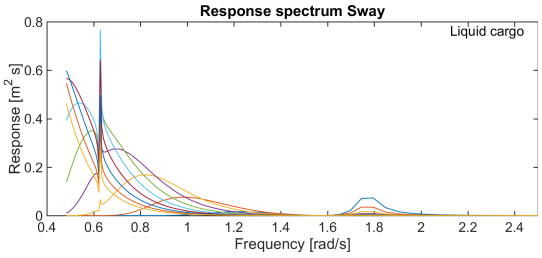

Figure C.10: Response spectrum sway for liquid cargo

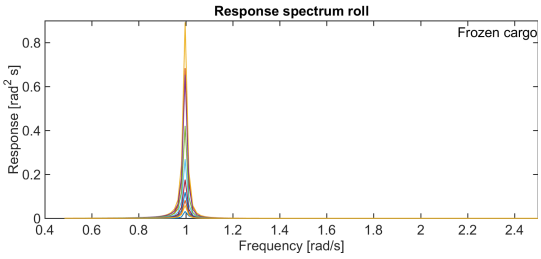

Figure C.11: Response spectrum roll for frozen cargo.

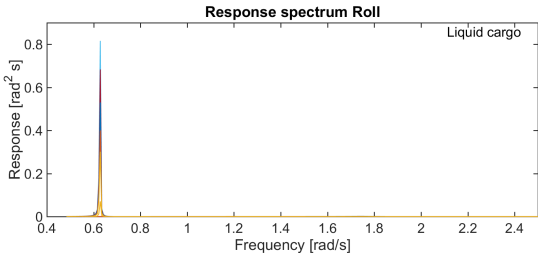

Figure C.12: Response spectrum roll for liquid cargo

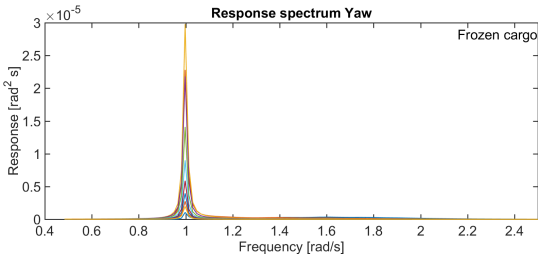

Figure C.13: Response spectrum yaw for frozen cargo.

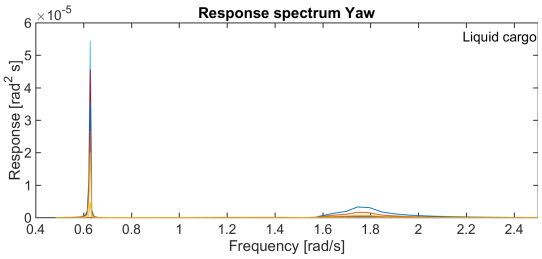

Figure C.14: Response spectrum yaw for liquid cargo

The figures show that the energy that is in the wave spectrum is higher for the frequency range in which the natural frequency of the barge is, than it is for the frequency range containing the natural frequency of the hopper. As a result, the effects of the waves on the motions of the barge will be more governing compared to their effect on the motions of the liquid cargo. From that the conclusion can be drawn that the motions of the barge that result from the motions of the liquid cargo are small compared to the motions of the barge due to the exterior waves. For the added mass terms that have to be found for the simulations this means that the added mass terms in the frequency range around the natural frequencies of the barge itself are expected to be of more importance than those in the range around the natural frequencies of the hopper.

The resulting added mass plots for sway, roll and yaw for both a frozen and liquid cargo are given in figures C.15 to C.17.

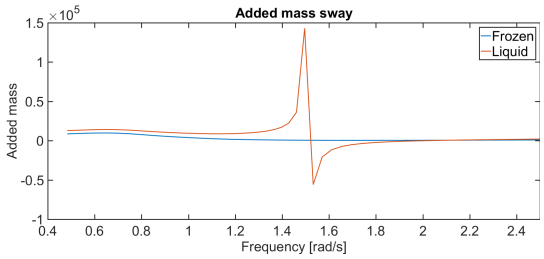

Figure C.15: Sway added mass

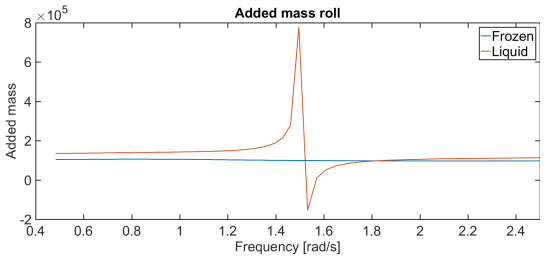

Figure C.16: Roll added mass.

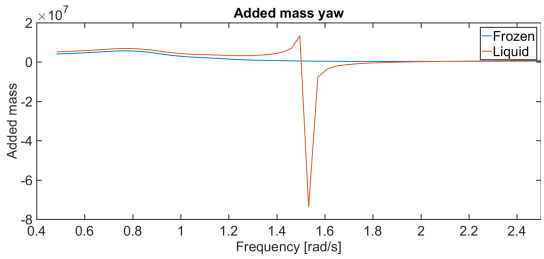

Figure C.17: Yaw added mass

From the added mass plots it can be seen that the effect of the liquid cargo on the added mass, can actually be described reasonably well using static term before and after the natural frequency of the tank. Since the conclusion was drawn that the non-linear effects around the natural frequencies of the hopper are not expected to cause significant effects, the large peaks found in the added mass plots for these frequencies are not expected to have significant influences as well. As a result, non-frequency dependent constant added mass matrices can be used for the AQWA model adjustments.

C.4. Conclusions

In this appendix the effect of the liquid cargo in the hopper of the SHB was elaborated on. From the coupled equations of motion of the barge and its hopper it was found that the effects can be captured by adding additional added mass and stiffness terms to the simulations. For the added mass, only the effects due to the liquid motions of the cargo in the hopper have to be added, the rigid added mass is already included in the simulations by considering the weight of the cargo in the hopper.

From the hydromechanics book by Journee (Journee & Massie, 2001) it was found that the additional stiffness that has to be considered when simulating the SHB with a liquid cargo, can be expressed using a reduction of the metacentric height. The reduction can be obtained using simple equations, the results can directly be implemented in the simulations.

To conclude on the additional added mass that has to be considered, the barge was simulated in WAMIT. From the motion RAO's it was found that significant effects of the liquid cargo are only expected in the sway, roll and yaw direction. From the response spectra of the barge with and without liquid cargo, it was found that for the directions of interest the effects in the frequency range surrounding the natural frequencies of the barge are most significant. From the added mass plots it was found that for the frequency ranges of interest the added mass due to a liquid cargo that is present in the hopper of the SHB can be described using a non-frequency dependent value. A non-frequency dependent added mass matrix can be implemented in AQWA directly.

D

Maximum resulting forces for multiple wave heights

D.1. Solid cargo

D.1.1. Required cylinder forces

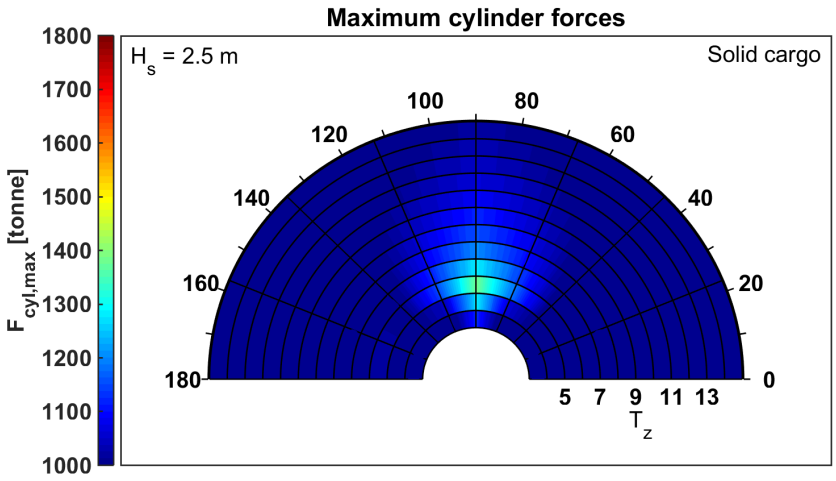

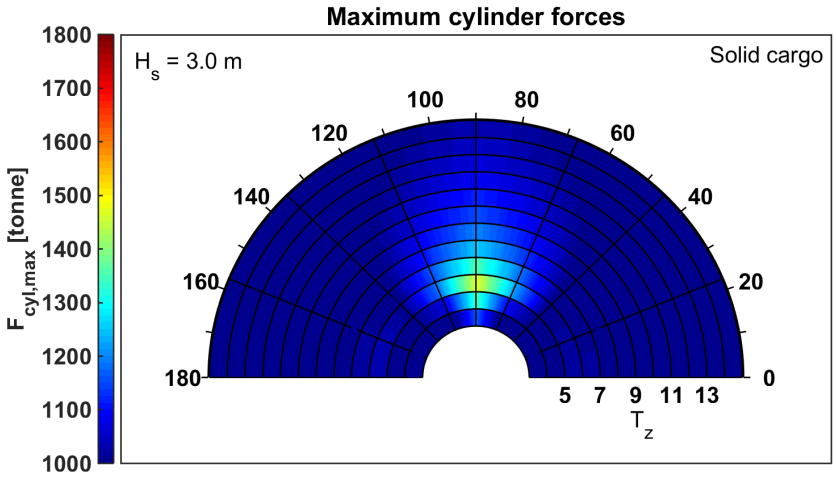

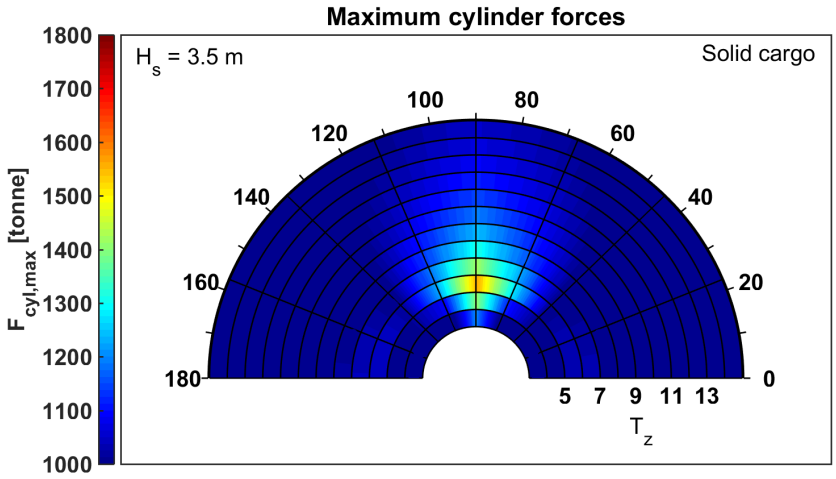

D.1.2. Hinges forces (fore)

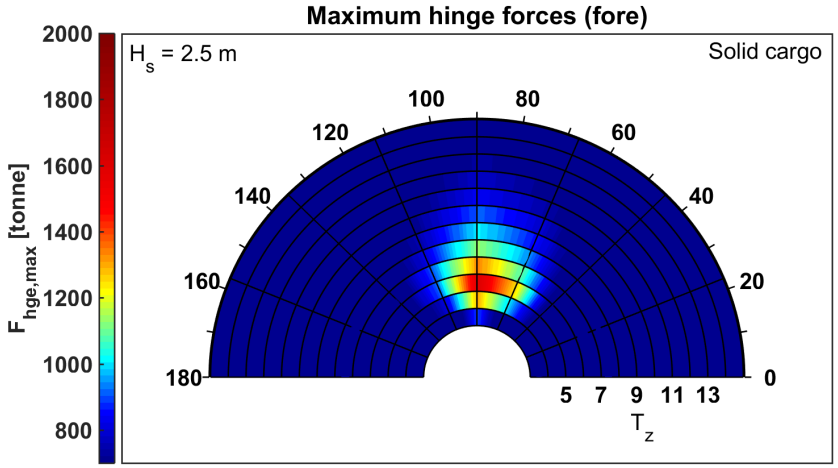

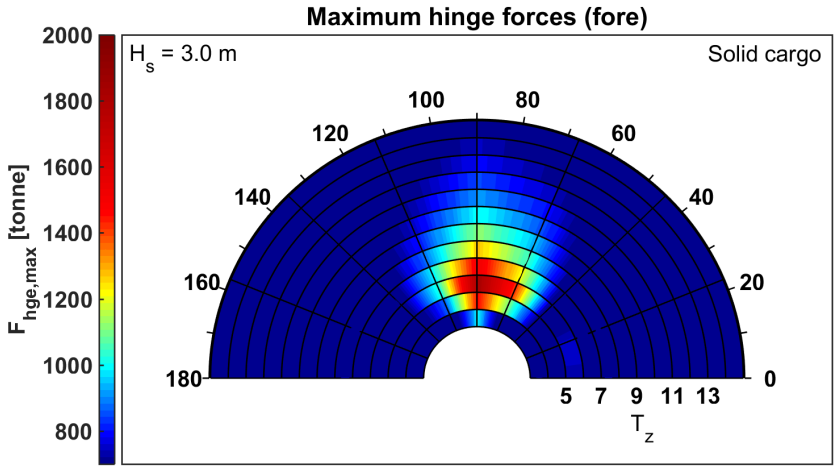

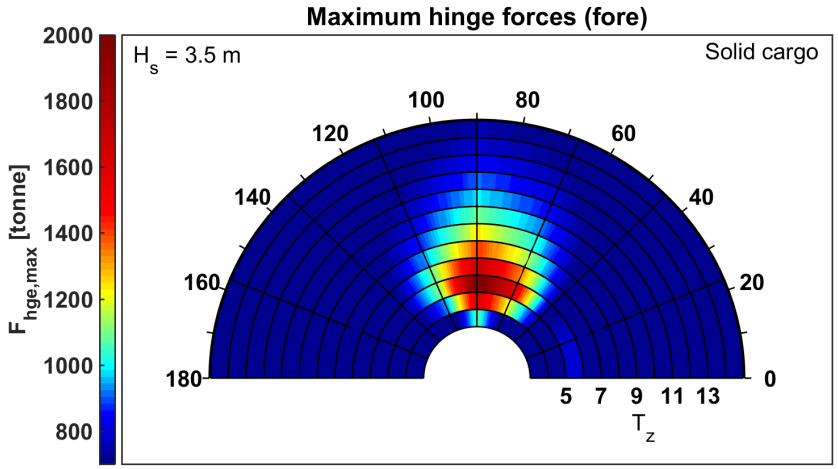

D.1.3. Hinges forces (aft)

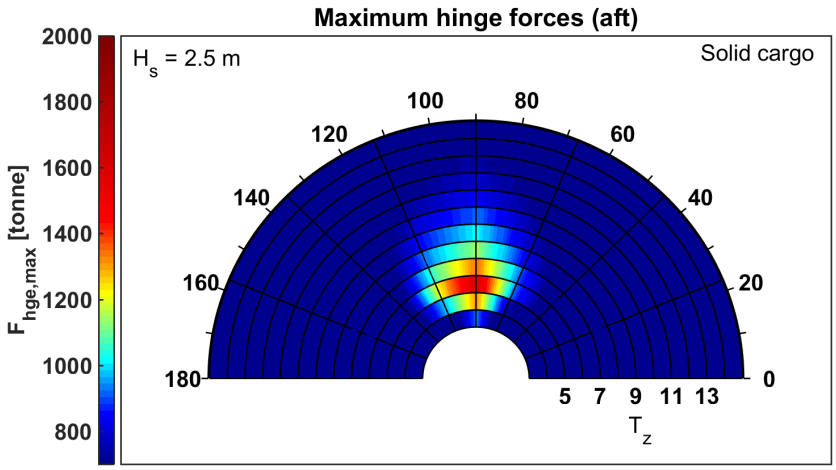

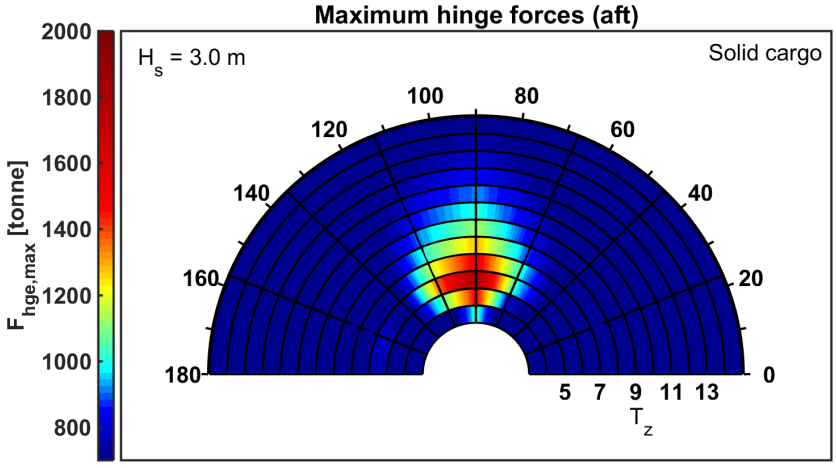

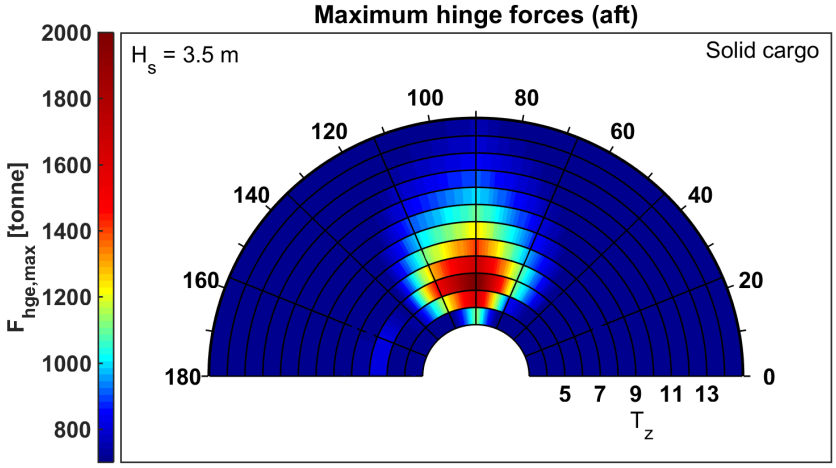

D.2. Liquid cargo

D.2.1. Required cylinder forces

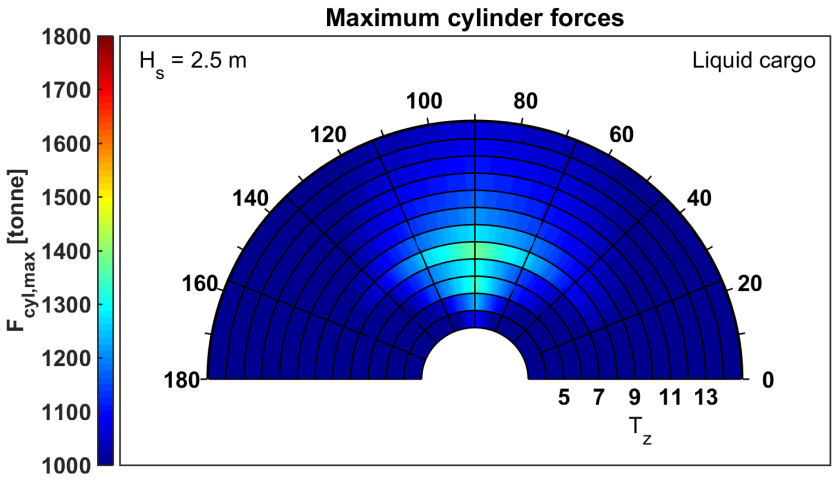

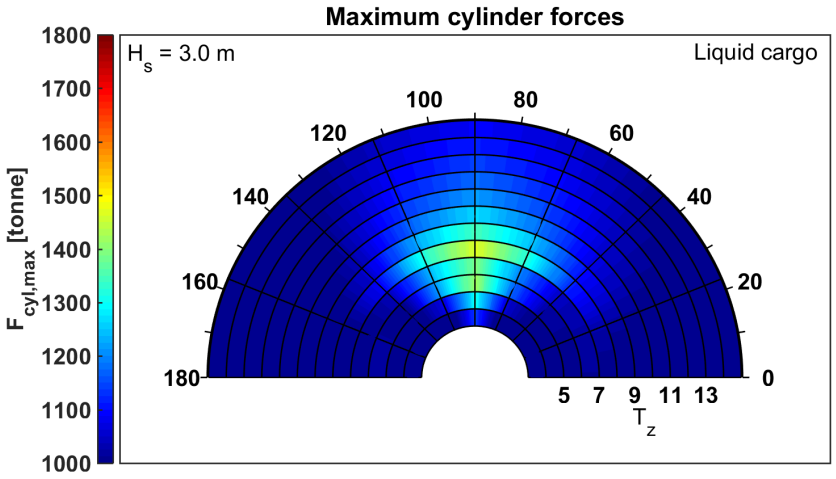

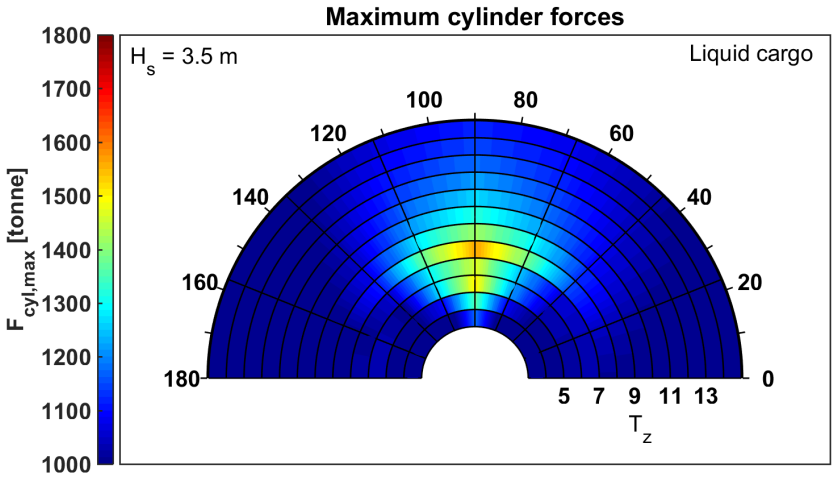

D.2.2. Hinges forces (fore)

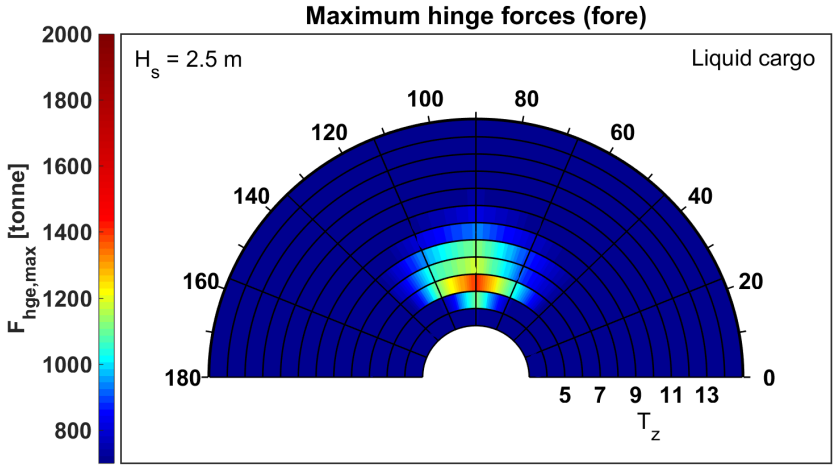

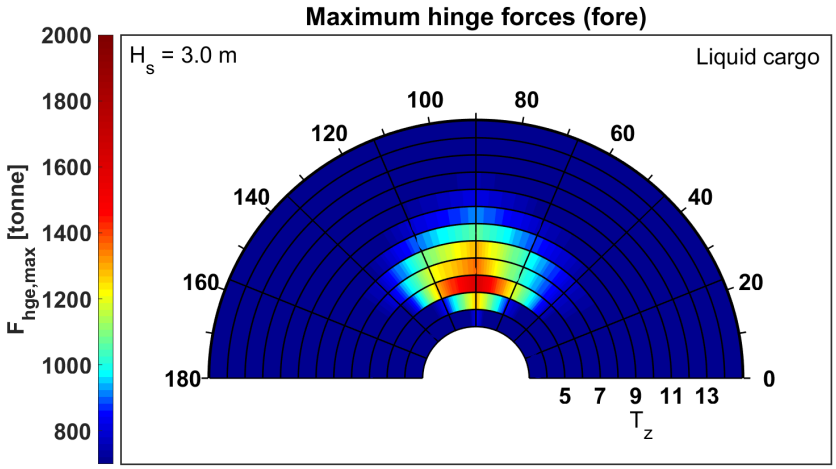

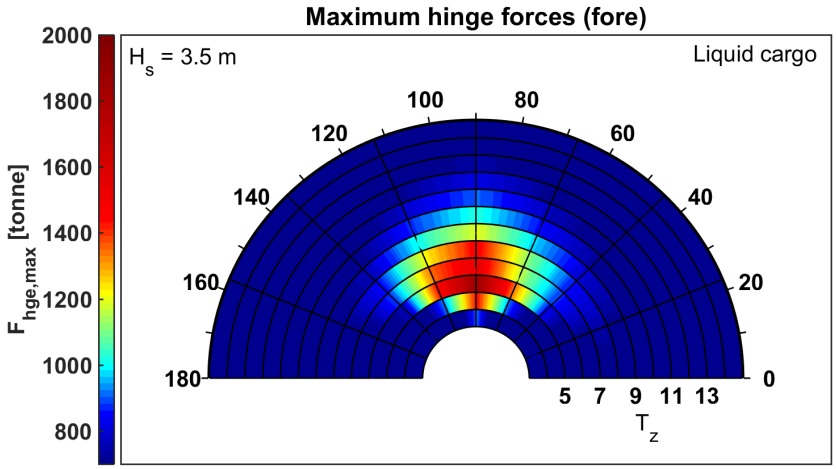

D.2.3. Hinges forces (aft)